Power Quality and Voltage Stability Enhancement of Terrestrial Grids and Shipboard Microgrids

Terriche, Yacine

Publication date:
2020

Document Version
Publisher's PDF, also known as Version of record

POWER QUALITY AND VOLTAGE STABILITY ENHANCEMENT OF TERRESTRIAL GRIDS AND SHIPBOARD MICROGRIDS

BY
YACINE TERRICHE

DISSERTATION SUBMITTED 2020

AALBORG UNIVERSITY
DENMARK

POWER QUALITY AND VOLTAGE STABILITY ENHANCEMENT OF TERRESTRIAL GRIDS AND SHIPBOARD MICROGRIDS

PH.D. DISSERTATION

by

Yacine Terriche

AALBORG UNIVERSITY
DENMARK

Dissertation submitted to
the Faculty of Engineering and Science at Aalborg University

for the degree of
Doctor of Philosophy in Electrical Engineering

.

Dissertation submitted: 07 September 2020

PhD supervisor: Professor Josep M. Guerrero
Aalborg University

Assistant PhD supervisor: Assistant Professor Yonghao Gui
Aalborg University

PhD committee: Associate Professor Samuel Simon Araya (chairman)
Aalborg Univeristy

Professor Jose Rodriguez
Universidad Andres Bello

Professor Haitham A. Abu-Rub
Texas A&M University at Qatar

PhD Series: Faculty of Engineering and Science, Aalborg University

Department: Department of Energy Technology

ISSN (online): 2446-1636
ISBN (online): 978-87-7210-805-6

Published by:
Aalborg University Press
Kroghstræde 3
DK – 9220 Aalborg Ø
Phone: +45 99407140
aauf@forlag.aau.dk
forlag.aau.dk

Printed in Denmark by Rosendahls, 2020

Curriculum Vitae

Yacine Terriche received a B.S. degree in electrical engineering from the University of Science and Technology, Constantine, Algeria in 2011, and an M.S. degree in Electrical Engineering from the University of Constantine 1, Constantine, Algeria. in 2013. He is currently working towards the Ph.D. degree at the Department of Energy Technology, Aalborg University, Denmark. His research interests include power electronics, modeling, control, signal processing, power quality issues, active and passive power filters, and maritime microgrids.

ENGLISH SUMMARY

Harmonic contamination is becoming a vital subject in electrical power systems (EPSs). It is inoffensive as long as its level is not significant. However, due to the large increase in the installation of power electronic converters, mainly the nonlinear loads such as AC and DC variable speed drives, harmonics are severely finding their way into shipboard and offshore applications.

Ensuring a good power quality of ships is not only earmarked to avoid serious damage of the EPSs, but also to avoid the severe possible accidents that might provoke the blackout of the ship. Hence, improving the safety of the passengers and/or crew with a privileged level of security, as well as reduces the specific emissions and fuel consumption. Therefore, harmonics generated by these nonlinear loads can be a potential risk if they are not well studied and mitigated, as they can also affect the voltage via the transmission lines' impedance and the sub-transient reactance of the synchronous generators, and thereby cause malfunction and fail of other loads.

The voltage stability is another issue, which can threaten the EPSs. The voltage stability hypothesis can be described as the attempt of the loads to absorb a larger power than the power supplies and transmission lines can deliver. If the load demand varies suddenly due to certain disturbances such as short circuits, the system might lose the equilibrium and results in the voltage collapse. Since the ships are characterized by the heavy variable loads that consume a large amount of power in a short duration, their EPS is prone to the voltage drop. If this drop exceeds the standards, it can cause the voltage collapse that can result in the blackout of the ship.

To deal with these issues, several static VAR compensators and filters have been suggested in the literature. The traditional method to reduce the harmonics and compensate for the power factor (PF) is to install the passive power filters (PPFs). Though these filters are featured by the low cost and ease of implementation, improving their harmonics rejection capability did not attract much attention. Hence, in this project, improving the harmonic attenuation factor and the filters sensitivity factor have been investigated.

Recently, based on the development of power converters, the application of the active power filters (APFs) is becoming an alternative solution to the PPFs. The main advantages gained from the APFs are the flexibility and fast dynamic response during the load variation, the capability to improve the current waveform using only one single filter, the ability to regulate the current/voltage unbalance, voltage sags, and PF. Therefore, in this project, the application of APFs and PPFs to improve the power quality issues of the EPSs of terrestrial grids and shipboard power systems (SPSs) has been investigated. Moreover, in order to enhance the filtering capability, flexibility,

and the dynamic response of the APFs, new algorithms such as the matrix pencil method and least square solutions are developed to extract the reference compensating currents. Furthermore, controlling the APF needs precise information about the voltage phase to perform the synchronization. Hence, some open-loop and closed-loop synchronization methods are developed to enhance the dynamic response of the APF.

Accurate assessment of harmonics provides substantial information on their circulation's danger, thus enables the engineers to verify if the harmonic distortion complies with the standards or requires interfering. Moreover, precise assessment of the harmonics helps the engineers to design the suitable filters, taking into consideration some important criteria such as the type of harmonics (odd/even harmonics, integer/non-integer multiple of the fundamental frequency), and the level of harmonic distortion. Furthermore, harmonics/interharmonics analysis can provide a comprehension diagnosis for fault detection, and fault location of the synchronous generators and motors. There are enormous techniques for estimating the harmonics of distorted signals. However, most of these techniques are frequency-dependent techniques, which implies that their performance degrades in the existence of interharmonics or frequency drifts. The dominant standards in the power quality field recommend the application of the discrete Fourier transform (DFT) with an aggregation of consecutive 12 cycle time intervals for a 60 Hz power system frequency. However, since the DFT can only operate in the steady-state condition, a window width of 12 cycles of a steady-state current is not practical for SMGs due to the large variation in the frequency and load in a short duration. Hence, following the standards recommendation may not be very practical for SMGs. In this regard, two signal periodicity-independent algorithms that can assess the harmonics/interharmonics accurately with a fast transient response under large frequency drifts are proposed in this project. The evaluation of these algorithms is carried out under MATLAB software and validated via analyzing the electrical power system current of a bulk carrier ship and a container ship during the operation of the mooring winches and the windlass, then the results are compared with the traditional methods.

DANSK RESUME

Harmonisk kontaminering er ved at blive et vigtigt emne i elektriske kraftsystemer (EPS). Det er uskadeligt, så længe niveauet ikke er signifikant. På grund af den store stigning i installationen af elektroniske omformere, hovedsageligt de ikke-lineære belastninger såsom vekselstrøms- og jævnstrømshastigheder, finder harmonikere på alvorlig vej til skibsports- og offshore-applikationer.

Det er ikke kun øremærket at sikre en god magtkvalitet for skibe til at undgå alvorlige skader på EPS'erne, men også for at undgå de alvorlige mulige ulykker, der kan fremkalde afbrydelse af torskibe. Derfor forbedres sikkerheden for passagererne og / eller besætningen med et privilegeret sikkerhedsniveau samt reducerer de specifikke emissioner og brændstofforbrug. Derfor kan harmoniske effekter genereret af disse ikke-lineære belastninger være en potentiel risiko, hvis de ikke er godt studeret og afbødet, da de også kan påvirke spændingsforsyningerne via transmissionslinjernes impedans og den underordnede reaktans af de synkrone generatorer og derved forårsagelige funktionsfejl og andre belastninger.

Spændingsstabiliteten er et andet problem, som kan true EPS'erne. Spændingsstabilitetshypotesen kan beskrives som et forsøg på belastningerne til at absorbere en større effekt end strømforsyningerne og transmissionsledningerne kan levere. Hvis belastningsbehovet pludselig varierer på grund af visse forstyrrelser, såsom kortslutninger, kan systemet miste ligevægten og resultere i spændingskollaps. Da skibene er kendetegnet ved de tunge variable belastninger, der forbruger en stor mængde strøm på kort varighed, er deres EPS tilbøjelig til spændingsfaldet. Hvis dette fald overstiger standarderne, kan det forårsage spændingskollaps, der kan resultere i afbrydelse af skibet.

For at tackle disse problemer er der foreslået flere filtre i litteraturen. Den traditionelle metode til at reducere harmoniske og kompensere for effektfaktoren (PF) er at installere de passive effektfiltre (PPF'er). Selvom disse filtre er kendetegnet ved de lave omkostninger og let at implementere, tiltrak forbedring af deres harmoniske afvisningskapacitet ikke meget opmærksomhed. I dette projekt er forbedring af den harmoniske dæmpningsfaktor og den filtre følsomme faktor undersøgt.

For nylig er applikationen af de aktive kraftfiltre (APF'er) ved at blive udviklet til en alternativ løsning til PPF'er baseret på udviklingen af strømkonvertere. De vigtigste fordele, der opnås ved APF'erne, er fleksibiliteten og den hurtige dynamiske respons under belastningsvariationen, evnen til at forbedre strømbølgeformen ved kun at bruge et enkelt filter, evnen til at regulere strøm / spændingsbalance og spændingssække og forbedre PF. Derfor er anvendelsen af APF'er og PPF'er i dette projekt undersøgt for strømkvalitetsspørgsmål for EPS'erne for jordnet og SPS'er. For at forbedre

filtreringsevnen, fleksibiliteten og den dynamiske respons af APF'erne udvikles derudover nye algoritmer såsom matrixblyantmetoden og mindst kvadratiske løsninger til at udtrække den referencecompenserende strøm. Endvidere har styring af APF brug for nøjagtig information om spændingsfasen for at udføre synkroniseringen. Derfor er nogle open-loop og closed-loop synkroniseringsmetoder udviklet til at forstærke den dynamiske respons fra APF.

Præcis vurdering af harmoniske giver væsentlig information om deres cirkulationsfare, og giver således ingeniørerne mulighed for at kontrollere, om den harmoniske forvrængning er i overensstemmelse med standarderne eller kræver interferens. Desuden hjælper en nøjagtig vurdering af harmonikerne ingeniørerne med at designe de passende filtre under hensyntagen til nogle vigtige kriterier såsom typen af harmoniske (ulige / endda harmoniske, heltal / ikke-heltal multiple af den grundlæggende frekvens) og niveauet for harmonisk forvrængning. Desuden kan harmoniske / interharmoniske analyser give en forståelsesdiagnose til fejlregistrering og fejlplacering af de synkrone generatorer og motorer. Der er enorme teknikker til at estimere harmonikken i forvrængede signaler. De fleste af disse teknikker er imidlertid frekvensafhængige teknikker, hvilket indebærer, at deres ydeevne forringes i eksistensen af interharmonik eller frekvensdrift. De dominerende standarder inden for kraftkvalitetsfeltet anbefaler anvendelse af den diskrete Fourier-transformation (DFT) med en sammenlægning af hinanden på følgende 12 cyklussers tidsintervaller for et 60 Hz kraftsystem. Da DFT imidlertid kun kan fungere i stabil tilstand, er en vinduesbredde på 12 cyklusser med en stabil tilstand på nuværende tidspunkt ikke praktisk for SMG'er på grund af den store variation i frekvens og belastning i en kort varighed. Derfor er det muligvis ikke særlig praktisk at følge standarderne anbefaling for SMG'er. I denne henseende foreslås to signal-periode-uafhængige algoritmer, der kan vurdere harmoniske / interharmonikere nøjagtigt med en hurtig forbigående respons under store frekvensdrev i dette projekt. Evalueringen af disse algoritmer udføres under MATLAB-softwaren og valideres ved analyse af det elektriske kraftsystemstrøm fra et bulkskib og et containerskib under driften af fortøjningsvinscherne og vindtassen, derefter sammenlignes resultaterne med de traditionelle metoder.

ACKNOWLEDGEMENTS

This Ph.D. dissertation entitled 'Power quality and voltage stability enhancement of terrestrial grids and shipboard microgrids', was carried out at the Department of Energy Technology, Aalborg University (AAU), Denmark. Under the supervision of Prof. Josep M. Guerrero.

First of all, I would love to express my sincere gratitude to Professor Josep M. Guerrero for the amazing opportunity to join his CROM group to peruse a Ph.D degree, which truly helped me to gain a large experience and develop lots of skills in his laboratory. I also highly appreciate his confidence, kindness, guidance, support, and patience during the period of the Ph.D.

I would love also to acknowledge the co-supervision of Saeed Golestan, and his precious advice on improving my research skills. I also appreciate his valuable time to discuss my ideas and correct my papers.

My sincere thanks also go to the co-supervisor Juan C. Vasquez for his support, help, and guidance to all my administration and laboratory needs, which made my Ph.D. procedures more convenient.

In addition, I also deeply acknowledge the help of Prof. Chien-lien SU, particularly, for his technical reports and materials regarding the electrical power system of shipboard power systems. I also highly appreciate his scholarship to support my stay during the study abroad a National Kaohsiung University of Science and Technology in Taiwan.

Finally, I take the opportunity to thank my lovely parents, brother and sister, the rest of my family, colleagues in CROM, and my friends for their support and encouragement.

TABLE OF CONTENTS

Chapter I. Introduction

Background and motivation

I. 1 Background of the harmonics sources of terrestrial grids and shipboard power systems

The term power quality indicates the ability of electrical equipment to consume the same quality of the power supplied to it. In other words, the ideal power quality of a system is achieved when there is no variation on the level of voltage/current waveform, frequency, phase, and balanced phases. Traditionally, most of the electrical power system (EPS) devices used to operate efficiently with relative variation in the voltage/current waveform, and frequency [1]. However, within the last decades, a tremendous spread of power electronic converters (PECs) based on semi-conductors technologies for AC/DC and AC/AC power conversion on the level of both terrestrial and non-terrestrial microgrids such as shipboard power systems (SPSs) [2]–[6]. Indeed, these PECs have contributed to increasing the controllability, reliability, and efficiency of several applications with a wide scale of power from a few watts to megawatts [6]. Examples of these PECs are the application of renewable energy to AC and DC microgrids such as wind turbines and photovoltaic solar panels, AC/DC conversion for energy storage using batteries, supercapacitor, electric vehicles, variable-voltage-variable-frequency drives for AC and DC shipboard power systems…etc [2], [4], [5], [7]. However, the non-linearity nature of PECs such as rectifiers draws a deformed waveform of current, which is full of harmonics and consequently results in affecting the power quality of the distribution system [8], [9]. The international standards such as the IEC61000-3-6 and IEEE Std 519™-2014 standards have imposed strict limits to the level of harmonics contamination as they cause severe problems in power systems such as augmenting the losses in the distribution units and transmission lines, reducing the lifetime of equipment, generating audible noise, causing interference with communication systems [10]. Therefore, mitigation of the power quality issues based on traditional and advanced techniques is mandatory to avoid harmful consequences. The SPSs, in every sense, can be considered as a self-sufficient microgrid, which is much similar to terrestrial microgrids, the differences between them are linked to some critical constraints such as [11], [12]:

- Operational modes: terrestrial microgrids operate in two operation modes (islanded and grid-connected), while the SPS operates in only one mode (islanded)

- Loading: SPSs are distinguished by dominant large pulsed loads (propulsion motors) that can consume 90% of the generated power.
- Stability and dynamic balancing: contrasting to microgrids that have a variety of renewable energy sources (PV systems, Fuel cell, wind turbines…etc.), the dominant source in SMPSs is finite inertia generators (synchronous generators driven by diesel motors). This kind of system is vastly prone to frequency drifts due to the large consumption of power (consumed by propulsion motors) in short time duration. Moreover, the electric power evolution in SPSs is always tended to enhance the performance, the efficiency, and the reliability of the ship by replacing the mechanically driven devices with the power electronic drives. Indeed, the controllability of the power flow consumed by large loads (propulsions and pumps …etc.) is easily achieved, and the dynamic response is optimized. However, this development might result in voltage instability caused by the constant power load.

Based on the similarity structure of the SPSs and terrestrial power systems, the power quality solutions applied to the terrestrial power systems can be generalized to SPSs, taking into considerations some constraints of the ships such as: the dynamic balancing (stability margin of voltage and frequency), the weight and the physical size of the proposed filters… etc. A good comprehension of the nature of the power quality issues, and detailed knowledge of their roots aid to provide the suited solutions

Fig. I. 1 presents a typical electrical power system (EPS) of the all-electric ship, which constitutes of four diesel generators that are shunted gradually depending on the demanded power, two propellers, connected to the main switchboard, and the hotel loads. Other loads such as the thrusters are not drawn for the sake of the simplicity. As the propellers, consume about 80% to 90% of the total power of the ship, their variable-speed drives cause the highest harmonic distortion. In addition to the potential risk that threatens the ELP and can leads to the blackout of the ship, the circulation of the harmonics in the EPS threatens also the lives of the crew/passengers.

I. 2 Power quality improvement

Several solutions have been proposed in the literature to improve the power quality issues of the EPSs. the application of the passive power filters (PPFs) to improve the power quality is one of the traditional and most used solution [13]. A PPF consists of a combination of an inductor and a capacitor to create a certain tuning for a specific harmonic. Several types of PPFs are proposed in the literature [14]. Fig. I. 2 depicts four types of PPFs where each type has advantages and disadvantages.

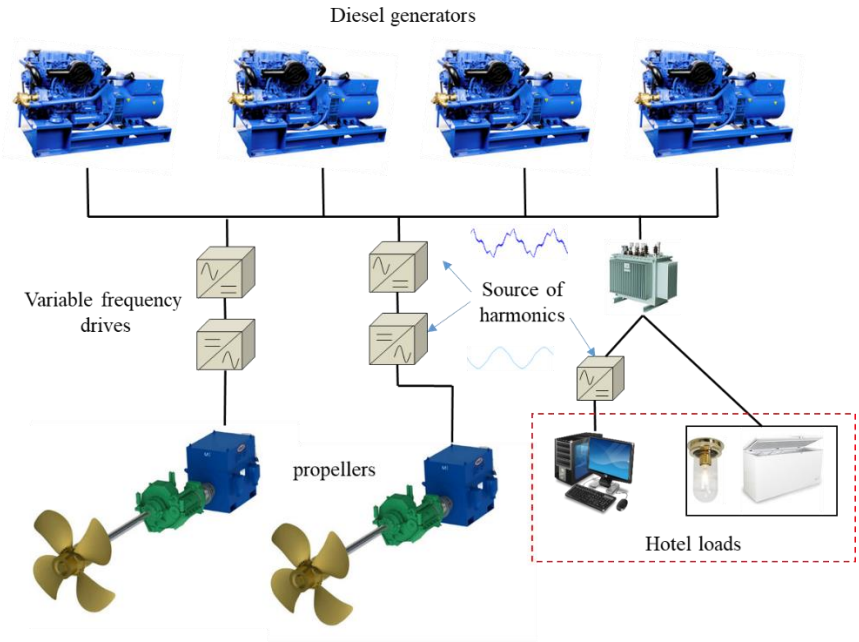

Fig. I. 1 Typical electrical power system of a ship

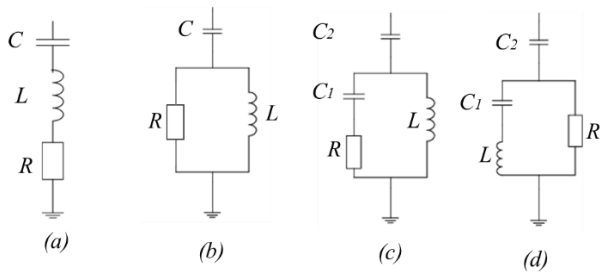

Fig. I. 2 Passive power filters: (a) single-tuned passive filter, (b) second-order high pass filter, (c) third-order high pass filter, and (d) C-type damped filter.

The pulse width modulation (PWM) voltage source rectifiers are widely utilized in uninterruptible power sources such as speed drive applications to replace thyristor and diode converters. Based on the bipolar transistors, the PWM rectifiers offer several advantages such as very low THD of the source current, bidirectional power flow, fast control of the DC voltage magnitude, and the ability to control the power factor. This type of rectifier has been utilizing in several applications such as variable

speed drives [15], DC, or AC microgrids [16], DC and AC shipboard power systems [17], [18]. Wind turbines and fuel cells.

The APFs are considered one of the advanced alternative solutions for power quality issues. In contradiction with traditional solutions such as PPFs that can only mitigate harmonics and compensate for a degree of reactive power, the APFs can suppress a wide range of harmonic components, and fully compensate for the power factor. Besides, the APFs can improve the voltage unbalance, sags, swells, and other perturbations. Besides, the controllability of the APFs offers the extra advantage of flexibility under the variation of load or grid parameters [19]. The APF consists of a two-level or multi-level inverter connected to the grid in shunt [20] or series [21], or combined (shunt and series) [22]. Usually, the shunt structure is applied for current perturbations, while the series one is utilized to improve the voltage perturbations. In case both voltage and current are distorted, then the application of the combined structure can solve the issue. Fig. I. 3 presents a basic schematic diagram of a shunt APF connected to improve the power quality issues caused by unbalanced non-linear loads of an EPS.

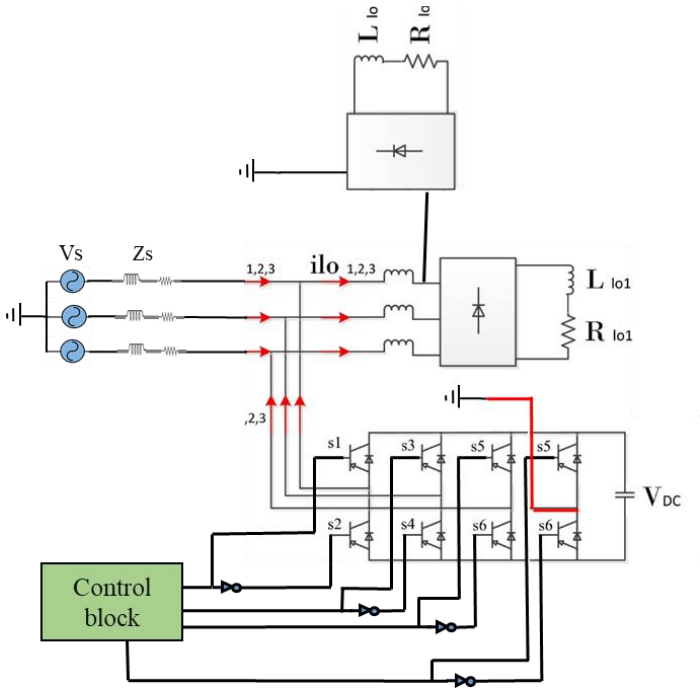

Fig. I. 3 schematic diagram of a two level four legs shunt APF.

The hybrid active power filters (HAPF) seem to be the most promising topology in the family of APFs due to the advantages they offer. Since the major disadvantage

of the APFs is the cost, particularly in medium and high power applications, the HAPF can be an alternative to reduce the power rating of the APFs, which therefore results in reducing the cost. The HAPF consists mainly of shunt or series APF connected in different structures with the passive power filters to improve the power quality issues with cheaper configurations [23]. Fig. I. 4 presents a hybrid structure of APF, which constitutes of shunt PPFs and a shunt APF. The PPFs are installed to filter the most dominant harmonics and compensate for a degree of the PF, while the shunt APF compensates for the higher-order harmonics and adjusts the PF under load variation.

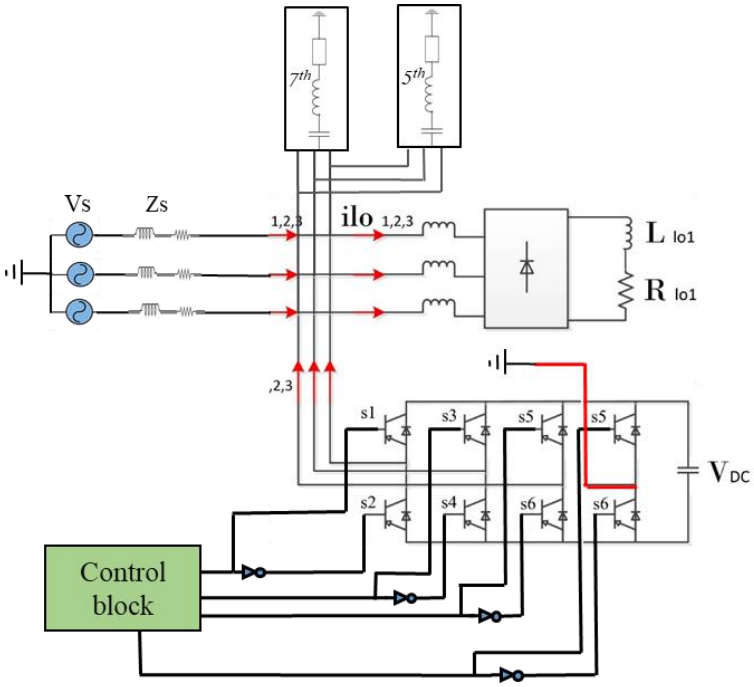

Fig. I. 4 schematic diagram of hybrid APF.

The FC-TCR is one of the static VAR compensators family [24], the fixed capacitor is implemented to compensate for the inductive reactive power, and generate extra capacitive reactive power, then based on the appropriate control, the TCR adjusts the power factor to be close to unity. In other applications, the FC-TCR can be implemented to inject capacitive reactive power to compensate for the voltage drops; hence, it ensures the voltage stability [25]. Moreover, in [26], the author proposed a series line impedance, which comprises an inductance connected in series with a capacitor tunned at the fundamental frequency. The goal of this line impedance is to create a very low path for the fundamental component and creates a high path for harmonics to force them to flow into the passive filter. Furthermore, it has been

demonstrated in [27] that if the FC-TCR is well designed, it can act as a low-pass filter and suppress all the harmonics after the cut-off frequency.

I. 3 Thesis objectives

The objective of this Ph.D. thesis is to make a study about the power quality issues and voltage stability of terrestrial grids and shipboard power systems for low-voltage and medium-voltage level. Then proposes the appropriate solutions, which conform to the size, type, and power level of the demanded power. Therefore, to realize this goal, the following objectives will be covered in this thesis.

- Analyzing and designing different algorithms such as synchronous reference frame method (SRF) and the least square approach to extract the reference compensating currents (RCCs) of the shunt active power filters (APFs) under adverse grid conditions. Then compare the proposed methods with the traditional ones to demonstrate their efficacy in enhancing the performance of the shunt APF and validate the simulation results experimentally.
- Designing developed open-loop and closed-loop synchronization methods based on some advanced effective filters such cascaded delayed signal cancelation technique, and complex coefficient filters to enhance the synchronization of the shunt APF under adverse grid conditions, then demonstrate the improved performance of the shunt APF by comparing the proposed methods with the traditional ones and validate the simulation results experimentally.
- Propose a signal periodicity-independent algorithm to assess the harmonics and interharmonics of shipboard power systems. This method, which is based on an enhanced MPM can estimate the harmonics and interharmonics with a short moving window width under large frequency drifts. The performance of the proposed method is evaluated under MATLAB software, then the experimental validation is attained by analyzing the current of a container ships.
- Perform a more in-depth harmonic analysis of the harmonic attenuation factor (HAF) and the filter sensitive factor (FSF) to enhance the harmonics rejection capability of the passive power filters (PPFs), then develop theoretical and analytical investigations to improve the trade-off between the HAF and FSF. After that, propose new topologies of the PPFs to achieve a good compromise between the HAF and the FSF. And finally, design the PPFs based on the proposed studies and validate their performance in reducing the harmonics and compensating the PF of the electrical power system of a hybrid ferry.

- Propose a combined topology of hybrid APF and FC-TCR compensator to enhance the power quality of SPSs. The FC-TCR is connected to reduce the distortion and compensates for the voltage drops. Thus, enhances the voltage stability, whereas the HAPF suppresses the dominant harmonic current.
- Propose an enhanced modeling based on a developed mathematical analysis to examine the mechanism of the harmonics mitigation of the FC-TCR compensator to improve the harmonics rejection capability. Then validate its performance in reducing the harmonics and compensate the PF of an SPS using the proposed analysis.
- Modeling and developing an FC-TCR compensator to filter the harmonics and compensates for the voltage sags and swells. Hence, ensures the voltage stability of the SPS.
- Develop simple and yet-effective numerical methods to estimate the firing angle of the FC-TCR compensator. These techniques that are based on the Bisection (BS) technique, Newton-Raphson (N-R) technique, and false position (FP) technique have the capability in providing an accurate firing angle estimation of the FC-TCR compensator under load variation and frequency drifts.

I. 4 Thesis outlines

The outcomes of this Ph.D. project are detailed in this thesis as a collection of journal papers, where most of them have already been published and one of them is still under review. The thesis is organized as follows:

CHAPTER I: Presents the introduction, which is the preamble of this thesis.

CHAPTER II: Presents analysis and design of an enhanced algorithm based on the least square approach to extract the reference compensating currents (RCCs) of the shunt active power filter (APF) under adverse grid conditions. Besides, it proposes developed open-loop and closed-loop synchronization methods based on some advanced effective filters such as cascaded delayed signal cancelation technique, and complex coefficient filters to improve the synchronization of the shunt APF under adverse grid conditions.

CHAPTER III: Presents a signal periodicity-independent algorithm to assess the harmonics distortion of shipboard power systems. This method, which is based on an enhanced MPM can estimate the harmonics and interharmonics with a short moving window width under large frequency drifts

CHAPTER IV: Presents a more in-depth theoretical and analytical investigations of the harmonics attenuation factor and filters' sensitivity factor of passive power filters to enhance the power quality of shipboard power systems. Then, it presents a combined topology of hybrid active power filter (APF) and FC-TCR compensator to improve the power quality of SPSs. After that, it describes the modeling and development of the FC-TCR compensator to filter the harmonics and compensates for the voltage sags and swells. Hence, ensures the voltage stability of SPSs. Finally, it ends by presenting simple and yet-effective numerical methods to estimate the firing angle of the FC-TCR compensator. These techniques that are based on the Bisection (BS) technique, Newton-Raphson (N-R) technique, and false position (FP) technique have the capability in providing an accurate firing angle estimation of the FC-TCR compensator under load variation and frequency drifts.

CHAPTER III: Summarizes the contributions of this thesis and provides suggestions and perspectives for the future works.

I. 5 List of publications

Journal papers

1. **Yacine Terriche**, Josep M. Guerrero, and Juan C. Vasquez. "Performance improvement of shunt active power filter based on non-linear least-square approach." Electric Power Systems Research 160 (2018): 44-55. ***J1***
2. Abderezak Lashab, Dezso Sera, Tamas Kerekes, **Yacine Terriche**, Aissa Bouzid, Juan Vasquez, Josep Guerrero *et al*., "A Cascaded H-bridge with Integrated Boosting Circuit," in *IEEE Transactions on Power Electronics.* ***J2***
3. Mutarraf, M., **Terriche, Y.**, Niazi, K., Vasquez, J., & Guerrero, J. (2018). Energy Storage Systems for Shipboard Microgrids—A Review. Energies, 11(12), 3492. ***J3***
4. **Terriche, Y.,** Mutarraf, M. U., Mehrzadi, M., Lashab, A., Guerrero, J. M., Vasquez, J. C., & Kerdoun, D., "Adaptive CDSC-Based Open-Loop Synchronization Technique for Dynamic Response Enhancement of Active Power Filters," in IEEE Access, vol. 7, pp. 96743-96752, 2019. ***J4***
5. **Terriche, Yacine**, Muhammad Umair Mutarraf, Saeed Golestan, Chun-Lien Su, Josep M. Guerrero, Juan C. Vasquez, and Djallel Kerdoun. "A Hybrid Compensator Configuration for VAR Control and Harmonic Suppression in All-Electric Shipboard Power Systems." *IEEE Transactions on Power Delivery* (2019). ***J5***

6. Mutarraf, Muhammad Umair, **Yacine Terriche**, Kamran Ali Khan Niazi, Fawad Khan, Juan C. Vasquez, and Josep M. Guerrero. "Control of Hybrid Diesel/PV/Battery/Ultra-Capacitor Systems for Future Shipboard Microgrids." Energies 12, no. 18 (2019): 3460. ***J6***

7. Lashab, A., Séra, D., Hahn, F., Camurca, L., **Terriche, Y.,** Liserre, M. & Guerrero, J. M. "Cascaded Multilevel PV Inverter with Improved Harmonic Performance During Power Imbalance Between Power Cells ,". 4 Mar 2020, (Accepted/In press) *IEEE Transactions on Industry Applications.* ***J7***

8. **Terriche, Yacine**, Muhammad U. Mutarraf, Abderrzak Laib, Chun-Lien Su, Josep M. Guerrero, Juan C. Vasquez, Saeed Golestan "A Resolution-Enhanced Sliding Matrix Pencil Method for Evaluation of Harmonics Distortion in Shipboard Microgrids." *IEEE Transactions on Transportation Electrification, 2020.* ***J8***

9. **Y. Terriche**, Chun-Lien Su, Abderrzak Lashab , Abderrzak Laib, Muhammad M. Mutarraf, , Josep M. Guerrero, Juan C. Vasquez, Saeed Golestan., "A Reliable Harmonics and inter-harmonics Estimation Method for Smart Maritime Microgrid Application," *IEEE Transactions on Smart Grids* (under review). ***J9***

10. **Yacine Terriche**, Abderezak Lashab 1, Muhammad. U. Mutarraf et al., "Voltage Stability and Harmonics Mitigation Analyses of Two Effective Compensators for More Electric Marine Vessel Applications," *IEEE Transactions on Industry Applications* (under review). ***J10***

11. Mojtaba Mehrzadi, **Yacine Terriche**, Chun-Lien Su, Muzaidi Bin Othman, Juan C. Vasquez & Josep M. Guerrero, 2020. "Review of Dynamic Positioning Control in Maritime Microgrid Systems," Energies, MDPI, Open Access Journal, vol. 13(12), pages 1-22, June. ***J11***

12. Mojtaba Mehrzadi, **Yacine Terriche**, Chun-Lien Su, Peilin Xie, Najmeh Bazmohammadi, Matheus N. Costa, Juan Carlos Vasquez, Josep Guerrero. " A Deep Learning Method for Short-Term Dynamic Positioning Load Forecasting in Maritime Microgrids," Applied Sciences. 2020 (accepted)

Conference papers

1. **Terriche, Y**., Golestan, S., Guerrero, J. and Vasquez, J.C. Vasquez. Multiple-Complex Coefficient-Filter-Based PLL for Improving the Performance of Shunt Active Power Filter under Adverse Grid Conditions. 2018 IEEE PES GENERAL MEETING. ***C1***

2. **Terriche, Y**., Mutarraf, M. U., Mehrzadi, M., Su, C-L., Guerrero, J. M., Vasquez, J. C. ''Power quality and Voltage Stability improvement of Shipboard Power Systems with Non-Linear Loads", 2019, EEEIC International Conference on

Environment and Electrical Engineering. ***C2***

3. **Y. Terriche,** et al, "More in-depth analytical investigations of two Effective Harmonics Filters for More Electric Marine Vessel Applications." 2019, 9th International Conference on Power and Energy Systems, 2019. ***C3***

4. Mutarraf, M. U., **Terriche, Y.**, Niazi, K. A. K., Su, C-L., Vasquez, J. C. & Guerrero, J. M., '' Battery Energy Storage Systems for Mitigating Fluctuations Caused by Pulse Loads and Propulsion Motors in Shipboard Microgrids" *International Symposium on Industrial Electronics (ISIE). 2019.* ***C4***

5. Mehrzadi, M., Su, C.L., **Terriche, Y**., Vasquez, J.C. and Guerrero, J.M., 2019, November. Operation Planning of Standalone Maritime Power Systems Using Particle Swarm Optimization. In 2019 1st International Conference on Electrical, Control and Instrumentation Engineering (ICECIE) (pp. 1-6). IEEE. ***C5***

6. Mutarraf, Muhammad Umair, **Yacine Terriche**, Mashood Nasir, Kamran Ali Khan Niazi, Juan C. Vasquez, and Josep M. Guerrero. "Hybrid Energy Storage Systems for Voltage Stabilization in Shipboard Microgrids." In Proceedings of 2019 9th International Conference on Power and Energy Systems. 2019. ***C6***

7. **Y. Terriche**., Su, C-L., Mutarraf, M. U., Guerrero, J. M., Vasquez, J. C ,"Harmonics Rejection Capability Enhancement of Passive Power Filters for All-Electric-Shipboard Micro-Grids." 2020 6th IEEE International Energy Conference (ENERGYCon 2020) (accepted). ***C7***

8. **Y. Terriche**., Su, C-L., Mutarraf, M. U., Guerrero, J. M., Vasquez, J. C, "Harmonics Mitigation in Hybrid AC / DC Shipboard Microgrids Using Fixed Capacitor-Thyristor Controlled reactor." 2020 6th IEEE International Energy Conference (ENERGYCon 2020) (accepted). ***C8***

Chapter II. Improving the power quality issues of terrestrial grids using active power filters

This chapter summarizes the contributions that are published in [28]–[30]. More details can be found in the attached publications of the Appendix.

II. 1 Summary of the contribution

Recently, the large spread of power electronic converters (PECs) have been growing vastly [7]. Certainly, this technology offers numerous advantages to the EPSs such as high efficiency and reliability, economical size, fast dynamic response, etc. The non-linearity characteristic of these PECs, however, draws a large number of harmonics that can cause a harmful effect to the EPS [8], [10]. Traditionally, The PPFs were applied to reduce the dominant harmonics and compensate for a degree of PF [31]. Though the installation of these filters is featured by the simplicity and lower cost, they, however, struggle from several deficiencies such as susceptibilities to series and parallel resonance, sensitivity to frequency variation, fixed tuning, heavyweight and large size, etc. In order to overcome these weaknesses, the APFs came as an alternative to the PPFs [32], [33]. Besides harmonics suppression, the APFs can compensate for the PF and unbalance [33]. A crucial part of installing the APFs is the reference compensating current (RCC) algorithm. [33] proposes a signal-periodicity independent-based RCC algorithm for APFs. This method, which is based on the matrix pencil method (MPM) can estimate the harmonics and interharmonics of the system without any information about the frequency of the grid. Hence, the frequency drifts of the power supply do not affect the performance of the APF. In [28], the dynamic performance of the APF under distorted and unbalanced grid voltage is enhanced by proposing a selective harmonic cancelation technique based on the multiple-complex coefficient-filter-based PLL (MCCF-PLL). The advantage of applying this type of PLL is to provide accurate information about each harmonic component of the voltage with its corresponding sequence during the estimation of the voltage phase/frequency. In [29], an optimized open-loop synchronization technique is proposed to enhance the dynamic performance of the APF. This technique, which is based on the non-linear least square (NLS) approach can extract the fundamental voltage and estimates its phase within only a half cycle in the presence of odd harmonics and dc offset. And last but not least, in [30], a fast and yet effective open-loop synchronization (OLS) technique based on Cascaded Delayed Signal Cancellation (CDSC) to improve the performance of the APF is suggested.

II. 2 Multiple-complex coefficient-filter-based PLL for shunt APF

The MCCF-PLL is one of the advanced SRF-PLL, which is featured by the capability of offering information about the sequence of each estimated harmonic component. The estimation block contains multiple modules of the complex coefficient filters (CCFs) that are working in a cooperative way as presented in Fig. II. 1 [28], [34]. In the case where the grid voltage is affected with unbalance and small harmonic distortion, the application of only two-modules (TW) set at the positive and negative sequences of the fundamental component is adequate for phase/frequency estimation. However, if the harmonic distortion is severe, then the application of the multiple-module (MM) system is necessary [35].

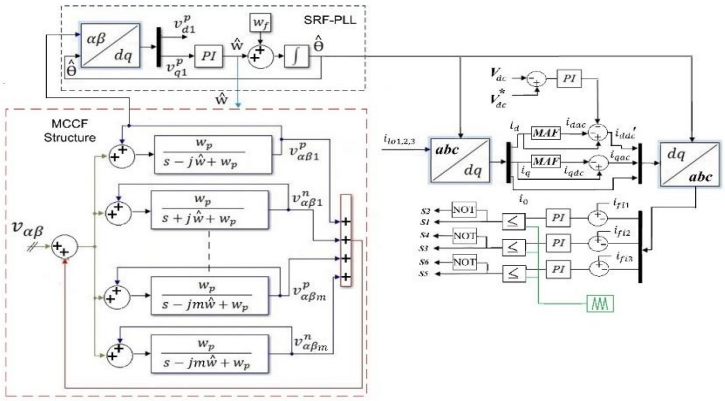

(a)

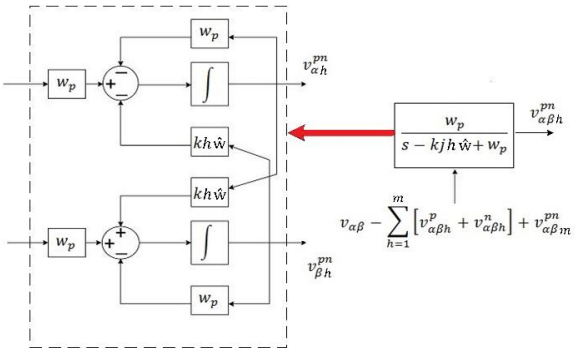

(b)

Fig. II. 1 Application of the MCCF-PLL to improve the synchronization of the shunt APF with the grid. (a) the control scheme of the APF. (b) A single submodule of the MCCF [28].

A grid-contaminated voltage can be formulated as:

$$V_{s1}(t) = \sum_{h=1}^{N} v_h^+ \cos(hwt + \phi_h^+) + v_h^- \cos(hwt + \phi_h^-) \quad \text{(II-1)}$$

$$V_{s2}(t) = \sum_{h=1}^{N} v_h^+ \cos\left(hwt + \phi_h^+ - \frac{2\pi}{3}\right) + v_h^- \cos\left(hwt + \phi_h^- + \frac{2\pi}{3}\right) \quad \text{(II-2)}$$

$$V_{s3}(t) = \sum_{h=1}^{N} v_h^+ \cos\left(hwt + \phi_h^+ + \frac{2\pi}{3}\right) + v_h^- \cos\left(hwt + \phi_h^- - \frac{2\pi}{3}\right) \quad \text{(II-3)}$$

where v_h^+, v_h^-, ϕ_h^+, ϕ_h^- are respectively the voltage amplitudes and phases of the positive and negative sequences of each harmonic frequency. The transformation of these signals into $\alpha\beta$ can be easily obtained as [28]:

$$\begin{bmatrix} v_\alpha(t) \\ v_\beta(t) \end{bmatrix} = \begin{bmatrix} v_\alpha^+(t) + v_\alpha^-(t) \\ v_\beta^+(t) + v_\beta^-(t) \end{bmatrix} = [\mathrm{T}] \begin{bmatrix} V_{s1}(t) \\ V_{s2}(t) \\ V_{s3}(t) \end{bmatrix} \quad \text{(II-4)}$$

where

$$[\mathrm{T}] = \frac{2}{3} \begin{bmatrix} 1 & \frac{-1}{2} & \frac{-1}{2} \\ 0 & \frac{\sqrt{3}}{2} & \frac{-\sqrt{3}}{2} \end{bmatrix}$$

$$[v_\alpha^+(t) + v_\alpha^-(t)] = \sum_{h=1}^{N} v_{\alpha h}^+(t) + \sum_{h=1}^{N} v_{\alpha h}^n(t) = \sum_{h=1}^{N} v_h^+ \cos(hwt + \phi_h^+) + \sum_{h=1}^{N} v_h^- \cos(hwt + \phi_h^-) \quad \text{(II-5)}$$

$$\left[v_\beta^+(t) + v_\beta^-(t)\right] = \sum_{h=1}^{N} v_{\beta h}^+(t) + \sum_{h=1}^{N} v_{\beta h}^-(t) = \sum_{h=1}^{N} v_h^+ \sin(hwt + \phi_h^+) - \sum_{h=1}^{N} v_h^- \sin(hwt + \phi_h^-) \quad \text{(II-6)}$$

After that, the transformation of Park is calculated as:

$$\begin{bmatrix} v_d(t) \\ v_q(t) \end{bmatrix} = \begin{bmatrix} v_d^+(t) + v_d^-(t) \\ v_q^+(t) + v_q^-(t) \end{bmatrix} = [\mathrm{T_1}] \begin{bmatrix} v_\alpha(t) \\ v_\beta(t) \end{bmatrix} \quad \text{(II-7)}$$

Where

$$[\mathrm{T_1}] = \begin{bmatrix} \cos(\hat{\theta}) & \sin(\hat{\theta}) \\ -\sin(\hat{\theta}) & \cos(\hat{\theta}) \end{bmatrix}, \hat{\theta} = \hat{w}t + \hat{\phi}_1^+$$

$$[v_d^+(t) + v_d^-(t)] = \sum_{h=1}^{N} v_{dh}^+(t) + \sum_{h=1}^{N} v_{dh}^n(t) = \sum_{h=1}^{N} v_h^+ \cos\left((hw - \hat{w})t + \phi_h^+ - \hat{\phi}_1^+\right) + \sum_{h=1}^{N} v_h^- \cos\left((hw + \hat{w})t + \phi_h^- + \hat{\phi}_1^+\right) \quad \text{(II-8)}$$

$$\left[v_q^+(t) + v_q^-(t)\right] = \sum_{h=1}^{N} v_{qh}^+(t) + \sum_{h=1}^{N} v_{qh}^-(t) =$$

$$\sum_{h=1}^{N} v_h^+ \sin\left((hw-\widehat{w})t+\phi_h^+-\hat{\phi}_1^+\right)-\sum_{h=1}^{N} v_h^- \sin\left((hw+\widehat{w})t+\phi_h^-+\hat{\phi}_1^+\right) \quad \text{(II-9)}$$

Under a quasi-locked condition ($\hat{\phi}_1^+ \approx \phi_1^+$ and $\widehat{w}=w$) (II-27) becomes

$$\begin{bmatrix} v_d \\ v_q \end{bmatrix} = \begin{bmatrix} v_{ddc} \\ v_{qdc} \end{bmatrix} + \begin{bmatrix} v_{dac} \\ v_{qac} \end{bmatrix} \quad \text{(II-10)}$$

Where v_{ddc} and v_{qdc} are the dc signals, and v_{dac} and v_{qac} represent the disturbance.

Fig. II. 1(a) displays the control method, which is based on the MCCF-PLL to synchronize the shunt APF. The transformation of the distorted voltage from *abc* stationary system into *αβ* is calculated using the formulas (II-24)-(II-26). Then, the positive sequence of the fundamental voltage $v_{\alpha\beta1}^+$ is estimated using the CCFs. After that, the SRF-PLL estimates the phase and frequency of $v_{\alpha\beta1}^+$. Next, the Park transform of the distorted currents ($i_{l1,2,3}$) is performed using the estimated phase of $v_{\alpha\beta1}^+$. The estimated frequency is fed back to the CCFs to adapt them during frequency drifts. When performing the Park transformation, the positive sequence of fundamental signal appear as continues signals (i_{ddc}) and (i_{qdc}). Whereas the harmonics appear as oscillations (i_{dac}) and (i_{qac}). The estimation of i_{ddc} and i_{qdc} can be easily performed using the moving average filter (MAV). The window size (T_w) of the MAF is chosen based on the type of harmonic distortion. If $i_{l1,2,3}$ is contaminated with the harmonics of the order $6h \pm 1$, then setting T_w to $6\times f$ is the ideal choice to provide accurate estimation and fast transient response. However, if the unbalance and the DC offset appear, then T_w should be selected respectively to $2\times f$ and f. Next, the inverse Park transform is performed to obtain the RCCs, which are sent to the pulse width modulation block. In this block, the RCC is compared with the output filter current of the shunt APF, and then via the traditional PI controller, the error is minimized. After that, the signal is compared with a triangular signal, whose frequency is 7 kHz. Finally, the pulses are fed to control the switches.

Fig. II. 1(b) presents the structure of one single sub-module of the CCF. Selecting *K* to 1 results in estimating the positive sequence of $v_{\alpha\beta h}$, while selecting *K* to -1 leads to estimate the negative sequence of $v_{\alpha\beta h}$. The positive sequences of the fundamental $v_{\alpha1}^p$ and $v_{\beta1}^p$ are formulated as [28]:

$$v_{\alpha1}^p = \frac{w_p}{s-j\widehat{w}+w_p} \times \left(v_\alpha - \sum_{h=1}^{m}\left[v_{\alpha h}^p + v_{\alpha h}^n\right] + v_{\alpha1}^p\right) \quad \text{(II-11)}$$

$$v_{\alpha1}^p = \frac{w_p}{s+w_p} \times \left(v_\alpha - \sum_{h=2}^{m} v_{\alpha h}^p - \sum_{h=1}^{m} v_{\alpha h}^n\right) - \frac{\widehat{w}}{s+w_p} \times v_{\beta1}^p \quad \text{(II-12)}$$

$$v_{\beta1}^p = \frac{w_p}{s-j\widehat{w}+w_p} \times \left(v_\beta - \sum_{h=1}^{m}\left[v_{\beta h}^p + v_{\beta h}^n\right] + v_{\beta1}^p\right) \quad \text{(II-13)}$$

$$v_{\beta 1}^{p} = \frac{w_p}{s+w_p} \times \left(v_\beta - \sum_{h=2}^{m} v_{\beta h}^{p} - \sum_{h=1}^{m} v_{\beta h}^{n} + v_{\beta 1}^{p} \right) + \frac{\hat{w}}{s+w_p} \times v_{\alpha 1}^{p} \qquad \text{(II-14)}$$

Based on [34], implementing the MCCF-OLL using only TM system to estimate the sequences of the fundamental is equivalent to the multiple reference frame based PLL (MRF-PLL) [29]. It means that the linearization of the MRF-PLL can be used for the MCCF-PLL. However, in the case of MM system, the disturbance input is modified accordingly to the number of CCFs. What distinguishes the complex band-pass filters (CBFs) from the real band-pass filters is the polarity selectivity. The RBFs, unfortunately, can not differentiate between the sequences of the estimated frequency. Hence, passes both of them. Whereas the CBFs can distinguish between the frequencies and pass only the desired one.

A typical CBF transfer function can be formulated in (II-15) for the positive sequence and in (II-16) for the negative sequence of any frequency.

$$G_F{}^{p}(s) = \frac{w_p}{s - jh\hat{w} + w_p} \qquad \text{(II-15)}$$

$$G_F{}^{n}(s) = \frac{w_p}{s + jh\hat{w} + w_p} \qquad \text{(II-16)}$$

where ŵ is the estimated frequency.

Usually w_p is selected to $0.707 w_f$ to offer a good compromise between transient response and damping ration in estimating the positive and negative sequence of the fundamental component [36]. In order to confirm this assertion, Fig. II. 2(a) is

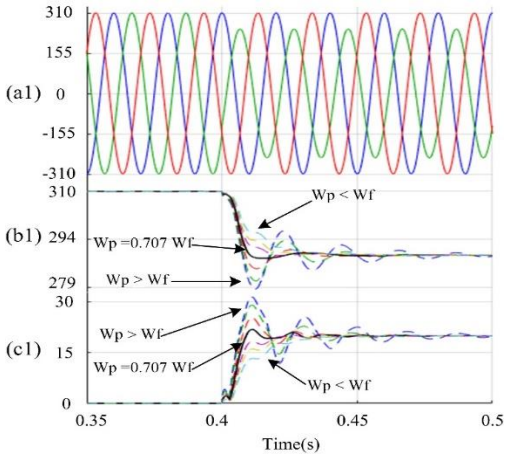

(a)

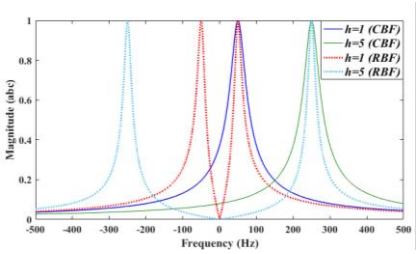

(b)

Fig. II. 2 Dynamic response and tuning behavior of the CBF. (a) analysis of w_p effect on the CBF dynamic behavior. (a1) grid voltage, (b1) the positive sequence of the fundamental frequency, and (c1) is the negative sequence of the fundamental frequency. (b) Bode plot of a first-order CBF and a second-order RBF[28].

displayed. It is clear that when the voltage subjects to an asymmetrical voltage drop, w_p with the values more than $0.707w_f$ have a faster transient response, but struggle from large oscillations. On the other hand, the values of w_p that are less than $0.707w_f$ provide accurate values but with slower transient response. Therefore, the optimum choice of w_p is to be selected to $0.707w_f$ since this value results in a good tradeoff between the overshoot and damping time. Fig. II. 2(b) presents the Bode diagram, which depicts the magnitude of a first-order CBF and second-order RBF. In this study case, the two filters are tuned at two frequencies (the fundamental and the fifth 5^{th} harmonic). The damping ratio values is set to ξ=0.707 and w_p=222.11 rad/s. It is obvious that the attenuation ration of the CCF has a unity only at one selected polarity (+50. +250). However, the second-order BPF has a unity gain at both polarities of each frequency (+50 Hz, +250 Hz, -50 Hz, -250Hz), which implies that this filter can not distinguish between them and passes them both.

II. 2. 1 Simulation and experimental results and discussions

The Simulation results are carried out under MATLAB/Simulink software. In this study case, the estimated frequency is not fed to the CCFs to assess their behavior under slight frequency drifts. The unbalance of the first stage occurs by dropping the second phase with 10 % of the nominal value in the first stage and 30% in the 2^{nd} stage. The injected harmonics are of the order -5^{th} and $+7^{th}$ respectively with the values 12.4V in the first stage and 31.1V in the second stage. In the instant 0.15s, a frequency variation occurs (from 50 Hz to 52 Hz). The PI controller parameters are selected to kp =220 and ki =2400.

Fig. II.3(a) displays the behavior of the MCCF-PLL in extracting the positive and negative sequences of the fundamentals using TM configuration. It is obvious that in the first stage, the MCCF-PLL can estimate a pure waveform of the fundamental

positive sequence $v_{\alpha 1}^{p}$, while the waveform of fundamental negative sequence $v_{\alpha 1}^{n}$ is relatively distorted. Though the frequency estimated by the MCCF-PLL has few ripples, these ripples are very small comparing to the ripples caused by the SRF-PLL. When the voltage disturbances increase in the second stage, it is obvious that $v_{\alpha 1}^{p}$ and its estimated frequency are not affected by that. Furthermore, the transient response of the measured phase error needs less than two cycles to reach the steady-state.

Fig. II.3(b) presents the performance of the MCCF-PLL under severe grid conditions using the MM configuration. In this study case, the MM configuration targets the sequences of the fundamental components and dominant harmonics. In the first stage, it is obvious that the waveform of $v_{\alpha 1}^{p}$ and $v_{\alpha 1}^{n}$ is sinusoidal, and the estimated frequency is free of ripples. Then in the second stage, when the perturbation increases, it is evident that the waveform of $v_{\alpha 1}^{p}$ is still sinusoidal, while the waveform of $v_{\alpha 1}^{n}$is slightly affected. In addition, the estimated frequency using the MCCF-PLL is very accurate during the small disturbance, then slightly affected under high disturbance with small ripples that can be disregarded. However, the frequency estimated by the traditional SRF-PLL struggles from the ripples under small and high disturbances. The two last plots of Fig. II. 3(b) portrays respectively the estimated -5th and 7th using the MCCF-PLL with the MM configuration. Since usually the purpose

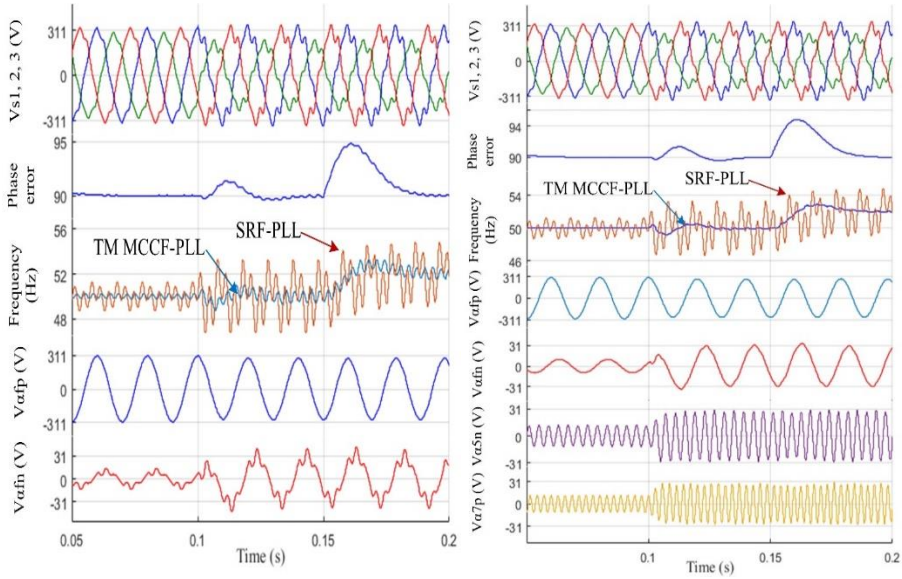

Fig. II. 3 Behaviour of the MCCF-PLL under sever grid conditions. (a) using TM configuration. (b) using MM configuration [28].

of the MCCF-PLL is to estimate the phase and frequency of only $v_{\alpha 1}^{p}$, then under small perturbations, the application of the TM configuration is sufficient. However, in the applications where the information about the sequences is important, then it is recommended to apply the MM configuration. As long as the magnitudes of harmonics decrease when their order increase, then it is sufficient to install the MM configuration with sub-modules tuned at the most dominant frequencies.

Fig. II. 4 displays the schematic diagram of the shunt APF connected to improve the power quality issues of the grid. Its schematic comprises a three-phase power supply, three-phase non-linear load that affects the current $i_{s1,2,3}$ waveform, and the shunt APF. The parameters of the studied EPS are summarized in Table II. 1.

Fig. II. 5 (a) shows the performance of the traditional SRF-PLL under sever voltage $V_{s1,2,3}$ conditions. Before the perturbation occurs, it is obvious that the SRF-PLL can accurately estimate the phase $\hat{\theta}$, which is fed to perform the *dqo* transform

Table II. 1 parameters of the simulation and practical systems [28].

Source	Grid Voltages RMS values:	
	Fundamental :	V_s = 230 V
	-5^{th} harmonic:	$V_{-5} = 40$ V
	7^{th} harmonic:	$V_7 = 30$ V
	-11^{th} harmonic:	$V_{-11} = 20$ V
	13^{th} harmonic:	$V_{13} = 10$V
	Main impedance:	$L_s = 0.005\ mH$
		$R_s = 0.5\ \Omega$
	Unbalance	$V_{s1} = 180$ V
		$V_{s1,3} = 230$ V
Shunt active power filter	dc link capacitor:	$C = 2200\ \mu F$
	dc link voltage references	$V_{dc} = 650\ V$
	output filters:	$L_f = 15\ mH$
		R_f =2 Ω
Load	Non-linear load:	$R_L = 153\ \Omega$
		$L_L = 10$ mH

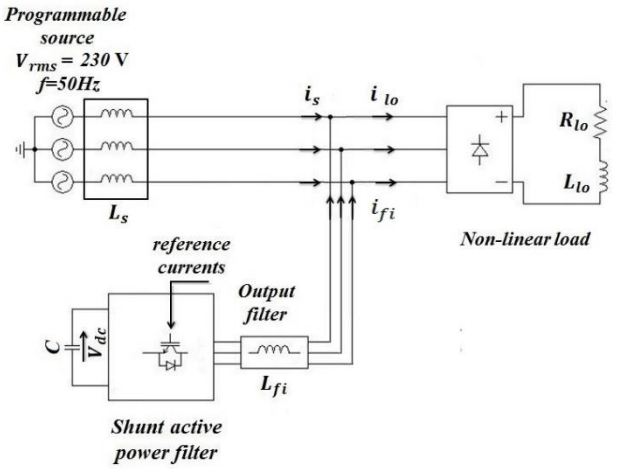

Fig. II. 4 Simulation and experimental scheme of the shunt APF [28].

of $i_{l1,2,3}$. Consequently, the harmonics rejection capability of the shunt APF is efficient and improves the THD of $i_{l1,2,3}$ from 29% to around 3.6%, which conforms with the IEC 61000-3-6 and IEEE 519-1992 standards. However, when the perturbation occurs to the voltage, the performance of the SRF-PLL tends to worsen. Consequently, the harmonic rejection capability of the shunt APF decreases by increasing the THD of $i_{s1,2,3}$ from 3.6% to 12.5%. Fig. II. 5(b) presents the behavior of the shunt APF under sever grid conditions using the MCCF-PLL. Since the voltage distortion is 12%, the application of 4 sub-modules tuned at (-1st, +1st, -5th, +7th) is enough to offer an accurate estimation of $\hat{\theta}$. In the instant 0.1s, the harmonics of the order -5th, +7th, -11th, +13th are superposed on $V_{s1,2,3}$. It is evident that the MCCF-PLL does not get affected by these harmonics and provides an accurate estimation of $\hat{\theta}$. Hence, the harmonics rejection capability of the shunt APF using the MCCF-PLL is improved. This can be seen in the THD of $i_{s1,2,3}$, which is decreased to 3.6%. Fig. II. 5(c) and (d) present, respectively, the behavior of the shunt APF using the SRF-PLL and MCCF-PLL under unbalanced and distorted voltage. The distortion of $V_{s1,2,3}$ is increased to 12.3%, while the unbalance is raised to 9%. From this figure, one can observe that when the unbalance is not significant, the SRF-PLL provides acceptable phase estimation. However, when the unbalance increases to 9%, the performance of the SRF-PLL tends to worsen. However, the capability of the MCCF-PLL to estimate the negative sequence of the fundamental enables the cancelation of the unbalance during the estimation of $v_{\alpha 1}^{p}$. Thus, the synchronization of the shunt APF is improved and yields to achieve an acceptable THD (3.7%) of $i_{s1,2,3}$, which respects the abovementioned Norms.

The experimental setup consists of a three-phase programmable source (Chroma model 61845) and a three-phase Danfoss inverter 2.2 kVA with an output L filter. The

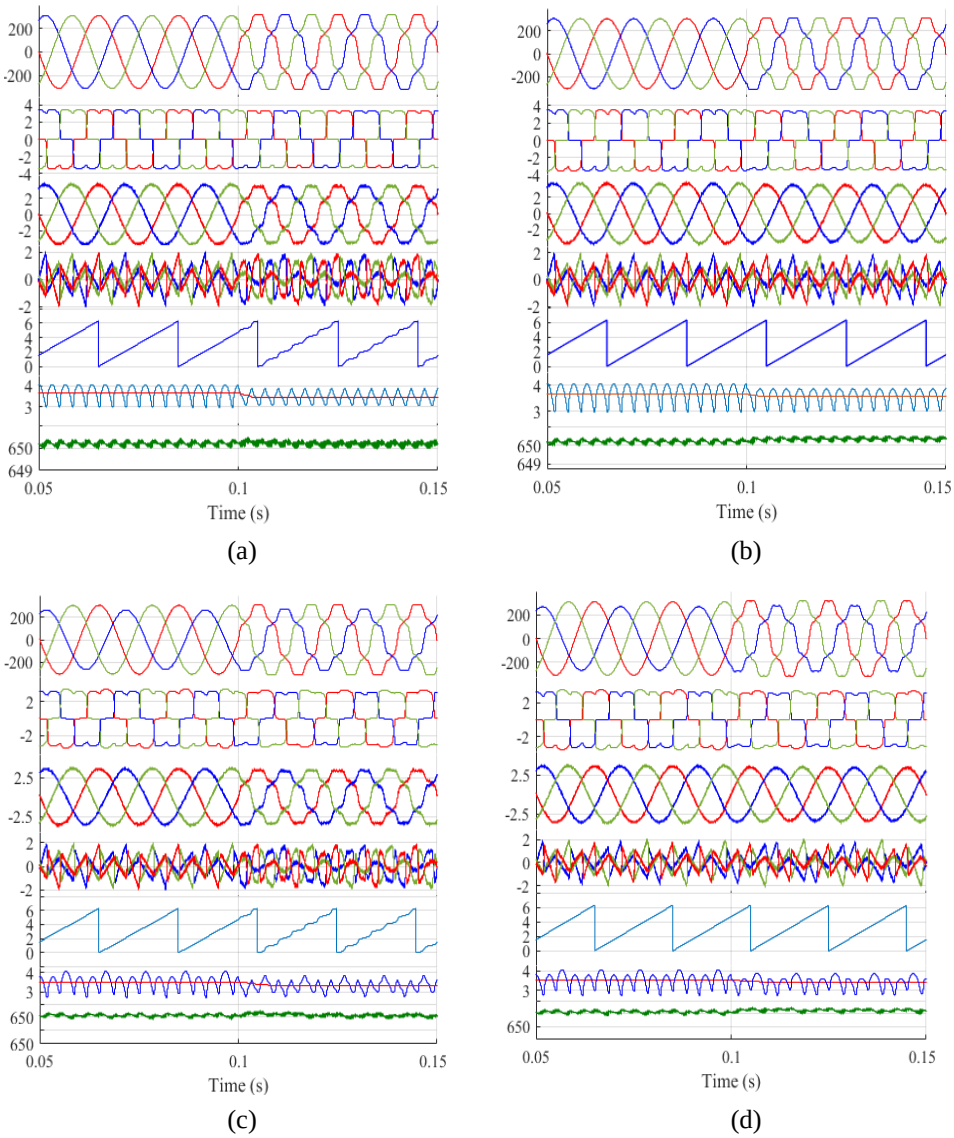

Fig. II. 5 Performance of the shunt APF using the SRF-PLL and MCCF PLL under distorted voltage ((a) and (b)) and distorted and unbalanced voltage ((c) and (d)) [28].

switching frequency is 10 kHz, the control algorithm is established under MATLAB/Simulink and implemented in a digital signal processor (dSPACE 1006 platform) with a sampling frequency of 10 kHz. The parameters of the experimental setup are presented in Table II. 1.

Fig. II. 6 shows the experimental performance of the shunt APF under distorted and unbalanced grid voltage utilizing the SRF-PLL (Fig. II. 6(a) and (c)), and the MCCF-PLL (Fig. II. 6(b) and (d)). The sampling time is set to 1e-4s. According to all plots of Fig. II. 6 it is obvious that the behavior of the shunt APF using the SRF-PLL and the MCCF-PLL are similar to the simulation results, which proves the MCCF-PLL can work efficiently in simulation and in experimental.

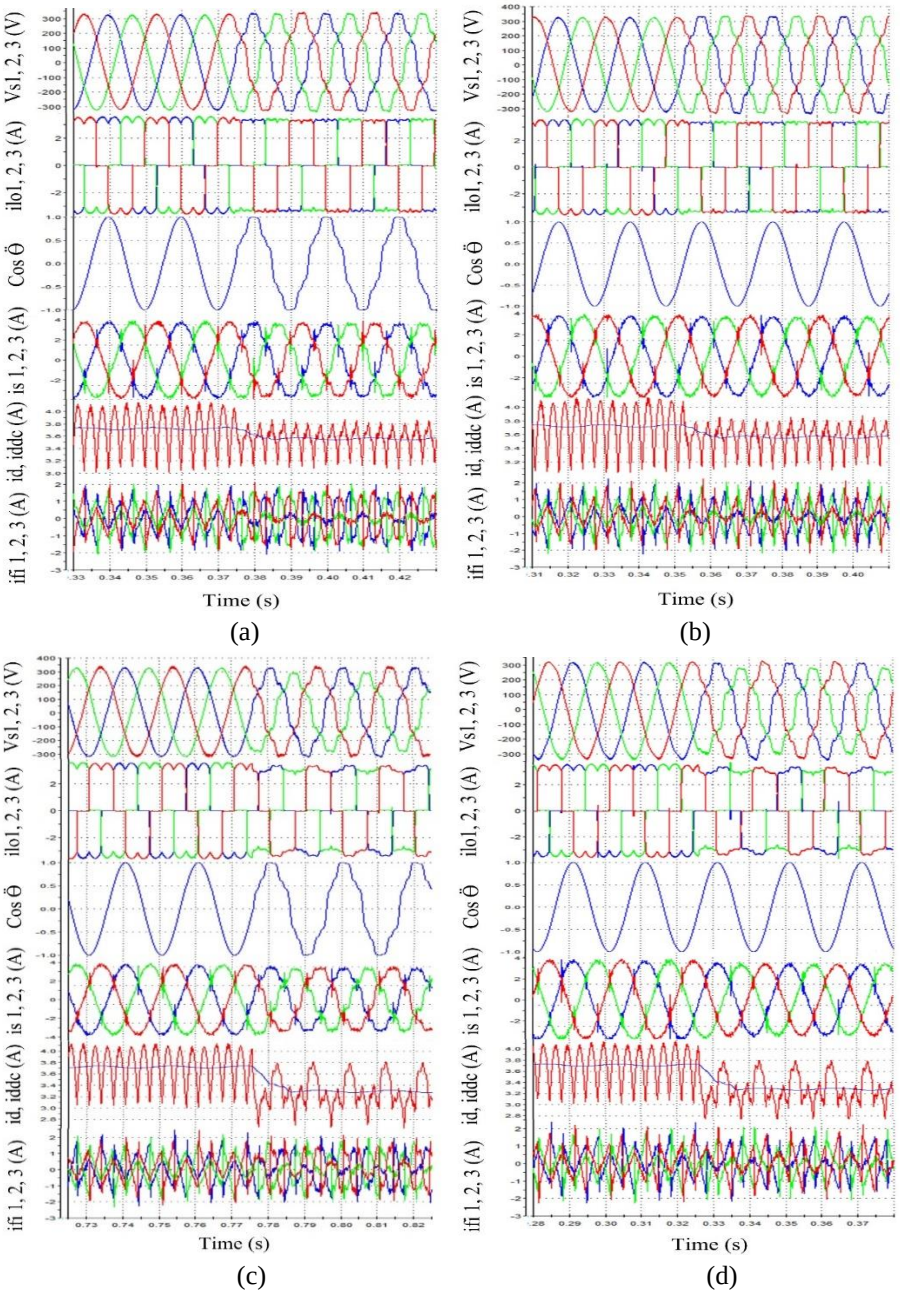

Fig. II. 6 Experimental results of applying the shunt APF to improve the power quality of the power grid using the SRF-PLL ((a) and (c)) and MCCF-PLL ((b) and (d)) under distorted voltage ((a) and (b)) and distorted and unbalanced voltage ((c) and (d)) [28].

II. 3 Non-linear least square approach to enhance the reference compensating current of shunt active power filter

The least-square method is a standard approach in regression analysis such as data fitting applications, harmonics, and frequency estimation. Recently, this approach has been extended to power converter applications such as APFs [37], [38], [39], [40]. In the case where there is no information about the grid frequency, the least square approach becomes non-linear (hereafter called NLS approach) [38].

Based on PM method, any contaminated voltage $V(t)$ can be approximated by a sum of exponentials and residues as [29]:

$$V(t) \approx \sum_{i=1}^{\mathcal{P}} \Re_i \cdot e^{(\Im_i t)} + \aleph(t) \tag{II-17}$$

Since in real applications, the data is measured with a finite number of samples Υ, (II-37 becomes):

$$V(\ell T_s) \approx \sum_{i=1}^{\mathcal{P}} \Re_i \cdot \mathcal{g}_i{}^{\ell} + \aleph(\ell T_s) \tag{II-18}$$

where: $\mathcal{g}_i = e^{(\Im_i Ts)}$. $\ell = 0,1, \ldots, \Upsilon - 1$. $i = 1,2, \ldots\ldots \mathcal{p}$. $\mathcal{p}$ is the tolerance.

The main goal of this approach is to perform the best approximation of (II-19), using the NLS approach as [29]:

$$\underbrace{\begin{bmatrix} V(0) \\ V(1) \\ \vdots \\ V(\Upsilon-1) \end{bmatrix}}_{\hat{V}} \approx \underbrace{\begin{bmatrix} 1 & 1 & \cdots & 1 \\ \mathcal{g}_1 & \mathcal{g}_2 & \cdots & \mathcal{g}_M \approx \\ \vdots & \vdots & \ddots & \vdots \\ \mathcal{g}_1^{(\Upsilon-1)} & \mathcal{g}_2^{(\Upsilon-1)} & \cdots & \mathcal{g}_M^{(\Upsilon-1)} \end{bmatrix}}_{g} \underbrace{\begin{bmatrix} \Re_1 \\ \Re_2 \\ \vdots \\ \Re_M \end{bmatrix}}_{\hat{\Re}} \tag{II-20}$$

$$\Re \approx g \backslash V \approx (g^T g)^{-1} g^T V \tag{II-21}$$

According to the NLS approach, if g is a vector that has a random amplitude and a frequency of 50 Hz, the equation (II- 40) extracts the pole of only the fundamental component. As long as the multiplication $(g^T g)^{-1} g^T$ provides the same amplitudes, then g can be selected at any amplitude. In order to reduce the computation burden of the NLS approach, it is wise to perform the multiplications $(g^T g)^{-1} g^T$ offline since the frequency is considered fixed or slightly fluctuated. Then, the obtained vectors can be stored in the signal processor cards. The fundamental component is estimated using a moving window and the magnitude and phase of this signal can be assessed using equations (II-41) and (II-42) in MATLAB software [29].

$$[Ma\ Ra] = max\big(\Re(:)\big) \tag{II-22}$$

$$\phi = \left(Ra \cdot T_s - \frac{1}{f \cdot 4}\right) \cdot \frac{180}{0.01} \tag{II-23}$$

where Ra is the rank of the maximum point of the filtered signal, and Ma is the magnitude of the maximum point of the filtered buffered signal. As the sinusoidal signal comprises only one sample, which corresponds to the maximum value, the multiplication of Ra and the sampling time T_s in (II-23) produces the phase angle of the signal that starts from the maximum value. As long as the sample of the maximum value of any sinusoidal signal is shifted from the first point by a quarter cycle ($\frac{\pi}{2}$), the subtraction ($-\frac{1}{f \cdot 4}$), which is a quarter cycle (0.005s), provide the real information of the phase ϕ. In contradiction with the PLL, whose dynamic response is long and its PI parameters need experts to design them, the equations (II-41) and (II-42) estimate the ϕ and the magnitude in an open-loop pattern, which is stable, has a faster transient response and does not require any control design.

In [38], [37] the NLS approach has been extended to the shunt APF. However, the application of this method in the *abs* stationary frame for the voltages and currents is computationally intensive. Moreover, in case the dc offset appears, this method needs a window size of one cycle to extract the fundamental component. The estimation of the PF and unbalance in the *abs* stationary requires extra-complicated calculations.

The approach, which is proposed in [29] integrates the NLS approach to the SRF method to perform the Park transformation, then the extraction of the harmonics is attained by the MAF. As a result, this approach benefits from several advantages such as low computation burden, faster transient response and easy compensation of the unbalance and PF. Moreover, the existence of the dc offset needs at least one cycle to be rejected. However, the proposed method in [29] needs only a half cycle to reject the dc offset.

Fig. II. 7 presents the RCC based on the NLS approach that is proposed in [29]. Its starts by transforming $V_{s1,2,3}$ from *abc* stationary frame to *αβ* stationary frame. Then, the transformed voltages $v_{\alpha,\beta}$ pass via a derivative, whose function is to eliminate the dc offset.

Fig. II. 8 is presented to elucidate the filtering procedures of v_α, which is affected by harmonics distortion and dc offset. Equation (II-24) presents the mathematical derivation of v_α. It is worthy to mention that v_β passes via the same processes, therefore, its calculation is not presented [29].

$$\frac{d\, v_\alpha}{dt} = \frac{d\,(v\sin(2\pi ft + \phi_h) + \sum_{h=2}^{m} v_h \sin(2\pi fht + \phi_h))}{dt}$$
$$= v2\pi f\sin(2\pi ft + \phi_h - 90^o)\sum_{h'=1,3,5..}^{m} v_h 2\pi fh' \sin(2\pi fh't + \phi_{h'} - 90^o)) \qquad \text{(II-24)}$$

(II-24) demonstrates that deriving v_α leads to a multiplication of respectively each frequency component by $2\pi f$ and $2\pi f h'$ and cause a phase shit of π/2. Deriving v_α leads to rejecting the dc offset from the distorted signal and keeps only the sinusoidal signals, then the obtained signal is divided by $2\pi f$ so that the magnitude of the estimated component remains fixed during the derivation process.

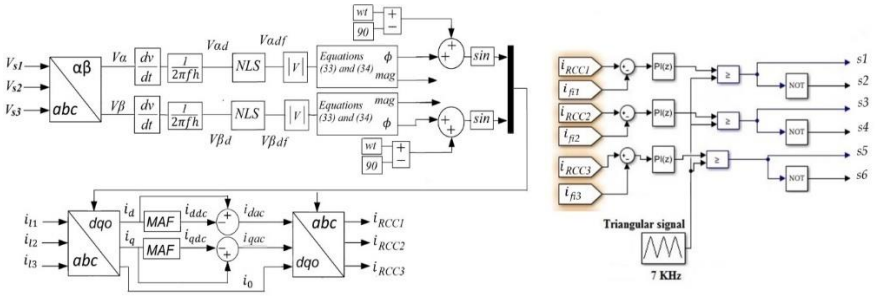

Fig. II. 7 The application of the NLS approach to enhance the RCC of the shunt APF [29].

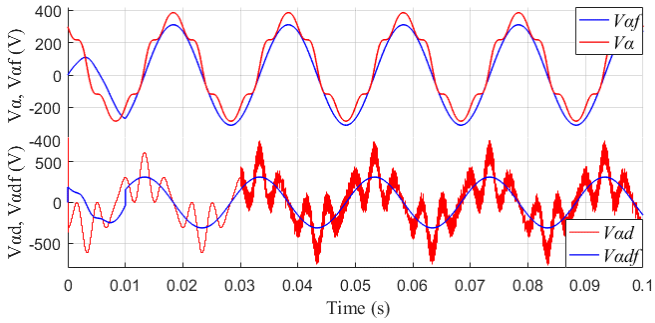

Fig. II. 8 Performance of the method proposed in [29] to estimate the fundamental component under noisy signal.

The extraction of the phase of $v_{\alpha df}$ is achieved by the equations (II-22) and (II-23) with a window size of one cycle. Seeking to decrease the window size to a half cycle to estimate Ra is not possible since the buffered second half cycle does not contain the maximum point. This is because for any fundamental signal, the first half cycle contains the maximum point and the second half cycle contains the minimum point. This issue can be solved by simply using the absolute function when estimating $v_{\alpha df}$. Since the derivative rejects the dc offset, it results in the equality of the maximum and minimum samples. Hence, the utilization of the absolute function($|v_{\alpha df}|$) provides two similar half-cycles that have the same Ra. Then, in

order to estimate the exact phase angle of ϕ , equations (II-25) and (II-26) are applied to differentiate between the order of the cycles [29].

$$.[Ma\ Ra] = max\left(\left|v_{\alpha df}(:)\right|\right) \tag{II.25}$$

$$If \max(\left|v_{\alpha df}(:)\right|) > \min\left(\left|v_{\alpha df}(:)\right|\right) \Rightarrow \phi = \left(Ra \cdot T_s - \frac{1}{f \cdot 4}\right) \cdot \frac{180}{0.01}$$

$$else\ \ \phi = \left(Ra \cdot T_s - \frac{1}{f \cdot 4}\right) \cdot \frac{180}{0.01} \tag{II-26}$$

After the estimation of ϕ, the shift resulted from the derivation of v_α is canceled by subtracting ϕ from π/2. As long as the phase shift between v_α and v_β is π/2, their fundamental signals are fed to the SRF method to extract the RCCs and send them to the PWM block to generate the pulses.

II. 3. 1 Simulation and experimental results

The simulation results are carried out under MATLAB/Simulink environment. The system parameters are presented in Table II. 2.

Fig. II. 9 presents the behavior of the proposed NLS approach under sever grid conditions [29]. In Fig. II. 9 (a), a voltage sag of 20% is caused in the period 0.1s to 0.16s. When applying Clark transform to $V_{s1,2,3}$, the sag perturbation appears on both $V_{\alpha\beta}$. Analyzing $V_{\alpha\beta}$ by NLS approach using a half cycle, results in the transient response of a half cycle with an accurate estimation of the phases ϕ_α and ϕ_β. Feeding these phases to the SRF method to perform the Park transformation of the current leads to extract the RCC accurately. Feeding the RCC to the APF results in improving the source current waveform with a THD of 4%, which respects the standards. Fig. II. 9(b) shows the performance of the proposed method in estimating the RCC under load variation. It is clear that in the instant 0.04s during the load variation, the APF controlled by the proposed method offers accurate estimation of the RCC with fast transient response.

Fig. II. 10 presents the experimental prototype, which compromises a three-phase programmable power supply (Chroma, model 61845), Danfoss 2.2 kVA inverter, digital signal processor (dSPACE-1006), and Hall effect sensors. The used sampling time is 0.1 ms. The parameters of this system are presented in Table. II-2.

Fig. II. 11 presented the experimental results of the proposed method, which is compared with the MAF-PLL, and MCCF-PLL under distorted and unbalanced voltage. The load current. $i_{lo1,2,3}$ is affected by the harmonics of the non-linear load and the harmonics of the voltage with a THD of 25% for the first and third line, and a THD of 39% for the second line. It is evident that the proposed method can estimate

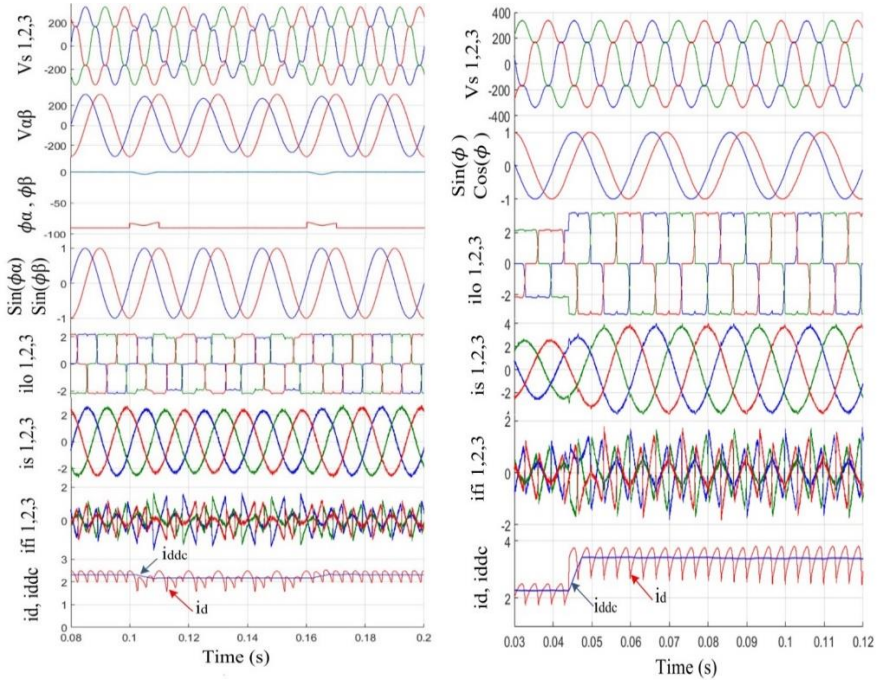

(a) (b)

Fig. II. 9 Performance of the proposed technique under: (a) voltage sag. (b) frequency drift and load variation [29]

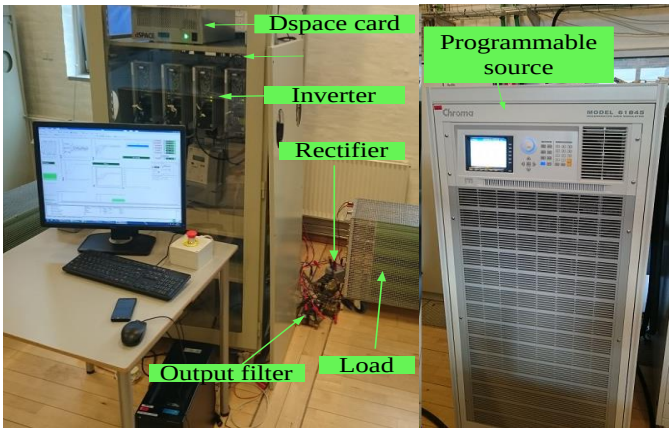

Fig. II. 10 Experimental prototype of the SAPF [29].

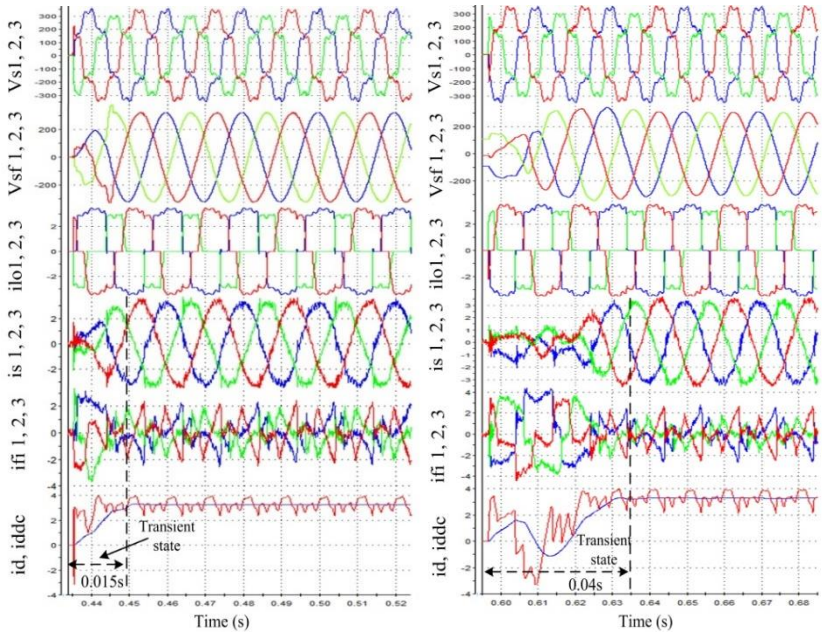

(a) (b)

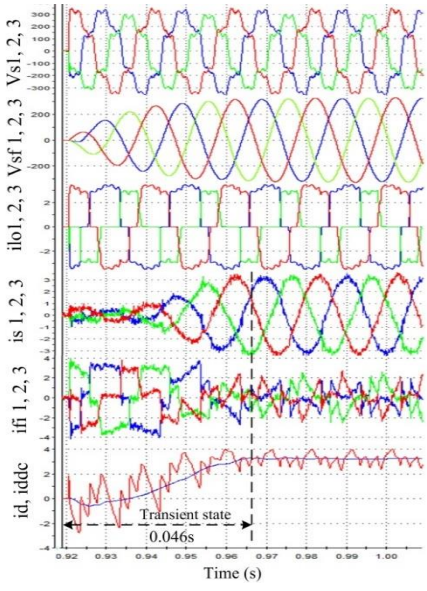

(c)

Fig. II. 11 Experimental results of SAPF in case of distorted unbalanced voltage. (a) The proposed method. (b) SRF method based on MCCF-PLL. (c) SRF method based on MAF-PLL [29].

the fundamental components of the voltages ($V_{sf1,2,3}$) in only a half cycle. Hence, serving their phases to the SRF method to extract the RCC requires a transient response in total only 0.15s to achieve a THD of 5%. While the SRF method based on the MCCF-PLL and MAF-PLL needs more than 2 cycles to reach the steady-state.

Fig. II. 12 presents the performance of the proposed method under a gird voltage, which is contaminated with harmonics and a dc offset. This latter is superposed on the voltage with 50V for the first and third phases and 100V for the second phase. In this study case, the magnitude of $V_{s1,2,3}$ is 200V, and its THD is about 30%. In contradiction with the MAF-PLL and MCCF-PLL that require a transient response of more than two cycles, the proposed method reaches the steady state only in a half cycle. Consequently, the estimation of the RCC using the proposed method needs about 0.024s to reach the steady-state with a THD of less than 5%. While the transient response of obtaining the RCC using the MCCF-PLL and MAF-PLL needs a larger transient response.

Table II. 2 Simulation and Practical parameters of the system [29]

Power supply	Voltages RMS values:	
	Fundamental :	V_s = 230 V
	-5^{th} harmonic:	$V_{-5} = 30$ V
	7^{th} harmonic:	$V_7 = 20$ V
	-11^{th} harmonic:	$V_{-11} = 10$ V
	13^{th} harmonic:	$V_{13} = 5$V
	Main impedance:	$L_s = 0.005\, mH$
		$R_s = 0.5\, \Omega$
	Dc offset	$V_{s1,3} = +50$ V
		$V_{s2} = +100$ V
	Unbalance	$V_{s1,3} = 230$ V
		$V_{s2} = 180$ V
SAPF	dc link voltage references	$V_{dc} = 650$ V
	dc link capacitor:	C = 2200 μF
	output filters:	$L_f = 14\, mH$
		$R_f = 2.5\, \Omega$
Load	Non-linear load:	$R_L = 153\ \Omega$
		$L_L = 10$ mH

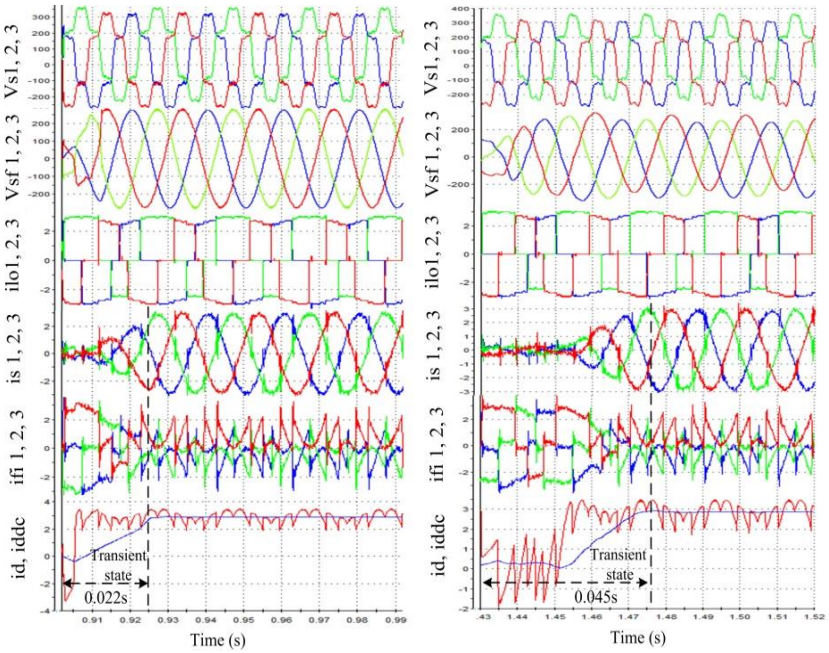

(a) (b)

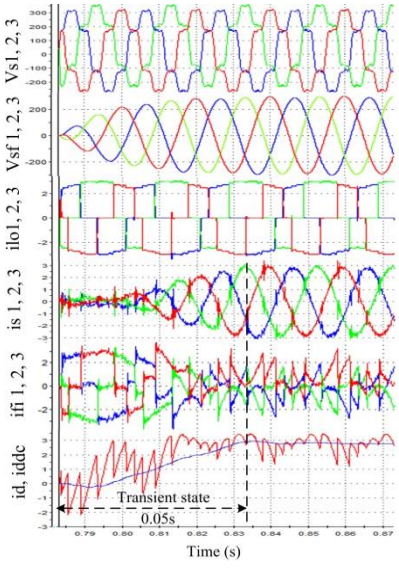

(c)

Fig. II. 12 Experimental results of SAPF in case of distorted voltage and dc offset. (a) The proposed method. (b) SRF method based on MCCF-PLL. (c) SRF method Based on MAF-PLL [29].

II. 4 Overview of OLS technique based on MAF and α-βCDSC

According to the fundamental theorem of algebra, the amplitude and the phase of the supply voltage can respectively be formulated as [30]:

$$V_{s\max} = \sqrt{V_\alpha(t)^2 + V_\beta(t)^2} \tag{II-27}$$

$$\hat{\theta} = \arctan\left(\frac{V_\beta(t)}{V_\alpha(t)}\right) \tag{II-28}$$

If we consider the voltages of the supply are balanced, then ((II-28) can be expressed as [30]:

$$\hat{\theta} = \arctan\left(\frac{V_{f\max}\sin(\omega t)}{V_{f\max}\cos(\omega t)}\right) = \arctan(\tan(\omega t)) = \omega t \tag{II-29}$$

In doing so, the frequency ω can be easily estimated as:

$$\frac{d\hat{\theta}}{dt} = d\omega t / dt = \omega \tag{II-30}$$

In the case where the grid voltage is not pure sinusoidal and harmonically contaminated, then it can be represented in the $\alpha\beta$ stationary frame as [30]:

$$\begin{bmatrix} \vec{V}_\alpha \\ \vec{V}_\beta \end{bmatrix} = \sum_{h=-\infty}^{\infty} V_{\alpha h} + j\sum_{h=-\infty}^{\infty} V_{\beta h} =$$

$$\sum_{h=-\infty}^{\infty} V_{\max h}\cos(h\omega t + \theta_h) + j\sum_{h=-\infty}^{\infty} V_{\max h}\sin(h\omega t + \theta_h) \tag{II-31}$$

where hwt and θ_h present respectively the phase angle of each existing frequency. The signs + and - denote respectively the sequences of each harmonic component. Estimating the phase angle in the existence of the perturbation becomes more complex resulting in the following complex equation [30]:

$$\tilde{\theta} = \arctan\left(\frac{V_{f\max}\sin(\omega t) + \sum_{h=\pm2,\pm3\ldots}^{\pm\infty} V_{h\max}\sin(h\omega t + \theta_h)}{V_{f\max}\cos(\omega t) + \sum_{h=\pm2,\pm3\ldots}^{\pm\infty} V_{h\max}\cos(h\omega t + \theta_h)}\right) \tag{II-32}$$

According to (II-28) and (II-32), it is obvious that $\tilde{\theta}$ and $\hat{\theta}$ have a repetitive signal of a right-angled waveform. Using the MAF can easily reject the perturbation if the window width T_w is well defined following the type of perturbation. The transfer

function of the MAF in both continues and discrete domains can be respectively presented as [30]

$$Y(t) = \frac{1}{T_w} \int_{t-T_w}^{t} A(t)dt \tag{II-33}$$

$$Y(k) = \frac{1}{N} \sum_{n=0}^{N-1} Y(K-n) \tag{II-34}$$

In the Laplace domain, the transfer function of the MAF is expressed as:

$$G_{MAF}(s) = \frac{1-e^{-T_w s}}{T_w s} \tag{II-35}$$

The application of Padé approximation results in:

$$e^{-T_w s} \approx \frac{1-(-T_w s/2)}{T_w s+(-T_w s/2)} \Rightarrow G_{MAF}(s) = \frac{1}{1+(T_w s/2)} \tag{II-36}$$

It is worthy to notice that the application of Park transformation and equation (II-50) have similar characteristics regarding the harmonics transformation. Hence, the fundamental component becomes a dc signal, while each harmonic component remains a sinusoidal signal with the order that is changed from *h* to the order *h-1*. Consequently, rejecting the harmonics of the order *6h ± 1* can be achieved with $T_w = 1/(6 \cdot f)$ that provides the faster transient response. Rejecting the harmonics of the order *6h ± 1* plus the tripplen harmonics (3rd, 6th, 9th, …etc.) needs T_w to be selected to $T_w = 1/(2 \cdot f)$. The existence of the dc offset, in addition, requires T_w to be selected to $T_w = 1/f$ (one cycle) to be rejected. The implementation of the MAF for OLS techniques, however, need the unwrap function to link each window output with the next window input as presented in [41]. Though this method is very effective and enhances the MAF performance, its implementation, however, in real systems is not practical due to the limitation of the digital signal processing and control cards memory. On the other hand, the implementation of the MAF in Park transform does not rely on the unwrap function. Hence, the method presented in [30] investigates the benefits of inserting the MAF into the SRF method to generate the RCC, whereas, the voltage is filtered using *α-β*CDSC method.

Fig. II. 13(a) presents the OLS method based on *α-β*CDSC filters, and Fig. II. 13(b) depicts one single operator of *α-β*CDSC filters. The transfer function of *α-β*CDSC can be formulated [26]-[28]:

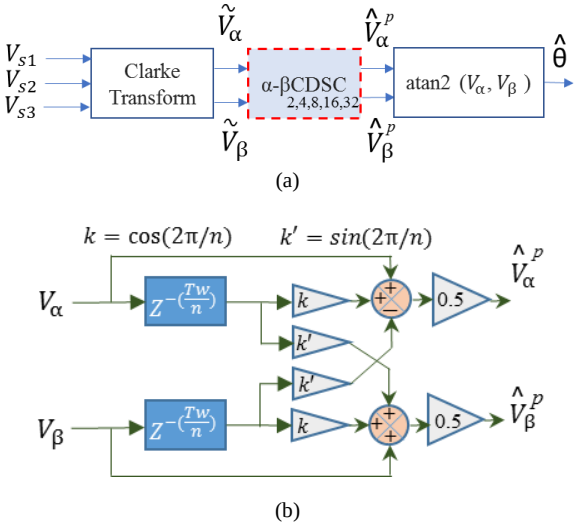

Fig. II. 13 OLS technique scheme. (a) OLS technique structure based on α-βCDSC. (b) Discrete-time domain of one α-βDSC operator [30].

$$\begin{bmatrix} \vec{V}_\alpha^p \\ \vec{V}_\beta^p \end{bmatrix} = \overbrace{\frac{1}{2}\left[1+e^{\frac{j2\pi}{n}}e^{\frac{-Tw}{n}s}\right]}^{\alpha-\beta\text{DSC}} \begin{bmatrix} \vec{V}_\alpha \\ \vec{V}_\beta \end{bmatrix} \tag{II-37}$$

where *p* refers to the positive sequence. *n* is the delayed factor, by selecting *n*=4, the *α-β*DSC filters can reject the -5th +7th and the negative sequence of the fundamental component caused by the unbalance [42]. The rejection of odd harmonics requires cascading 4 operators of *α-β*DSC in series with *n* selected to *n*=4,8,16,32, which increases the response time to ½ cycle. Furthermore, adding a series cascaded operator with *n*=2 results in rejecting the dc offset. Hence, the response time of the total operators gets closer to one cycle. The cascaded series operators can be expressed as [30]:

$$\begin{bmatrix} \vec{V}_\alpha^p \\ \vec{V}_\beta^p \end{bmatrix} = \prod_{n=2,4,8,16,32} \frac{1}{2}\left[1+e^{\frac{j2\pi}{n}}e^{\frac{-Tw}{n}s}\right] \begin{bmatrix} \vec{V}_\alpha \\ \vec{V}_\beta \end{bmatrix} \tag{II-38}$$

The proposed OLS technique [30] is developed to reject the dc offset with a disregarded delay. Fig. II. 14 presents the proposed method, which implements two different estimators. These estimators are connected in parallel, where the first one is installed to estimate the frequency in an open-loop manner, and the second one is installed to estimate the voltage phase. The idea behind separating the estimators is to ensure the stability of the frequency estimator in case the phase estimator subjects

to malfunctioning under certain issues. In order to illustrate the contribution of this technique, let's assume that the voltage is superposed by only the dc offset. Hence, its mathematical formulation might be expressed as [30]

$$\begin{bmatrix} V_{\alpha}^{p}(t) \\ V_{\beta}^{p}(t) \end{bmatrix} = \begin{bmatrix} V_{dc\alpha} \\ V_{dc\beta} \end{bmatrix} + \begin{bmatrix} V_{\alpha 1}^{p} e^{j(\omega t + \theta_{\alpha 1}^{p})} \\ V_{\beta 1}^{p} e^{j(\omega t + \theta_{\beta 1}^{p})} \end{bmatrix} \tag{II-39}$$

If we substitute *s* by *jw* and put $T_w = 1/f$ in (II-59), applying α-βDSC with n=2 to the voltages leads to [30]:

$$\begin{bmatrix} V_{\alpha}^{p}(t) \\ V_{\beta}^{p}(t) \end{bmatrix} = \begin{bmatrix} V_{dc\alpha} \\ V_{dc\beta} \end{bmatrix} + \begin{bmatrix} V_{\alpha 1}^{p} e^{j(\omega t + \theta_{\alpha 1}^{p})} \\ V_{\beta 1}^{p} e^{j(\omega t + \theta_{\beta 1}^{p})} \end{bmatrix} \frac{1}{2} \left[1 + e^{\frac{j2\pi(1 - Tw \cdot f)}{n}} \right] \tag{II-40}$$

$$\begin{bmatrix} \hat{V}_{\alpha}^{p}(t) \\ \hat{V}_{\beta}^{p}(t) \end{bmatrix} = \begin{bmatrix} V_{\alpha 1}^{p} e^{j(\omega t + \theta_{\alpha 1}^{p})} \\ V_{\beta 1}^{p} e^{j(\omega t + \theta_{\beta 1}^{p})} \end{bmatrix} \tag{II-41}$$

where ^ denotes the filtered signals. Based on (II-41) it is obvious that the dc offset needs a delay of at least n=2 to be cancelled.

From (41), one can conclude that the dc offset requires a delay of n=2 to be rejected. However, the proposed method, which is presented in Fig. II. 14(a) can reject the dc offset with the use of a derivative before the filters as expressed in (II-42). Hence, no time delay is resulted due to the cancelation of the dc offset [30].

$$\begin{aligned} \frac{d}{dt}\begin{bmatrix} V_{\alpha}^{p}(t) \\ V_{\beta}^{p}(t) \end{bmatrix} &= \frac{d}{dt}\left(\begin{bmatrix} V_{dc\alpha} \\ V_{dc\beta} \end{bmatrix} + \begin{bmatrix} V_{\alpha 1}^{p} e^{j(\omega t + \theta_{\alpha 1}^{p})} \\ V_{\beta 1}^{p} e^{j(\omega t + \theta_{\beta 1}^{p})} \end{bmatrix} \right) \\ &= wj \begin{bmatrix} V_{\alpha 1}^{p} e^{j(\omega t + \theta_{\alpha 1}^{p})} \\ V_{\beta 1}^{p} e^{j(\omega t + \theta_{\beta 1}^{p})} \end{bmatrix} \end{aligned} \tag{II-42}$$

It is obvious that (II-42) is similar to (II-41). However, (II-42) is obtained without any time delay. The frequency ω in (II-42) is canceled during the estimation of θ as demonstrated in (II-41). Adding $\frac{-\pi}{2}$ to $\hat{\theta}$ as presented in Fig. II. 14(a) compensates the shift that is caused by the derivative as

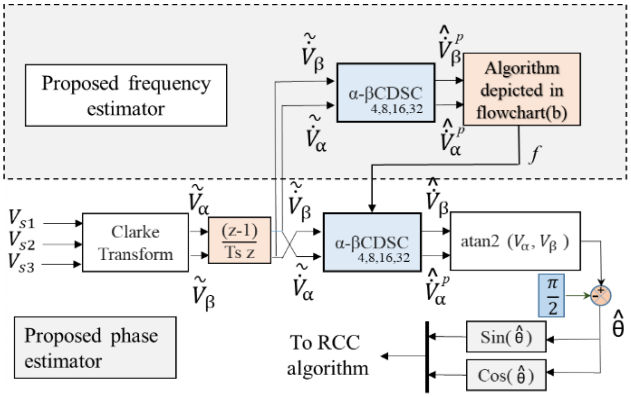

(a)

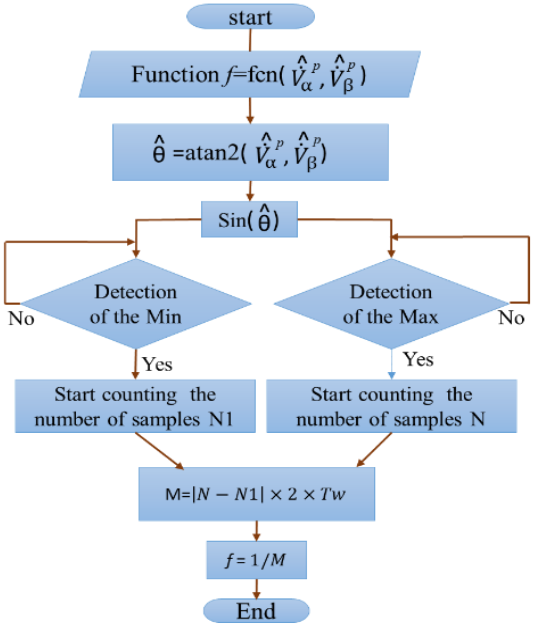

(b)

Fig. II. 14 The proposed OLS technique. (a) Phase and frequency estimator. (b) the flow chart of the proposed frequency estimator [30].

$$\hat{\theta} = \arctan\left(\frac{\hat{V}_{\beta}(t)}{\hat{V}_{\alpha}(t)}\right) - \frac{\pi}{2} \qquad \text{(II-43)}$$

According to (II-40), in case there is no frequency drift, the product $Tw\cdot f$ tends to unity for the fundamental positive sequence voltage. However, under frequency drifts, the product $Tw\cdot f$ does not tend to unity anymore and undergoes some perturbations, which leads to a degraded accuracy of the α-βCDSC. So far, deriving the phase of the voltage is one of the most applied methods to estimate the grid frequency [43], [44]. However, these methods do not have good performance, particularly in the applications that have poor sampling time. A simple yet effective estimator based on α-βCDSC is proposed in [45] to reduce the error of the solution proposed [43], [44]. However, as demonstrated in [30], its performance decreases under severe grid conditions. In order to overcome this deficiency, an efficient frequency estimator is proposed in [30]. As it is shown in Fig. II. 14(a), the process begins by applying Clark transformation to the grid voltage, then using a derivative in series to cancel any appearance of the dc offset with no delay time. After that, the operators α-βCDSC$_{4,8,16,32}$ are cascaded to filter the signal. Next, the algorithm, which is presented in Fig. II. 14(b) is applied to estimate the frequency. After estimating an accurate θ and perform its sinus, the algorithm detects the maximum and the minimum of it. Then, sums the number of samples N and N_1 that are located between the maximum and the minimum points of each half-cycle. Finally, the grid frequency is calculated as [30]:

$$f = \frac{1}{\left|N - N_1\right|\cdot 2\cdot Tw} \tag{II-44}$$

II. 4. 1 Simulation and experimental results.

The simulation results are carried out under the MATLAB/Simulink environment. Fig. II. 15 presents the performance of the proposed frequency estimator under harmonically contaminated signal and frequency drifts. The first subplot presents contaminated signal $V_{\alpha\text{-}\beta}$, and the second subplot presents the derived distorted signal $\dot{V}_{\alpha\text{-}\beta}$. The third subplot portrays the performance of the α-βCDSC$_{4,8,16,32}$ operators in filtering the signal $\dot{V}_{\alpha\text{-}\beta}$. It is evident that the filtered signal is pure sinusoidal under nominal frequency. However, when the frequency subjects to a drift of 4%, the signal is slightly affected. Hence, the frequency estimated by the traditional methods still struggles from some ripples. The proposed method can accurately estimate the frequency even under frequency drifts.

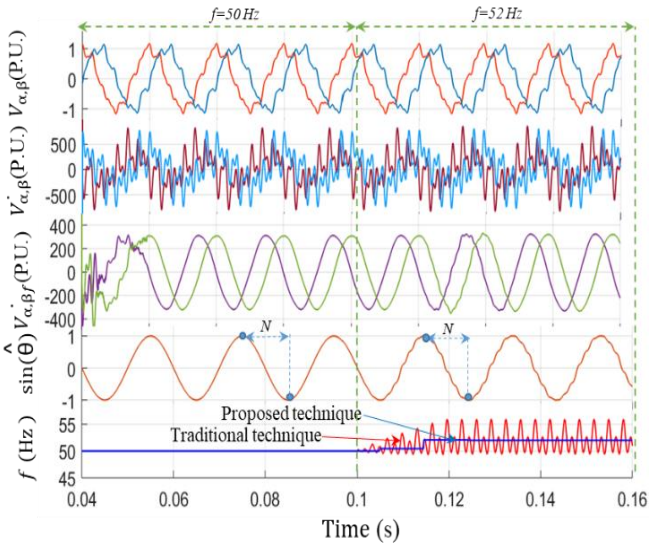

Fig. II. 15 behavior of the proposed frequency estimator under harmonic contamination and frequency variations [30].

Fig. II-16 Demonstrate the efficacy of the proposed OLS technique in estimating the frequency and phase under severe grid conditions. The grid voltage is affected by the odd harmonics and dc offset. It is obvious that the proposed OLS technique provides an accurate estimation of the phase/frequency with the fastest transient response compared with the enhanced true open-loop synchronization technique (ETOLS) that is presented in [45]. Besides, during the frequency drift in the instant 0.061, it is clear that the transient response of the proposed method is faster (needs only 0.01s) than the ETOL, which requires 0.028s to reach the steady-state. In addition, during the phase jump and frequency drop in the instant 0.11s and 0.16s, the proposed method provides the faster transient response with a more accurate estimation.

Fig. II-17 presents the effectiveness of the proposed frequency estimation with different sampling time T_s. it clear that even when T_s changes from 20 μs to 0.5 ms, the accuracy of estimating the frequency is slightly affected, with a value that can be disregarded.

Fig. II-18 Presents the experimental prototype of the shunt APF. The types of equipment of the experimental prototype are the same that are mentioned in the previous section. The parameters of the experimental configuration are summarized in Table II. 3.

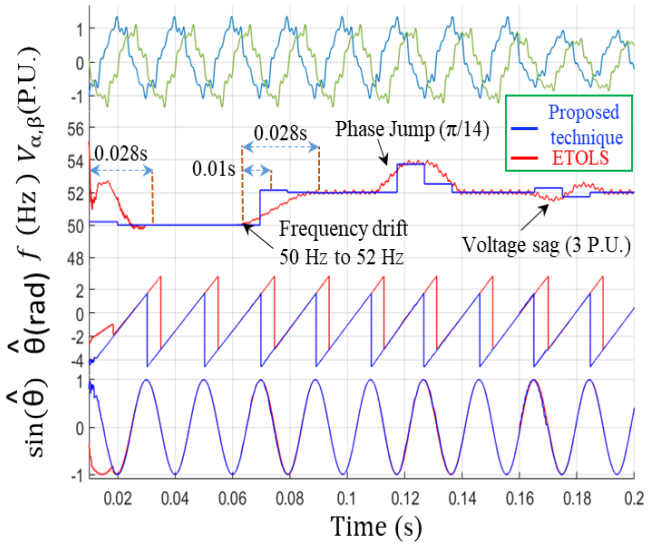

Fig. II. 16 presents the performance of the proposed OLS technique to estimate the frequency and phase under sever grid conditions [30].

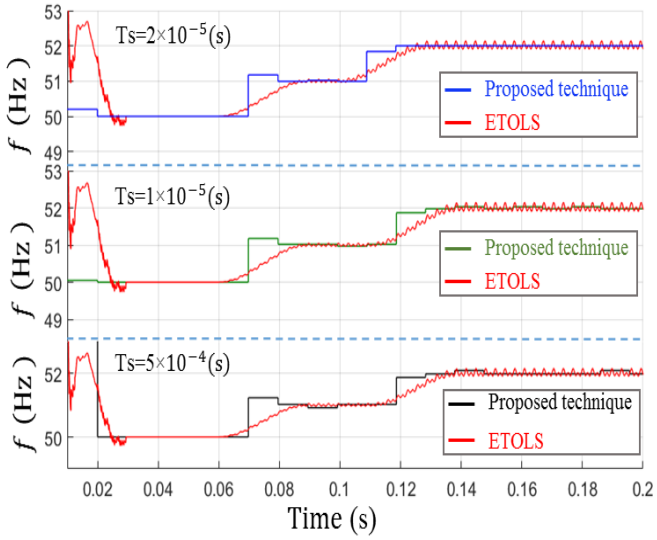

Fig. II. 17 Performance of the proposed OLS method under different sampling time [30].

Table II. 3 Parameters of the experimental prototype [30]

Devices	Parameters	Values
Power supply	Fundamental Voltages (RMS) :	V_s = 230 V
	-5th harmonic:	V_{-5} = 30 V
	7th harmonic:	V_7 = 20 V
	-11th harmonic:	V_{-11} = 10 V
	13th harmonic:	V_{13} = 5 V
	Main impedance	L_s = 0.007 *mH*, R_s = 0.7 Ω
	Dc offset	$V_{s1,2,3}$ = +50 V
	Unbalance	$V_{s1,3}$ = 230 V, V_{s2} = 180 V
SAPF	dc link voltage	V_{dc} = 650 V
	dc link capacitor:	$C = 2200\ \mu F$
	output filters:	L_f = 15 *mH*, R_f = 1.9 Ω
Load	Non-linear load:	R_L = 280 Ω, L_L = 7 *mH*

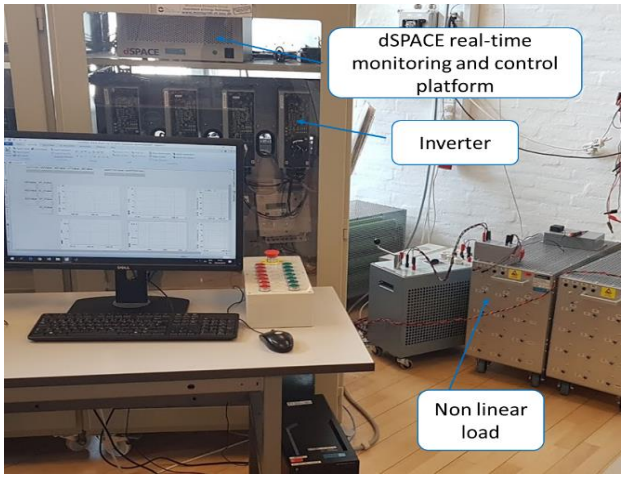

Fig. II. 18 Experimental prototype of SAP [30].

Fig. II. 19 and 20 present respectively the dynamic behavior of the SAPF under distorted and unbalanced voltage (Fig. II.19) and distorted voltage and dc offset (Fig. II. 20). The proposed OLS method, which is presented in Fig. II. 14 is compared with two traditional methods that are DFT [29], [30], and self- tuning filter (STF) [31]. The subplots of Fig. II- 19 and 20 present respectively the grid contaminated voltage V_s, the fundamental filtered voltage V_f, the distorted current of load i_{lo}, the filtered source current i_s and its RMS value i_{sRMS}, and the injected filter current i_{fi}.

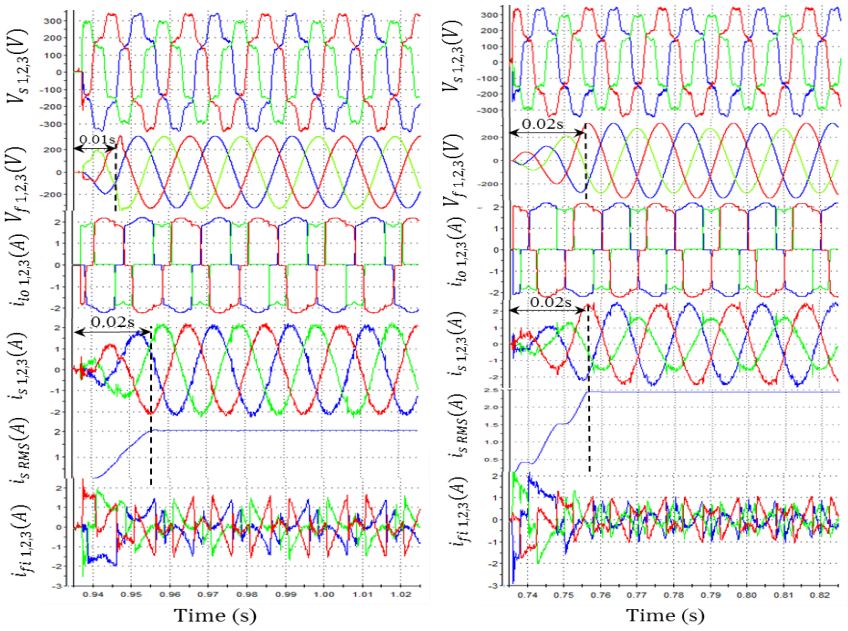

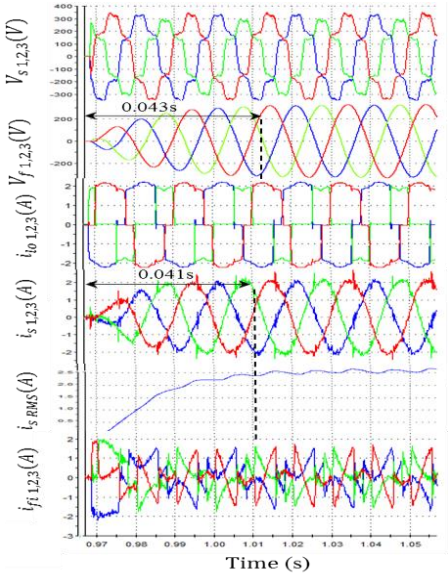

Fig. II. 19 Performance of the proposed OLS technique in enhancing the dynamic response of the shunt APF under distorted and unbalanced voltage. (a) Proposed OLS technique. (b) DFT. (c) STF [30].

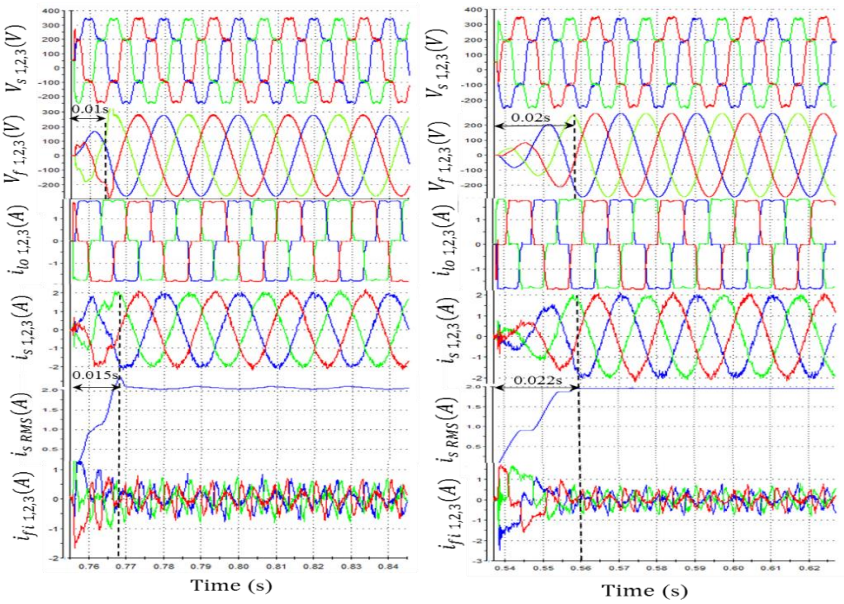

(a) (b)

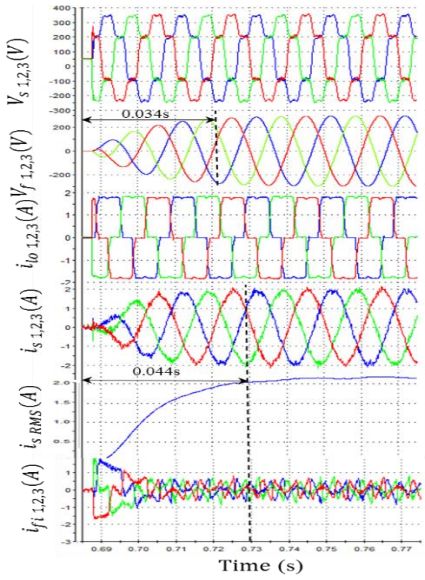

(c)

Fig. II. 20 Performance of the proposed OLS technique in enhancing the dynamic response of the shunt APF under distorted voltage and DC offset. (a) Proposed OLS technique. (b) DFT. (c) STF [30].

According to Fig. II- 19 and 20, it is obvious that the method presented in Fig. II. 14 provides a faster transient response (half cycle) than the traditional methods whose transient responses are more than one cycle. Moreover, it is clear in Fig. II. 19 that the DFT can not cancel the unbalance since it is applied in the *abs* stationary frame. Sending the estimated $\hat{\theta}$ of V_f to the SRF method to extract the RCC and control the shunt APF improves the waveform of i_s by reducing the THD from 29% to about 5%, and thus, conforms with the IEC 61000-3-6 and IEEE 519-1992 standards. Though i_s improved by applying the DFT has a THD of about 5%, it, however, still struggle from the unbalance. Furthermore, the STF method can cancel the unbalance of i_s , but its transient response is very long (more than two cycles).

Chapter III. Signal periodicity-independent method to assess the harmonics on board shipboard power systems

This chapter summarizes the contribution of the following paper: [49]. More details can be found in the attached publications at the appendix.

III. 1 summary of the contribution

Over recent years, due to the widespread use of power electronic converters (PECs) on board shipboard power systems (SPSs), harmonic distortion is becoming a severe issue. Attaining precise information of harmonics is very crucial to assess the total distortion and verify if it respects the norms or poses a threat. There are several ships classifications standards and rules that deal with harmonic issues [5]. Most of them resemble the dominant power quality standards like the IEC standards 61000-4-7/30 [6], [7]. In order to ensure security on-board ships, these standards have imposed some restrictions on the harmonics contamination. However, these standards have some recommendations, mainly in the existence of the inetrharmonics and frequency drifts that are not suitable for SPSs such as the application of the fast Fourier transform FFT with a window width of 10/12 times of the fundamental frequency [18], [50]. To deal with this issue, a signal periodicity-independent algorithm is proposed in [49], to assess the harmonics and interharmonics of distorted signals. this method, which is based on an enhanced matrix pencil method (MPM) can estimate the harmonics and interharmonics with a short moving window width under large frequency drifts. the performance of the proposed method is evaluated under MATLAB software, then the experimental validation is attained by analyzing the current of a bulk carrier ship.

III. 2 A resolution-enhanced signal periodicity-independent method for evaluation of harmonics distortion in shipboard microgrids

The DFT is one of the most used methods in different analysis areas and signal processing. For any distorted signal, the DFT can be formulated as [51], [49]:

$$X(k)=\sum_{n=0}^{N-1} x(n)\ W_N^{kn} \quad =\sum_{n=0}^{N-1} x(n)\left[\cos(\frac{2\pi}{N}kn)-i\cdot\sin(\frac{2\pi}{N}kn)\right] \qquad \text{(III-1)}$$

where $W_N=e^{-j2\pi/N}$, $k=0,...,N-1$, $x(n)$ is the input sequence with the length N and all integers n ($x(n)=x_0,\ x_1,\ \ldots,\ x_{N-1}$),

The inverse DFT of the domain $n\in[0,N-1]$ is presented as [49]:

$$x(n) = \frac{1}{N} \sum_{k=0}^{N-1} X(k)\ W_N^{-kn}\ ,\quad n \in \mathbb{Z}\ . \tag{III-2}$$

The FFT is a technique, which performs the DFT in an efficient manner to obtain similar results with a computation burden that is decreased from $O(N^2)$ to $O(N \log N)$ [52]. From (III-2), if we set the product $X(k)\ W_N^{-kn}$ =A, then (III-3) equals the formula of the MAF that is expressed in the discrete and continues time-domain respectively as [29], [49]:

$$x(n) = \frac{1}{N} \sum_{k=0}^{N-1} A(k) \tag{III-3}$$

$$x(t) = \frac{1}{T_w} \int_{t-T_w}^{t} X(\tau)\ d\tau \tag{III-4}$$

where T_w denotes the window width. The transfer function of the MAF using Laplace can be formulated as [53], [49]:

$$MAF_{con}(s) = \frac{x(s)}{A(s)} = \frac{1 - e^{-T_w s}}{T_w s} \tag{III-5}$$

Based on Padé approximation, $e^{-T_w s}$ can be simplified as [49]:

$$e^{(-T_w s)} = e^{(-\frac{1}{2}T_w s)} / e^{(\frac{1}{2}T_w s)} = (1 - T_w s/2)/(1 + T_w s/2) \tag{III-6}$$

Substituting (III-6) in (III-5) provides

$$MAF_{con}(s) \approx 1/(1 + (0.5\ T_w s)) \tag{III-7}$$

From (II-7) we observe that the DFT/MAF can act as an ideal low-pass filter if T_w is set to $T_w = 1/nf$, and $n = 1,2,3 \ldots etc.$

Setting $s = j\omega$ in (III-7) leads to [49]:

$$MAF_{con}(j\omega) = \frac{1}{T_w j\omega} - \frac{\cos(-T_w\omega) + j\sin(-T_w\omega)}{T_w j\omega} \tag{III-8}$$

Based on (III-8) it is obvious that if the system frequency is nominal, then the production $f \cdot T_w$ provides a unit gain, which tends (III-8) to 0 ($MAF_{con}(j\omega) \approx 0$). This prove is visualized in Fig. III. 1, which demonstrates that the MAF/DFT tends to zero only when the product $f \cdot T_w \approx 1$ is fulfilled.

The contribution of this work is to present the weakness of the traditional MPM, then proposes a novel method on how to optimize it.

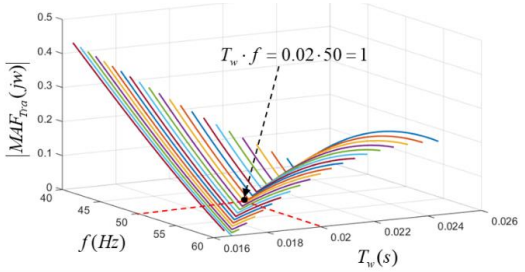

Fig. III. 1 Effect of the frequency drifts on the accuracy of the MAF/DFT [49].

According to PM method, any distorted signal can be approximated by a sum of exponentials and residues as presented in (III-9) and discretized in (II-10) [49].

$$A(t) \approx \sum_{i=1}^{M} \Re_i \; e^{(-\alpha_i + j\omega_i)t} + \mathrm{N}(t) \tag{III-9}$$

$$A(kT_s) \approx \sum_{i=1}^{M} \Re_i \; e^{(-\alpha_i + j\omega_i)kT_s} + \mathrm{N}(kT_s) \tag{III-10}$$

In opposite to the most applied methods to estimate the harmonics that are frequency-dependent techniques such as the DFT, the MPM can estimate the harmonics and interharmonics in half/one cycle, depends on the sampling time as [49]:

$$\Upsilon = \frac{1}{c \cdot (f + |\Delta f_{\max}|) \cdot T_s}, \quad \begin{matrix} c = 1 & if & T_s > 5e^{-4} \\ c = 1/2 & if & T_s \le 5e^{-4} \end{matrix} \tag{III-11}$$

where Υ is the number of samples, $\Delta f_{\max}$ is the maximum frequency deviation that can occur to the signal. After the selection of Υ, the Hankel matrix is built as [49]:

$$[B] = \begin{bmatrix} b(1) & b(2) & \dots & b(L+1) \\ b(2) & b(3) & \dots & b(L+2) \\ \vdots & \vdots & \ddots & \vdots \\ b(\gamma - L) & b(\gamma - L + 1) & \dots & b(\gamma + 1) \end{bmatrix}_{(\gamma - L)(L+1)} \tag{III-12}$$

The pencil parameter L is usually selected as $\frac{\gamma}{3} \le L \le \frac{\gamma}{2}$ to provide better performance under noisy contaminated data $\frac{\gamma}{3} \le L \le \frac{\gamma}{2}$ [54], [55]. The main weakness of the MPM is that the number of harmonics *Nh* that can be estimated is constrained to *L* as [49]:

$$Nh = \frac{\sigma_{2L+2}}{2} = \frac{L+1}{2}, \qquad \frac{\gamma}{3} \le L \le \frac{\gamma}{2} \tag{III-13}$$

where σ_{2L+2} is the maximum number of the singular values. For example, if we set $L = \gamma/2$, it implies that the maximum number of harmonic components can be assessed by the MPM is $Nh = \gamma/4$. As long as Υ and L are proportional to each other, and Υ is proportional to T_s, it means that Nh is inversely proportional to T_s. Hence, the increase of T_s results in decreasing the number of harmonic components can be extracted. Besides, in case the harmonics of the order that is more than Nyquist frequency $f_{\max} = 1/(2T_s)$ exists, the algorithm cannot detect them. In this regard, a novel method is proposed in [49] to enhance the resolution of the traditional MPM. It starts by selecting two matrices $[A_a]$, and $[A_b]$ from (II-3) as [49]:

$$[A_a] = \begin{bmatrix} u(2) & u(3) & \dots & u(L+2) \\ u(3) & u(4) & \dots & u(L+3) \\ \vdots & \vdots & \ddots & \vdots \\ u(\gamma-L) & u(\gamma-L+1) & \dots & u(\gamma+1) \end{bmatrix}_{(\gamma-L-1)(L+1)} \tag{III-14}$$

$$[A_b] = \begin{bmatrix} u(1) & u(2) & \dots & u(L+1) \\ u(2) & u(3) & \dots & u(L+2) \\ \vdots & \vdots & \ddots & \vdots \\ u(\gamma-L-1) & u(\gamma-L) & \dots & u(\gamma) \end{bmatrix}_{(\gamma-L-1)(L+1)} \tag{III-15}$$

where $[A_a]$, and $[A_b]$ are respectively built by deleting the head and the bottom rows of [B]. Then, the mean value between every two samples of [B] are attained as [49]:

$$[A_C] = \frac{[A_a] + [A_b]}{2} \tag{III-16}$$

After that, the developed new Hankel matrix is constructed by fitting $[A_c]$ in [B] as [49]:

$$[A_e] = \begin{bmatrix} a(1) & \frac{a(1)+a(2)}{2} & \dots & a(2L+1) \\ \frac{a(1)+a(2)}{2} & a(2) & & \\ a(2) & \frac{a(2)+a(3)}{2} & \dots & a(2L+2) \\ \vdots & \vdots & \ddots & \vdots \\ a(2\gamma-2L) & a(2\gamma-2L+1) & \dots & a(2\gamma+1) \end{bmatrix}_{(2\gamma-2L)(2L+1)} \tag{III-17}$$

Fig. III. 2 is added to demonstrate the influence of L in extracting the maximum number of harmonics using both methods (Traditional MPM and the enhanced MPM). From this figure, we can observe that the increased value of L increases the number of harmonics that can be estimated. However, the increased value of T_s limits the number of harmonics that can be estimated. On the other hand, the proposed method can estimate the double number of harmonics with the same L and T_s. Hence, enhances the THD assessment.

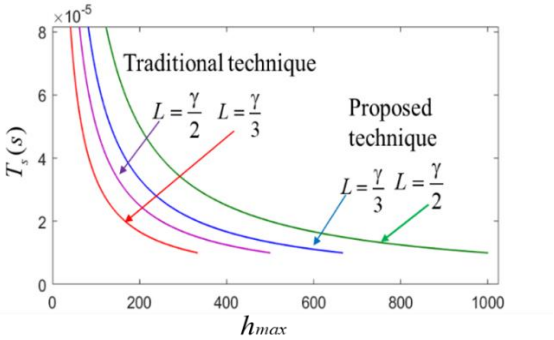

Fig. III. 2 Influence of the parameter L on the MPM to estimate the maximum number of harmonics [49].

After obtaining $[A_e]$, the rest of the matrix is performed as explained [49].

Fig. III. 3 displays the proposed method that is buffered with a short sliding window $\psi(k)$, If we assume that the signal is noiseless, then the enhanced MPM with a short sliding window is expressed as [49]:

$$A(kT_s) \approx \sum_{m=1}^{M}\sum_{i=1}^{M} \Re_i \cdot \Im^{kT_s} \psi(k - m\frac{\gamma}{y}),\ m\frac{\gamma}{y} \in [1, P] \qquad \text{(III-18)}$$

where $\Im = e^{(-\alpha_i + j\omega_i)}$. P is the width of the analyzed data. m refers to the windows' number of windows. y denotes to the overlapping between the windows. As real signals are not steady-states signals, particularly in case of the power of shipboard power systems that is distinguished by the large variation of load and frequency in a short time, it is wise to set $\psi(k)$ to short window size. After operating the proposed method, it detects if the contaminated signal contains interharmonics using several methods. One of the easiest methods that can be performed under MATLAB software is to use the following equation [49]:

$$f_{\text{int}er}(i) = \left| f_i - round(f_i) \right|,\ f_i \in \mathbb{Z}^+,\ round(f_i) \in \mathbb{N}^+ \qquad \text{(III-19)}$$

The role of the function $round(f_i)$ is to approximate f_i to their natural values

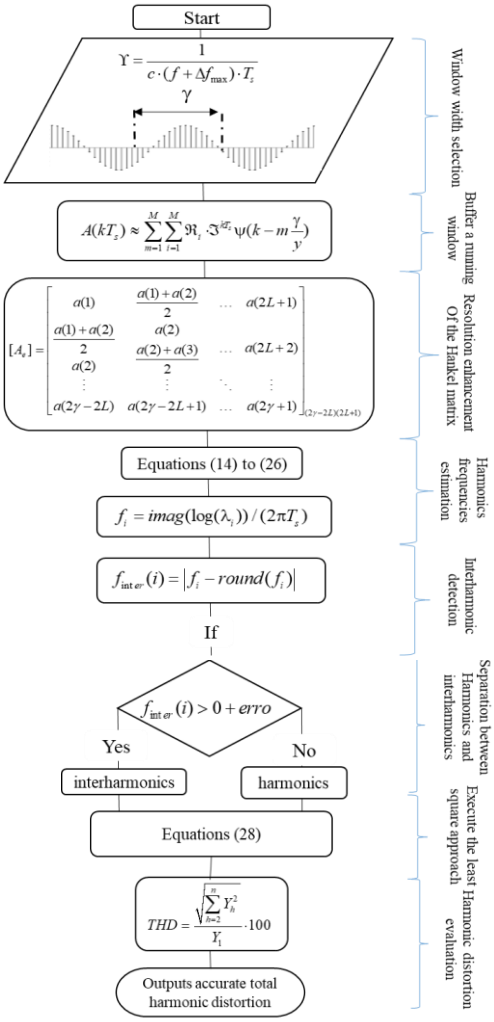

Fig. III. 3 Flow chart of the enhanced MPM [49].

by deleting their digits. Then, it compares if or no. If the result is yes, it means that the signal is contaminated with the interharmonics. is the error that can occur due to the noise, sampling time, or measurement error. For providing a good trade-off between the accuracy and the number of the extracted frequencies, the error is set to $erro = 0.1$ in [49]. After selecting the harmonics and interharmonics separately, the engineers can decide to calculate the global THD using both harmonics and interharmonics or calculate them individually.

III. 2. 1 Simulation results and discussions

The simulation results are carried out under MATLABsoftware. Fig. II. 4 displays the behavior of the standard FFT, the FFT with a short window width, the traditional MPM, and the enhanced MPM. The signal is contaminated with the harmonics and interharmonics. The nominal frequency is 60 Hz, which changes with 8% of the nominal one in the instant 0.27s, and the load varies in the instant 0.16s. As long as the FFT fails to estimate the frequency, in this study case, only the traditional MPM and the proposed method are applied to estimate the frequency. According to the second plot of Fig. III. 4 it is obvious that due to the poor sampling time, the traditional MPM fails to estimate the frequency. However, the proposed method can estimate the frequency accurately and follows the frequency drift in the instant 0.27s with fast transient response. The last plot of Fig. III. 4 portrays the THD estimated by the aforementioned methods. It is obvious that the FFT with a short window fails to estimate accurate THD due to the existence of interharmonics, which results in the appearance of the picket-fence effect and leakage that are clear in the harmonic spectrum of Fig. III. 5(a). Though the standard FFT can overcome the weakness of the ripples and provide better performance in the existence of the interharmonics (see Fig. III. 4), it, however, requires a large transient response (12

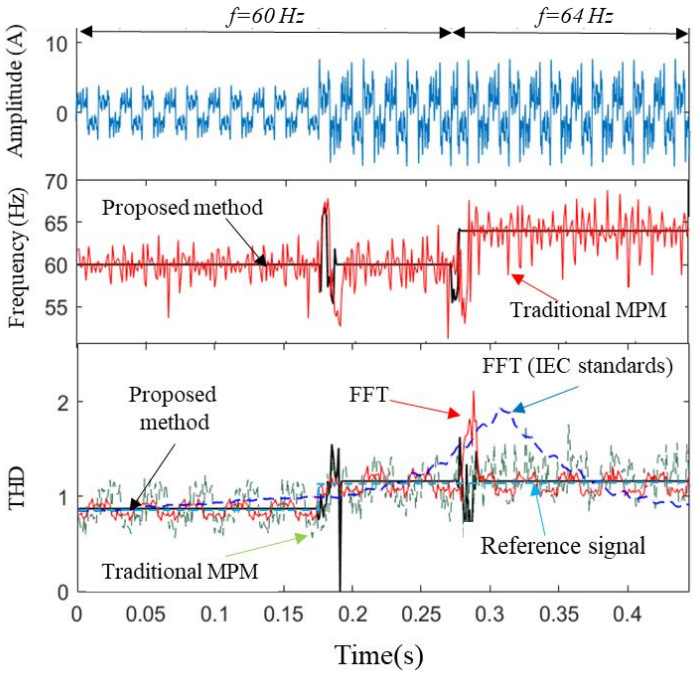

Fig. III. 4 Performance of the traditional MPM, FFT, standard FFT recommended by IEC standards, and the enhanced MPM method in estimating the THD under frequency and load variation [49].

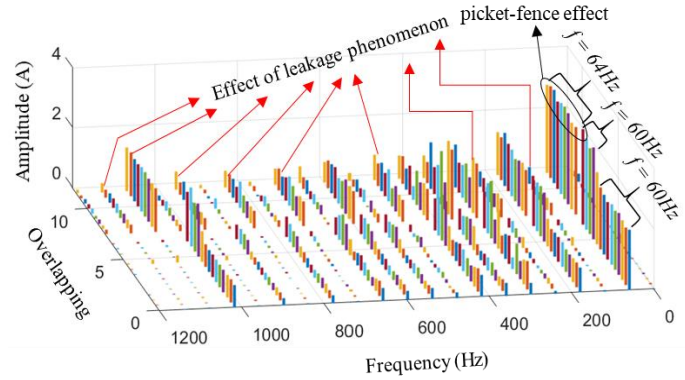
Effect of leakage phenomenon
picket-fence effect
f = 64Hz
f = 60Hz
f = 60Hz
Amplitude (A)
Overlapping
Frequency (Hz)

(a)

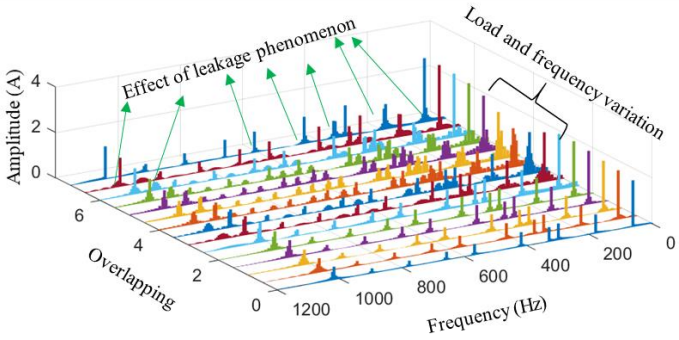
Effect of leakage phenomenon
Load and frequency variation
Amplitude (A)
Overlapping
Frequency (Hz)

(b)

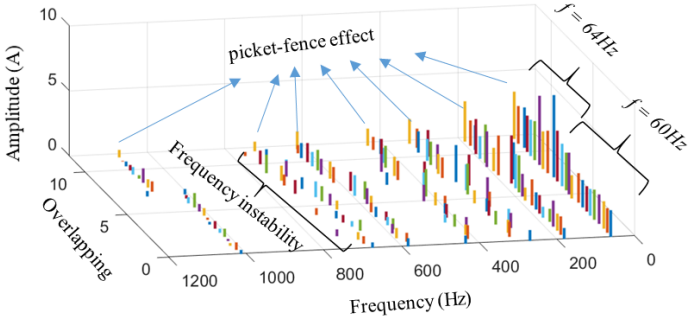
picket-fence effect
f = 64Hz
f = 60Hz
Frequency instability
Amplitude (A)
Overlapping
Frequency (Hz)

(c)

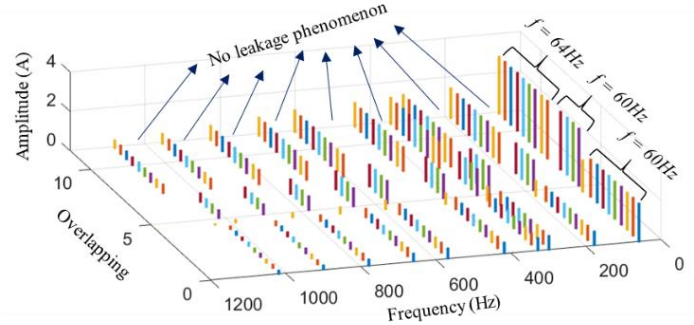

(d)

Fig. III. 5 3D harmonics spectrum extracted by: (a) FFT. (b) Standard FFT. (c) Traditional MPM. (d) Enhanced MPM [49].

cycles) to reach steady-state. Hence, results in the leakage phenomenon as demonstrated in Fig. III. 5(b), which degrades its performance. Furthermore, according to the last plot of Fig. III. 4, the traditional MPM fails to provide accurate estimation as the sampling time is poor, while the proposed method can provide accurate estimation and fast transient response due to the enhanced resolution. This evidence is clear in Fig. III. 5(d) where the spectrum does not struggle from the spectral leakage and the picket-fence.

III. 2. 2 Experimental results and discussions

The experimental results are validated by analyzing the current of a container ship, which is depicted in Fig. III. 6(a). The studied case is selected during the operation windlass and the mooring winches that are presented in Fig. III. 6(b). The distorted current is recorded using Hioki 8847 Memory HiCorder, which presented in Fig. III. 6(c). The current is distorted due to the application of the variable speed drives that are presented in Fig. III. 6(d). The parameters of the electrical power are summarized in Table III. 1.

Fig. III. 7 displays the behavior of the enhanced MPM to assess the THD and frequency of the experimental current. The first plot portrays the distorted current. The second plot displays the supply frequency assessed by the enhanced MPM. The third plot presents the THD estimated by the enhanced MPM and standard FFT. And the fourth plot shows the half symmetry waveform of the distorted current. From the second plot, it is obvious that the real frequency of the SPS varies from 3 to 8% in a short duration. Hence, the application of frequency-dependent methods with short windows may not be good solutions. Moreover, according to the third plot, it is clear that the proposed method can follow the variation of the load with a very small delay.

TABLE III-1
PARAMETERS OF THE CONTAINER SHIP ELECTRICAL SYSTEM [49]

Items and Equipment	Parameters	Values
Main AC bus voltage	Vabc[Vrms]	440 V
	f [Hz]	60 Hz
Diesel generator (3sets)	Vg[Vrms]	450 V
	Pg[kW]	1900 kW
	Xd'[%]	24.6
	Xd''[%]	17.2
	Cos(ψg)	0.8
Windlass & mooring winch (8 sets)	Vm[Vrms]	440 V
	Pm[kW]	45 kW
Main engine	Pm[kW]	20500 kW
Fuel tank	Weight[t]	202 tons
Speed	Knots	21 Knots

Whereas the standard FFT suffers from a front delay due to the large window size, which results in inaccurate values during the load variation.

Fig. III. 8 presents the 3D experimental spectrums estimated by the enhanced MPM and the standard FFT. According to Fig. III. 8 (a) it is obvious the standard FFT fails to estimate the harmonics and interharmonics accurately due to spectral leakage and picket-fence effect. Moreover, during the load variation, it is obvious that the fundamental and harmonics/interharmonics components estimated by the standards FFT have a very slow response to achieve the steady-state. On the other hand, it is evident that the enhanced MPM does not suffer from spectral leakage nor the picket-fence effect. Hence, it can accurately estimate the poles of the signal. Besides, the transient response of the enhanced MPM under load variation is very fast compared to the standard FFT.

(a) (b)

(c) (d)

Fig. III. 6 Experimental measurements. (a) the selected nominated container ship. (b) Windlass and mooring winch. (c) Recording devices (Hioki 8847 Memory HiCorder). (d) variable speed drives [49].

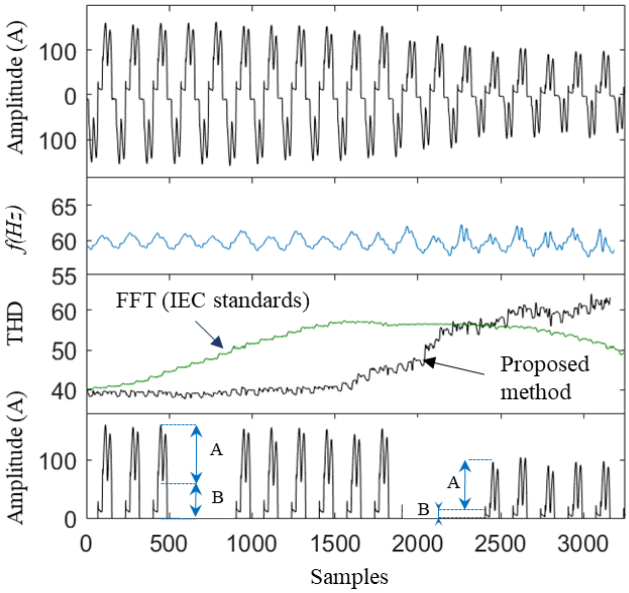

Fig. III. 7 Experimental validation of the enhanced MPM method and standard FFT to estimate the THD [49].

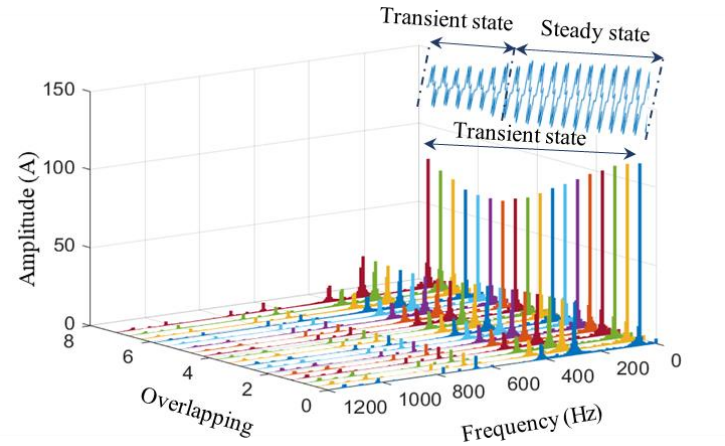

(a)

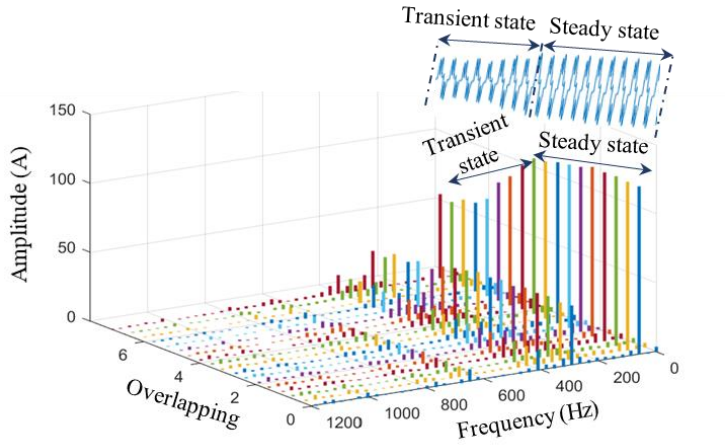

(b)

Fig. III. 8 3D experimental spectral analysis. (a) Using the enhanced MPM. (b) Using the standard FFT [49].

Chapter IV. Power quality improvement of shipboard power systems

This chapter summarizes the contributions of the following papers [27], [56]–[60]. More details can be found in the attached publications of the Appendix.

IV. 1 Introduction

Recently, due to the large increase of power electronics converters (PECs) onboard shipboard power systems (SPSs), harmonics contamination is becoming a serious issue. to deal with this issue, several cost-effective topologies have been proposed in the literature [27], [56]–[60]. The PPFs is one of the most used solutions to mitigate the harmonics and compensate for a degree of the PF [31], [61]. Contrary to the APFs, the PPFs are featured by the cheap price, ease of installation, and maintenance, free of control complexity, and they can be applied in all rates of power (low, medium, and high power). Therefore, their extension to be applied in SPSs benefits from several advantages such as harmonic mitigation, PF compensation, energy efficiency, fuel consumption enhancement, and decrease the emissions [62]. Tuning the PPFs accurately at the aimed harmonics cannot always provide a good harmonics rejection. The most important key factor, which can provide better information about the filtering performance of the PPFs is the harmonic attenuation factor (*HAF*). The smaller the *HAF* is, the better the filtering performance. However, seeking to decrease the *HAF* can affect the filtering sensitivity factor (*FSF*) if the filters are not properly designed. Therefore in [59], a more in-depth harmonic analysis of the *HAF* of PPFs is investigated and improved. Moreover, a theoretical and analytical investigation on how to improve the trade-off between the *HAF* and *FSF* is addressed. Furthermore, new topologies of the PPFs are suggested to achieve a good compromise between the *HAF* and the *FSF*. In [56], a combined topology of hybrid APF and FC-TCR is proposed to enhance the power quality of SPSs. The FC-TCR is connected to reduce the distortion and compensates for the voltage drops. Thus, enhances the voltage stability, whereas the HAPF filters the dominant harmonic currents. In [27], it has been demonstrated that if the FC-TCR compensator is well designed, it will function as a low-pass filter with a cut-off frequency that is lower than the frequencies of the low-order harmonics. Hence, it filters both the dominant and high-order harmonics. Moreover, the control algorithm of the FC-TCR compensator that is proposed in [27] can compensate for the power factor accurately. Hence, improves the efficiency of the SPS. However, According to [63], [64] tending the PF near to unity does not mean good voltage stability. Seeking to tend to the PF towards unity can lead to the overvoltage in some cases. To deal with this issue, in [51] and [52] the FC-TCR compensator is developed to reduce the harmonics and compensates for the voltage sags and swells. Hence, ensures the voltage stability of

the SPS. The estimation of the firing angle to control the FC-TCR is not easy due to the non-linearity characteristic [65]. The traditional method of this obstacle is to use an offline calculation of several values of the FC-TCR inductance, then store it in the microprocessor using the lookup table [25]. Though this technique can provide approximate values of the real inductance needed to be generated by the FC-TCR, its performance, however, suffer under frequency drifts, which is a common problem in SPSs. The numerical methods can be an effective alternative for the lookup table to solve the non-linear equations [66]. Unfortunately, these methods did not attract much attention in controlling the FC-TCR. In this regard, three simple and yet-effective numerical methods are suggested to estimate the firing angle of the FC-TCR compensator in [60]. These techniques that are based on Bisection (BS) technique, Newton-Raphson (N-R) technique, and false position (FP) technique have demonstrated their capability in providing an accurate firing angle estimation of the FC-TCR compensator under load variation and frequency drifts.

IV. 2 Harmonics rejection capability enhancement of passive power filters for all-electric-shipboard microgrids

The PPFs are largely applied in industries to reduce the harmonics and compensate for a degree of PF. There are several types of PPFs such as single tuned filters and high-pass filters [67]. The single tuned topology is the most applied due to its simplicity and capacity to tackle the dominant harmonics. Fig. IV.1 (a) displays the EPS in a single line diagram of the studied hybrid ship. It contains two parallel diesel generators, two propellers that move the ship, an energy storage system to enhance the fuel consumption, and hotel loads. The installed PPFs are tuned at the most dominant harmonics (5^{th} and 7^{th}). Designing the PPF to filter the harmonics and injects the right amount of the capacitive reactive power, which improves the PF can be attained using the following formulas [59]:

$$X_{Lh} = X_{Ch} \Rightarrow \ \omega_n = \frac{1}{\sqrt{LC}} \tag{IV-1}$$

$$X_f = \frac{V_{Lo}^2}{Q_C} \tag{IV-2}$$

where ω_n is the aimed frequency. V_{Lo} is the load voltage. X_f is the equivalent impedance at the fundamental frequency. Q_C is the amount of the capacitive reactive power should be delivered by the PPF and can be calculated as:

$$Q_C = V_{Lo} \cdot i_{Lo} \cdot \sin(\phi) \tag{IV-3}$$

However, tuning the PPF at the aimed harmonic component will not ensure a good harmonic rejection capacity. Hence, studying the *HAF* is crucial to define the

filtering capability of the PPFs. Fig. IV-1(b) portrays the single line diagram of the EPS of the hybrid ship to facilitate the harmonics analysis. Fig. IV.1(c) presents the harmonic equivalent circuit that shows the behavior of PPF in only filtering the harmonics. Therefore, the voltage is short-circuited and the linear load is open-circuited [59]. According to Fig. IV.1(c) the *HAF* can be formulated as:

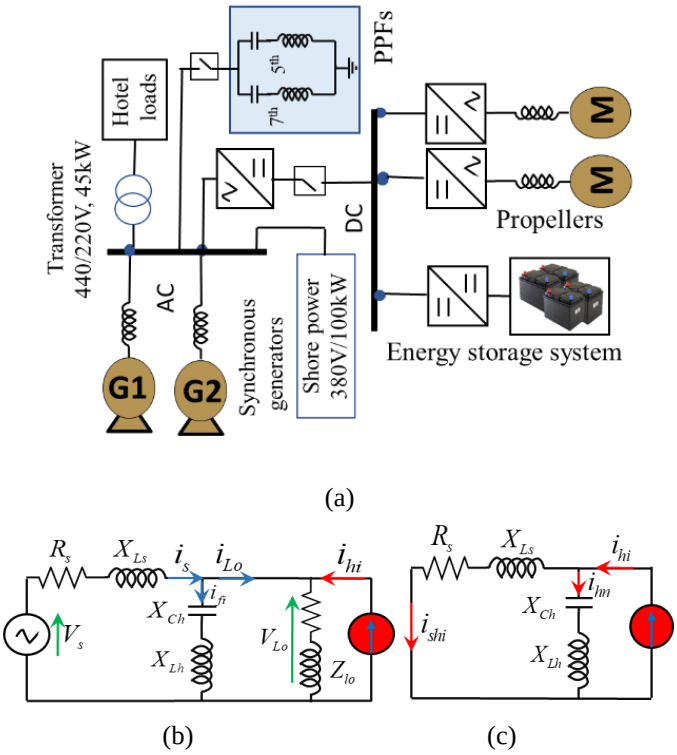

Fig. IV. 1 Schematic diagram of the EPS of the hybrid ferry. (a) single line diagram of EPS. (b) The equivalent circuit of Fig. IV.1(a) in a per-phase base form. (c) the equivalent harmonic circuit in a per-phase base form of Fig. IV.1(b) [59].

$$\partial = \frac{I_{shi}}{I_{hi}} = \frac{\left|X_{Lh} - X_{Ch} + R_{fi}\right|}{\left|X_{Lh} - X_{Ch} + X_{Ls} + R_{fi} + R_s\right|} \tag{IV-4}$$

After some mathematical improvement, (IV-4) becomes [59]:

$$\partial = \frac{\left|(2\cdot\pi\cdot f\cdot h\cdot L - 1/(2\cdot\pi\cdot f\cdot h\cdot C))\,j + R_{fi}\right|}{\left|(2\cdot\pi\cdot f\cdot h\cdot L - 1/(2\cdot\pi\cdot f\cdot h\cdot C) + 2\cdot\pi\cdot f\cdot h\cdot L_s)\,j + R_{fi} + R_s\right|} \tag{IV-5}$$

$$\partial = \frac{\left|2\cdot\pi\cdot f\cdot h\cdot j(L-1/((2\cdot\pi\cdot f\cdot h)^2 C))+R_{fi}\right|}{\left|(2\cdot\pi\cdot f\cdot h\cdot j(L+L_s-1/((2\cdot\pi\cdot f\cdot h)^2 C))+R_{fi}+R_s\right|} \quad \text{(IV-6)}$$

According to Fig IV.2 (a) and (b), it is clear that the larger X_{Lh} and X_{Ch} are, the larger value of X_{Ls} is needed to attenuate the *HAF*. Therefore, if X_{Ls} is not high enough, the performance of the PPF degrades. Moreover, according to Fig. IV.2 (c) and (d) the behavior of the *HAF* of the PPF resembles the one presented in Fig IV.2 (a) and (b). However, the increase of the filter resistance degrades the filtering performance. Hence, it is crucial to select an optimal quality factor Q_f during designing the PPF to enhance the harmonic rejection capability of the PPFs.

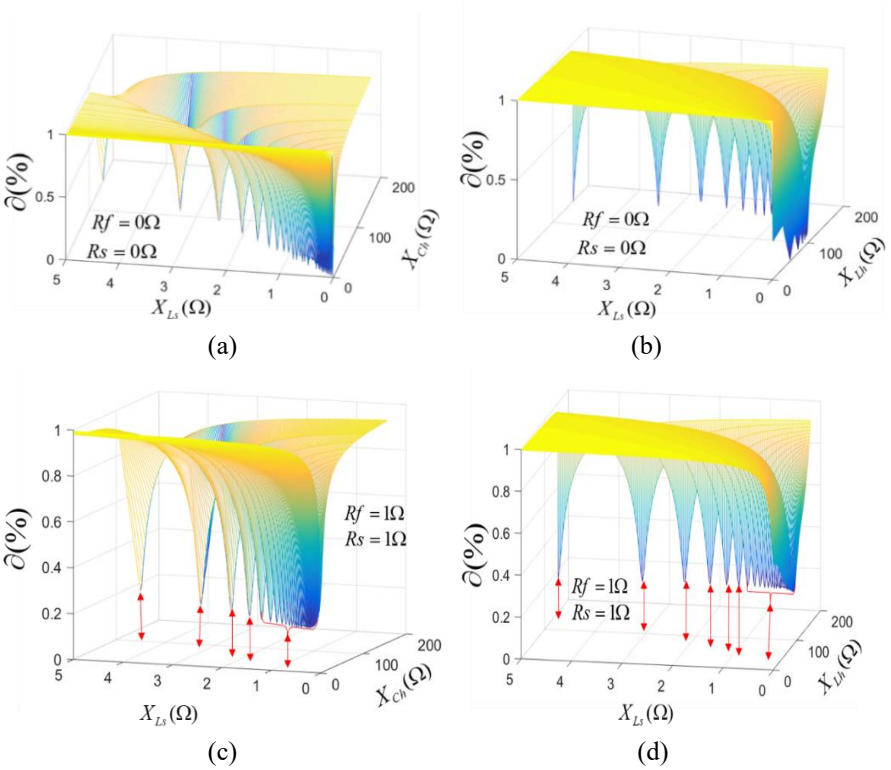

Fig. IV. 2 *HAF* of the PPFs. (a) *HAF* of the PPF in terms of the variation of X_{Ls} and X_{Ch}. (b) *HAF* of the PPF in terms of the variation of X_{Ls} and the X_{Lh}. (c) *HAF* of the PPF in terms of the variation of X_{Ls} and X_{Ch} with $R_f = R_s = 1\ \Omega$. (d) *HAF* of the PPF in terms of the variation of X_{Ls} and the X_{Lh} with $R_f = R_s = 1\ \Omega$ [59].

The *FSF* of the PPFs can be expressed as [59]:

$$FSF_L = \frac{M}{2 \cdot \pi \cdot f \cdot h \cdot L} \tag{IV-7}$$

$$FSF_C = D \cdot 2 \cdot \pi \cdot f \cdot h \cdot C \tag{IV-8}$$

where FSF_L is the *FSF* of the inductance and FSF_C is the *FSF* of the capacitance of the PPF, M and D are respectively the numbers of the shunted inductors and capacitors. Fig. IV.3 is added to portray the behaviour of the *FSF* of the fundamental component and the 5th and 7th harmonic components. Fig. IV. 3(a) displays the behaviour of FSF_C with different values of the PPF capacitance and frequency variation. It is obvious that seeking to enhance the *HAF* by increasing C results in increasing FSF_C, which deteriorates the EPS stability. Furthermore, the *FSF* behaves differently with the order of harmonics, where the larger order is, the more sensitivity is. Fig. IV. 3(b) portrays the behaviour of FSF_L with different values of the PPF inductor and frequency variation. It is clear that seeking to enhance the *HAF* by decreasing the inductance of the PPF results in increasing FSF_L, which affects the system stability and can result in disastrous consequences. In addition, based on Fig. IV. 3(c) it proves that varying the PPF parameters to enhance the *HAF* does not affect the filter total impedance Z_{tot} at the aimed frequency. Therefore, enhancing the *HAF* can affect the *FSF,* but it does not appear at the total filter impedance.

According to [59], in order to enhance both the *HAF* and the *FSF*, the PPF can be shunted as displayed in Fig. IV. 4. The *HAF* is enhanced by decreasing the parameters of the PPFs, and adding extra inductance to compensate for the reactive power caused by this decrease. Whereas the *FSF* is enhanced by paralleling the PPFs instead of decreasing their parameters. Hence, the novel *HAF* becomes [59]:

$$\partial_2 = \frac{I_{shi}}{I_{hi}} = \frac{\left| \frac{X_{Lh} \cdot X_{Lh}}{X_{Lh} + X_{Lh}} - \frac{X_{Ch} \cdot X_{Ch}}{X_{Ch} + X_{Ch}} + \frac{R_{fi} \cdot R_{fi}}{R_{fi} + R_{fi}} \right|}{\left| \frac{X_{Lh} \cdot X_{Lh}}{X_{Lh} + X_{Lh}} - \frac{X_{Ch} \cdot X_{Ch}}{X_{Ch} + X_{Ch}} + \frac{R_{fi} \cdot R_{fi}}{R_{fi} + R_{fi}} + X_{Ls} + R_s \right|} \tag{IV-9}$$

After some mathematical development (IV-9) becomes [59]:

$$\partial_2 = \frac{\left| \frac{1}{2} X_{Lh} - \frac{1}{2} X_{Ch} + \frac{1}{2} R_{fi} \right|}{\left| \frac{1}{2} X_{Lh} - \frac{1}{2} X_{Ch} + X_{Ls} + \frac{1}{2} R_{fi} + R_s \right|} \tag{IV-10}$$

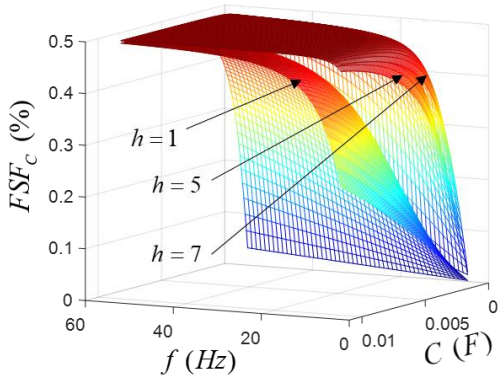

(a)

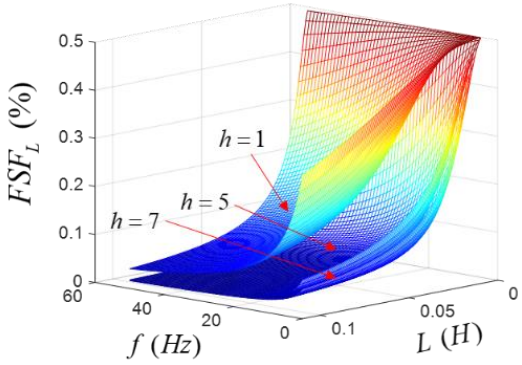

(b)

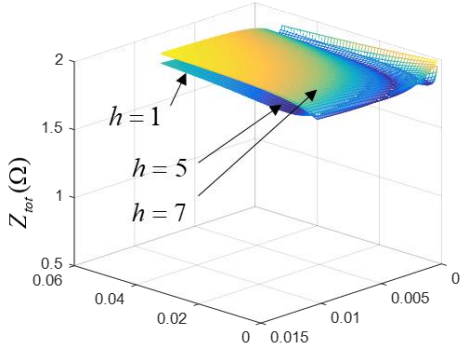

(c)

Fig. IV. 3 (a) Behaviour of the *FSF* in terms of the PPF capacitance and frequency variation. (b) behaviour of the *FSF* in terms of the PPF inductance and frequency variation. (c) behavour of Z_{tot} in terms of its capacitance and inductance [59].

Based on (IV-10) it is obvious that the topology proposed in Fig. IV. 4 can decrease the *HAF* without affecting the *FSF*.

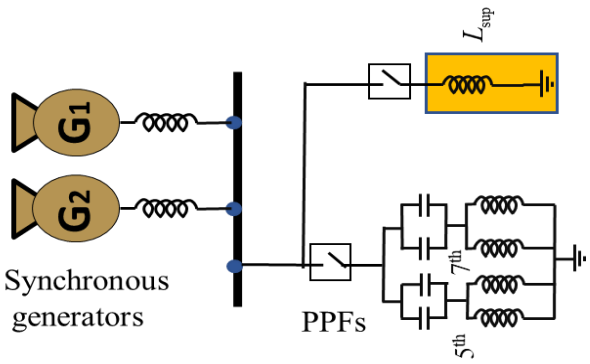

Fig. IV. 4 Modified topology of the PPF to enhance the *HAF* without affecting the *FSF* [59].

IV. 2. 1 Simulation results and discussion

The simulation results are carried out under MATLAB/Simulink software. The main system parameters are listed in Table IV.1. Fig. IV.5 and 6 portray the behaviour of the PPFs in harmonic suppression of the EPS of the hybrid ferry. The plots of this figure present respectively the load voltage V_{Lo}, the load current i_{lo}, the source current i_s, the filter current, and the THD of i_{lo} and i_s. As long as the *HAF* is not considered in this study case, it is obvious that when connecting the PPFs in the instant 0.06s, the THD of i_s is reduced only by 9% (from 26% to 17%). However, when the *HAF* and *FSF* are taken into account based on the topology depicted in Fig. IV. 4, it is clear in Fig. IV. 6 that when connecting the PPFs in the instant 0.06s, the THD is reduced by 14% (from 26% to 12%). It is worthy to declare that the THD can be enhanced to less than 12% if more filters for other aimed harmonics are installed.

Fig. IV. 7 displays the harmonics spectrum of i_s. It is observable that when using the proposed topology based on the enhanced HAF and FSF, the spectrum has fewer harmonics.

Table IV.1: System Parameters [59]

Category	Parameters	Values
Synchronous generators	RMS voltage	V=450V
	Electric Power	P= 2x88 ekW
propellers	Rated power	2x112kW/1620rpm
Hotel loads	Nominal power	P=35 ekW
PPFs	5^{th} harmonic filter	$L = 0.006 / 0.016H$ $C = 67.54/25.3302\ \mu F$
	7^{th} harmonic filter	$L = 0.006 / 0.016H$ $C = 34.46/12.92\ \mu F$
	Supporter inductance	$L_{sup} = 0.06H \quad R = 2\Omega$

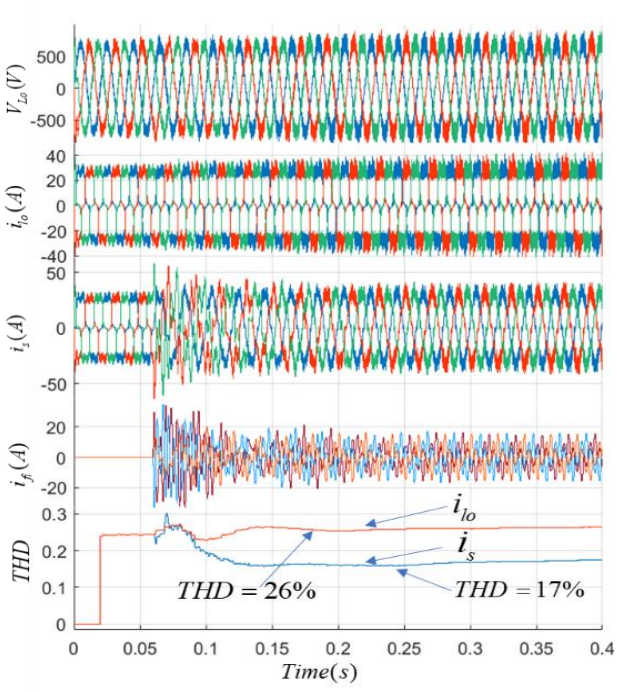

Fig. IV. 5 Performance of the PPF without considering the *HAF* [59].

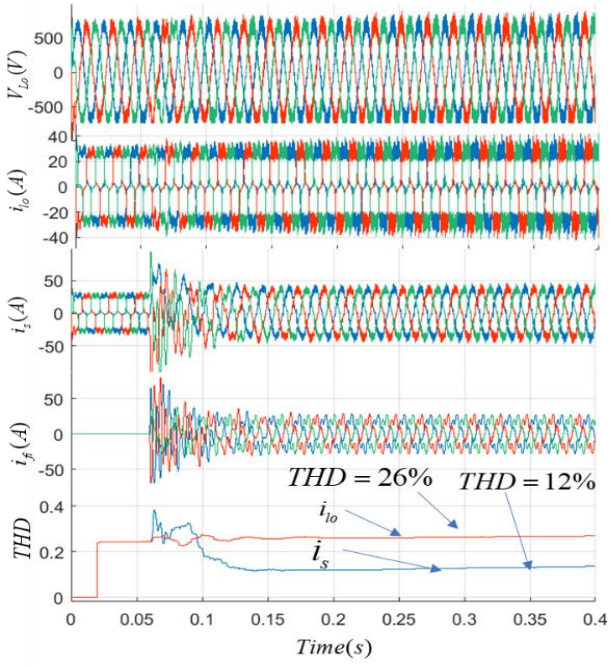

Fig. IV. 6 Performance of the PPF with low *HAF* and high *FSF* [59].

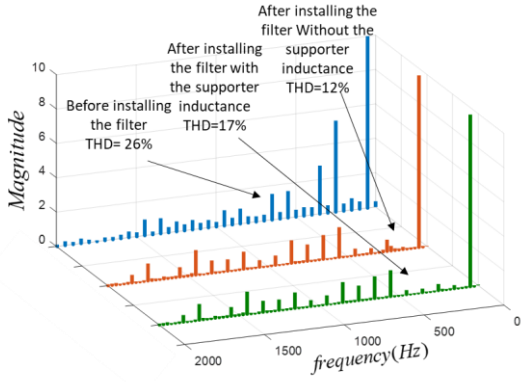

Fig. IV. 7 Harmonics spectrum of i_s before and after installing the proposed topology [59].

IV. 3 A hybrid compensator configuration for var control and harmonic suppression in all-electric shipboard power systems

The common solutions for improving the power quality issues cannot always be ideal solutions for some applications such as medium voltage SPSs. For example, the PPFs are one of the most used solutions to reduce the dominant harmonics and compensate for the PF [31],[68]. Although this solution is distinguished by the ease of installation and maintenance, it, however, suffers from several deficiencies such as the fixed tuning characteristic, bulkiness, limited amount of reactive power, risk of inducing the resonance …etc. On the other hand, the APFs can over the drawbacks of the PPFs [69], [55], [70]. However, their application to medium or high power applications requires a high-cost implementation. Besides, implementing the APFs in EPSs that have a contaminated voltage with a THD that is more than 8% leads to shorten the lifetime of the dc-link capacitor [26], [71].

In this regard, a cost-effective compensator is developed in [27] to overcome the drawbacks of the traditional filters. This compensator, which is based on the FC-TCR compensator can act as a low-pass filter, thus, filters all the harmonics after the cut-off frequency and tends the PF towards unity. Furthermore, this compensator is featured by the low switching losses; thus, its implementation for medium and high power applications is efficient. Fig. IV. 8 presents the single line diagram of the FC-TCR compensator connected the switchboard of the EPS of an SPS. The studied ship is a Semi-Submersible Deck Cargo/Heavy-Lift Carrier.

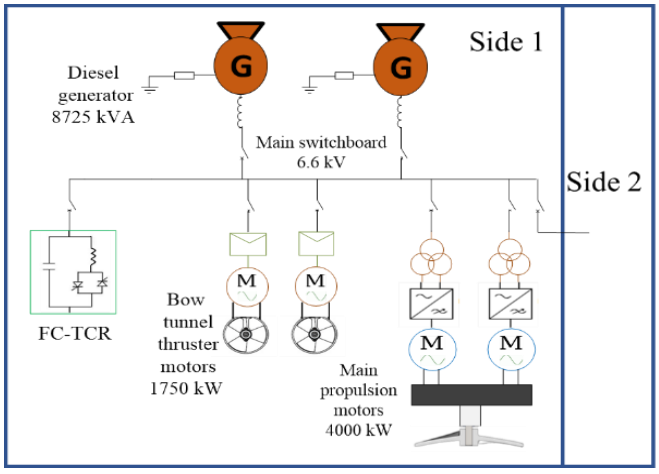

Fig.IV. 8 single-line diagram of the FC-TCR compensator connected to the EPS of the selected ship [27].

The simplified single line diagram of the FC-TCR compensator that is connected to the EPSs of the ship is depicted in Fig. IV. 9. Fig. IV. 9(a) displays the equivalent circuit in a per-phase form. Fig. IV. 9(b) simplifies Fig. IV. 9(a) by considering the nonlinear loads as a linear load plus sources of harmonics, then Fig. IV. 9(c) considers only the harmonics behavior with the filter. Thus, the source is shortcircuited and the linear load is open-circuited.

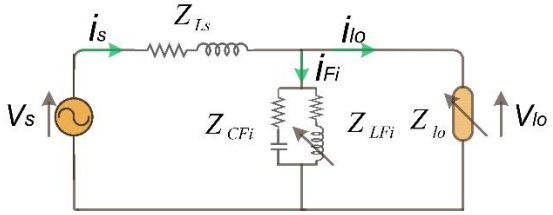

(a)

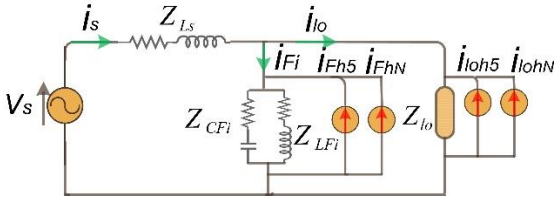

(b)

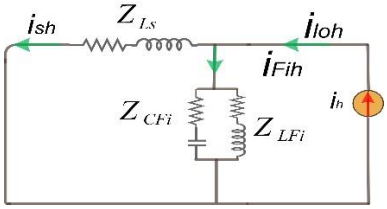

(c)

Fig. IV. 9 The single-line schematic basic principle of the proposed filter. (a) The equivalent circuit of Fig. IV. 8 in a per-phase base form. (b) A simplified circuit of Fig. IV. 9 (a). (c) The equivalent harmonic circuit of Fig. IV. 9(a) [27].

Based on Fig. IV. 9(c), the harmonic attenuation factor ∂, which shows the harmonic rejection capability of the FC-TCR compensator is calculated as [27]:

$$\partial = \frac{I_{sh}}{I_{loh}} = \frac{\left| \frac{Z_{LFi} \cdot Z_{CFi}}{Z_{LFi} + Z_{CFi}} \right|}{\left| \frac{Z_{LFi} \cdot Z_{CFi}}{Z_{LFi} + Z_{CFi}} + Z_{Ls} \right|} \qquad \text{(IV-11)}$$

The smaller ∂ is, the better harmonic rejection capability, after some mathematical manipulations (IV-11) becomes [27]:

$$\partial = \frac{\left| \frac{(X_{LFi} + R_{LFi}) \cdot (X_{CFi} + R_{CFi})}{X_{LFi} + R_{LFi} + X_{CFi} + R_{CFi}} \right|}{\left| \frac{(X_{LFi} + R_{LFi}) \cdot (X_{CFi} + R_{CFi})}{X_{LFi} + R_{LFi} + X_{CFi} + R_{CFi}} + X_{Ls} + R_{Ls} \right|} \quad \text{(IV-12)}$$

$$\partial = \frac{\left| \frac{X_{LFi} \cdot R_{CFi} + X_{LFi} \cdot X_{CFi} + R_{LFi} \cdot X_{CFi} + R_{LFi} \cdot R_{CFi}}{X_{LFi} + R_{LFi} + X_{CFi} + R_{CFi}} \right|}{\left| \frac{X_{LFi} \cdot R_{CFi} + X_{LFi} \cdot X_{CFi} + R_{LFi} \cdot X_{CFi} + R_{LFi} \cdot R_{CFi}}{X_{LFi} + R_{LFi} + X_{CFi} + R_{CFi}} + X_{Ls} + R_{Ls} \right|} \quad \text{(IV-13)}$$

$$\partial = \frac{1}{\left| 1 + \frac{X_{LFi} \cdot X_{Ls} + R_{LFi} \cdot X_{Ls} + X_{CFi} \cdot X_{Ls} + R_{CFi} \cdot X_{Ls} + X_{LFi} \cdot R_{Ls} + R_{LFi} \cdot R_{Ls} + X_{CFi} \cdot R_{Ls} + R_{CFi} \cdot R_{Ls}}{X_{LFi} \cdot R_{CFi} + X_{LFi} \cdot X_{CFi} + R_{LFi} \cdot X_{CFi} + R_{LFi} \cdot R_{CFi}} \right|} \quad \text{(IV-14)}$$

Fig. IV. 10(a) portrays the behavior of ∂ in terms of X_{CFi} and X_{LFi} with different values of the resistance of the capacitor. It is obvious that the smaller X_{CFi} is, the higher the rejection capability is. While the variation of X_{LFi} has no effect on the filtering capability. Moreover, the increase of the fixed capacitor resistance increases ∂, which results in affecting the filtering capability of the filter. Fig. IV. 10(b) presents the behavior of ∂ in terms of X_{CFi} and X_{LFi} with different values of the resistance of the main impedance R_{Ls}. Contrary to the capacitor resistance, which affects the filtering capability, the increase of the main impedance enhances the harmonic rejection capability of the FC-TCR by forcing the harmonics to flow into the capacitor. Fig. IV. 10(c) portrays the behavior of ∂ in terms of X_{CFi} and X_{LFi} with different values of the resistance of the TCR inductance R_{LFi}. It is clear that the variation of R_{LFi} does not influence on the filtering capability of the FC-TCR since the harmonics flow into the capacitor during the filtering process. Fig. IV. 10(d) presents the behavior of ∂ in terms of X_{Ls} and X_{LFi} with different values of X_{CFi}. It is clear that both the increase of X_{Ls} or the decrease X_{LFi} contributes to enhancing the filtering performance of the FC-TCR compensator. Whereas the variation

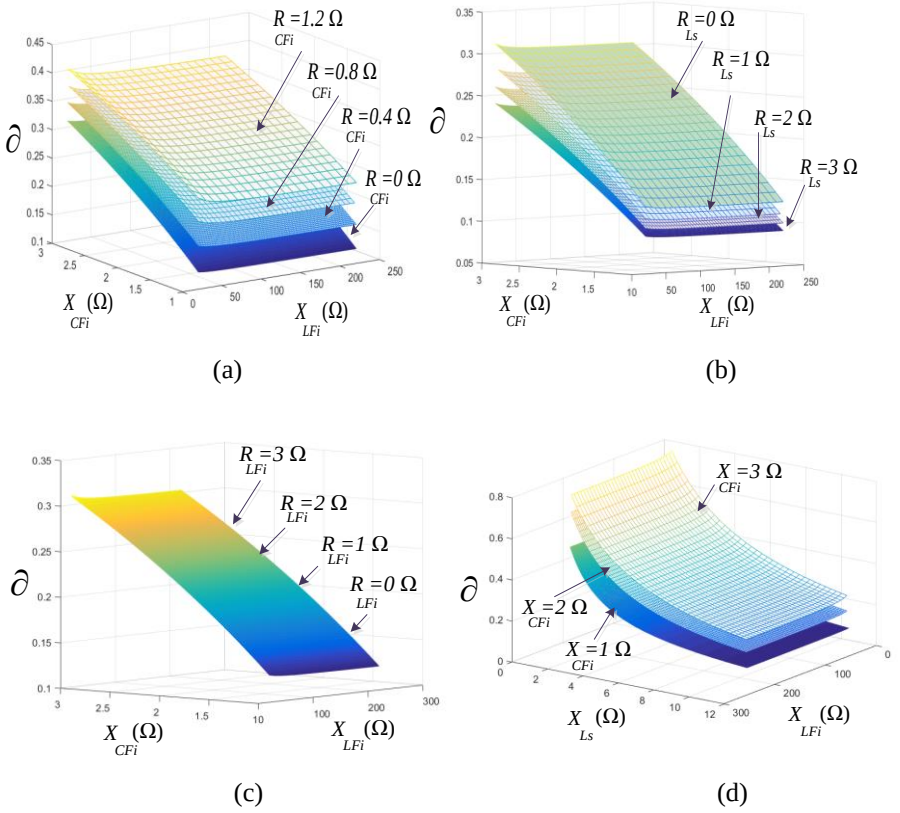

Fig. IV. 10 behaviour of harmonic attenuation factor under system parameter variation. (a) Behaviour of ∂ during the variation of the fixed capacitor resistance in terms of X_{LFi}, X_{CFi}. (b) Behaviour of ∂ during the variation of the main impedance resistor in terms of X_{LFi}, X_{CFi}. (c) Behaviour of ∂ during the variation of the TCR resistance in terms of X_{LFi}, X_{CFi}. (d) Behaviour of ∂ during the variation of X_{CFi} in terms of X_{Ls}, X_{LFi} [27].

of the parameters of X_{LFi} does not affect the filtering performance. From these figures, we can observe that there is a compromise between increasing X_{LFi} or decreasing X_{Ls} to reduce ∂. Hence, for an acceptable harmonic rejection capability of the FC-TCR, the following equation should be guaranteed [27].

$$\left|\frac{(X_{LFi}+R_{LFi})\cdot(X_{CFi}+R_{CFi})}{X_{LFi}+R_{LFi}+X_{CFi}+R_{CFi}}\right| << \left|X_{Ls}+R_{Ls}\right| \qquad \text{(IV-15)}$$

IV. 3. 1 Simulation results

The numerical analysis are taken under MATLAB/Simulink software using the structure of Fig. IV. 8. Fig. IV. 11 depicts the control method of the FC-TCR, which is performed in an open-loop manner. Hence benefits from several advantages such as simplicity and fast dynamic response. The parameters of the EPS are listed in Table. IV. 2.

Fig. IV. 12 shows the performance of the FC-TCR compensator to filter the harmonics and compensate for the PF. The load voltage V_{lo} and the current are harmonically contaminated with a THD of respectively 42%, and 10% that exceeds the IEC61000-3-6 and IEEE Std 519™-2014 standards, whereas the PF is 0.82, which does not respect the standards as well. The voltage distortion is a bit high to demonstrate the efficacy of the harmonic rejection capability of the FC-TCR. In the instant 0.06s, only the capacitor of the FC-TCR is connected. It is obvious that the amount of capacitive reactive power generated by this capacitor moves the lagging PF to be a leading PF. Besides, by ensuring the formula (IV-15), it is obvious that the waveform of V_{lo} and I_s is improved by decreasing the THD to less than 5%, which respects the abovementioned standards. In addition, when connecting the TCR in the instant 0.12s, it is observable that the controlled inductive reactive power of the TCR tends the PF towards unity, while the THDs of V_{lo} and I_s remain stable. During the load variation in the instant 0.24s, it is clear that the FC-TCR has a fast dynamic response in suppressing the harmonics and compensating the PF.

Table IV. 2 parameters of the EPS of the SPS [27]

Category	Parameters	Values
Synchronous generators	Nominal voltage	V=6.6 kV (+6%, -10%)
	Electric Power	P=6980 ekW,
	Apparent power	S=8725 kVA,
propellers	Rated power	P=4000 kW
thrusters	Rated power	P=1750 kW
Shifted Transformers	Transformed voltage	V=6.6 kV/715V
Non-linear loads	Rated power	P=700kW
FC-TCR compensator	Main impedance	$L_{Ls}=0.006\ H\ \ R_{Ls}=0.5\ \Omega$
	Switched capacitor	$L_{Fi}=450\ \eta F\ \ R_{CFi}=0.5\ \Omega$
	TCR inductor	$L_{Fi}=5\ mH\ \ R_{LFi}=0.5\ \Omega$

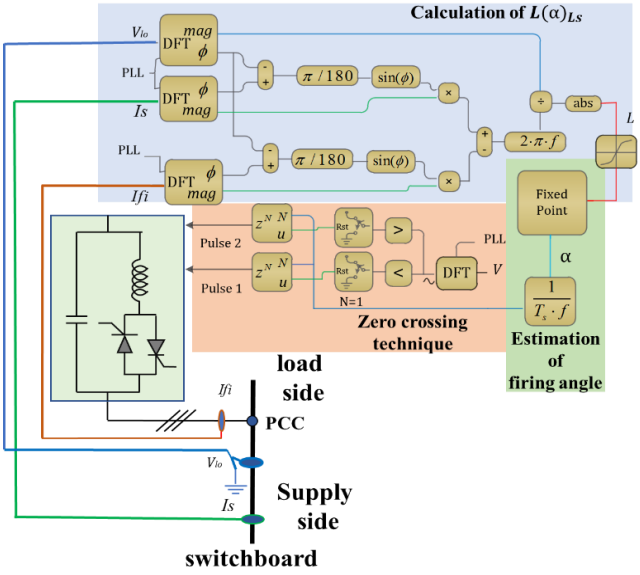

Fig. IV. 11 Control algorithm of the FC-TCR compensator [27].

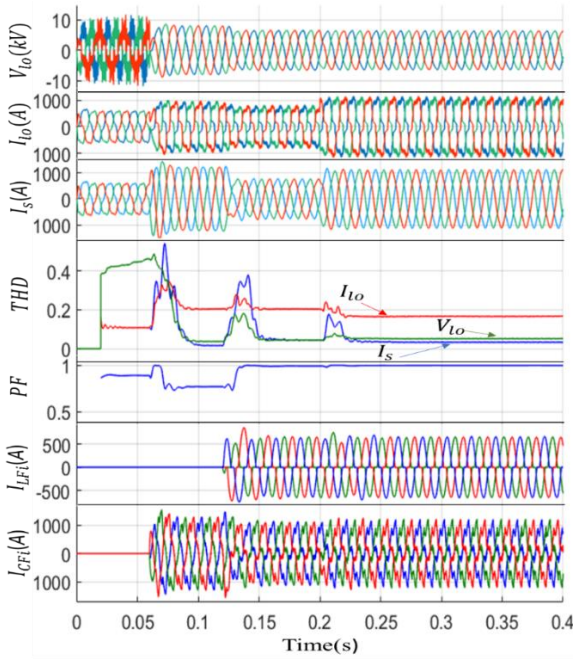

Fig.IV. 12 Performance of the FC-TCR compensator in filtering harmonics and compensating the PF under load variation [27]

IV. 4 Voltage stability and harmonic mitigation of shipboard power systems

In [27], it has been demonstrated that the FC-TCR compensator can suppress the harmonics of SPSs and compensates for the PF. However, according to [63], [64] in some cases, tending the PF near to unity does ensure good voltage stability. In this regard, the authors in [56]–[58] apply the FC-TCR to reduce the harmonics and compensate for the voltages sags. Hence, ensures voltage stability.

The voltage stability hypothesis can be described as the attempt of the loads to absorb a larger power than the power supplies and transmission lines can deliver. If load demand varies suddenly due to certain disturbances such as short circuits, the system might lose the equilibrium and results in the voltage collapse. Hence, the engineers of SPSs should ensure adding some solutions such as the static var compensators (SVCs) or batteries to provide a surplus power to guarantee the stable operation of the EPS under worse conditions to avoid the blackout of the ship [72]. Furthermore, based on some ship classification societies and standards such as the IEEE 45:2002[73], IEC 60092-101:2002[74], ABS 2008[75], when compensating the reactive power, the overvoltage must not exceed +6%.

Based on Fig. IV. 9(b), before connecting the FC-TCR compensator, the load current is presented as [58]:

$$\bar{I}_S = \bar{I}_{lo} = \frac{\bar{V}_s - \bar{V}_{lo}}{-jX_{Ls}} = \frac{\bar{V}_s}{(X_{lo} + X_{Ls}) \cdot j + R_{lo}} \tag{IV-16}$$

From (IV-16), the load power can be formulated as:

$$P = \frac{V_s^{\,2} \cdot R_{lo}}{(X_{lo} + X_{LS})^2 + R_{lo}^{\,2}} \tag{IV-17}$$

where $Z_{lo} = R_{lo} + X_{lo}$. According to the complex impedance plane, we have

$$\tan(\phi) = \frac{X_{lo}}{R_{lo}} \Rightarrow X_{lo} = R_{lo} \cdot \tan(\phi) \tag{IV-18}$$

Substituting (IV-18) in (IV-17) leads to

$$P = \frac{V_s^{\,2} \cdot R_{lo}}{(R_{lo} \cdot \tan(\phi) + X_{Ls})^2 + R_{lo}^{\,2}} \tag{IV-19}$$

The condition to calculate the maximum amount of power, which the EPS can deliver to the load is

$$\frac{\partial P}{\partial R_{lo}} = 0 \quad \Rightarrow \quad X_{Ls} = \sqrt{R_{lo}^{\,2} + R_{lo}^{\,2} \cdot \tan^2(\phi)} \tag{IV-20}$$

For the sake of simplicity, if we assume that the PF is close to unity ($\phi \approx 0 \Rightarrow \cos(\phi) \approx 1$), then (IV.20) becomes

$$X_{Ls} \approx R_{lo} \tag{IV-21}$$

It implies that the maximum power can be drawn by the load is:

$$P_{\max} = \frac{V_s^{\,2}}{2 \cdot R_{lo}} = \frac{V_s^{\,2}}{2 \cdot X_{Ls}} \tag{IV-22}$$

Fig. IV. 13(a) presents the maximum power, which the system can supply. The positive part of the Y-axis indicates the inductive reactive power, while the negative part indicates the capacitive reactive power. It is obvious that the increase of the inductive reactive power limits the amount of active power that can be drawn by the load. However, the increase of the capacitive reactive power helps the load to draw more active power. Fig. IV. 13(b) displays the parabola, which shows the behavior of the voltage during consuming the active and reactive power. The upper half area of each parabola presents the stable area, while the lower area presents the unstable area. The points that connect the unstable areas with the stable ones are known as the critical points and represent the maximum amount of the active power that can be absorbed. It is obvious that the increase of $\tan(\phi)$ on the positive side leads to minimizing the amount of active power due to the absorption of the inductive reactive power. However, the increase of $\tan(\phi)$ in the negative side results in increasing the amount of the active power that can be absorbed due to the increase of capacitive reactive power. Hence, this study demonstrates that the injection of capacitive reactive power can compensate for the voltage sags and improve voltage stability. However, a large injection causes over-voltage and rises the critical points. Hence, performing the voltage stability analysis before compensating the PF is crucial.

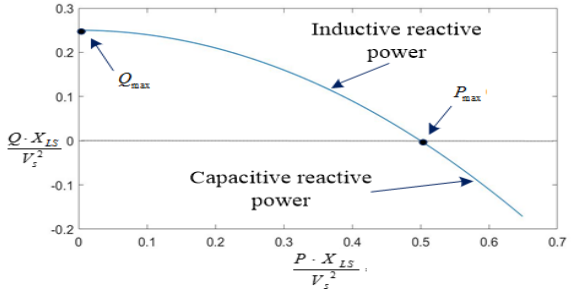

(a)

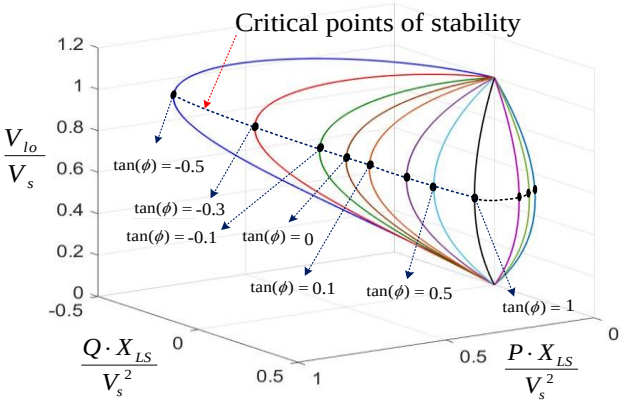

(b)

Fig.IV. 13 voltage stability of the EPS (a) Maximum power can be drawn by the load. (b) 3D PV curve [58]

IV. 4. 1 Numerical results and analysis

The simulation results of modelled SPS, which is presented in Fig. IV. 8 are carried out under MATLAB/Simulink environment, and the parameters of the system are summarized in Table .VI. 3.

Fig. IV. 14(a) presents the voltage control model of the FC-TCR compensator. This method starts by comparing the load voltage V_{lo} with a reference voltage, then apply PI controller to correct the error. In order to enhance the stability of the algorithm, the limitation function is applied to confine the maximum and minimum values of the inductance that the TCR can deliver. Then, the linearization block uses the following formula to estimate the firing angle [57].

$$-2\alpha + \sin(2\alpha) = \pi\left(\frac{L_{FI}}{L_{FI}(\alpha)} - 2\right) \tag{IV-23}$$

The last step is to use the estimated firing angle to perform the zero-crossing method to supply the pulses to the TCR. In order to extract the fundamental component of the voltage to perform the zero-crossing method, any method such as the DFT can be used.

Fig. IV. 14(b) presents the voltage control-based average model of the FC-TCR compensator connected to the EPS of the SPS. Based on this model, the open-loop transfer function is calculated as [58]:

Table. IV. 3 System Parameters [57]

Synchronous generators	Nominal voltage Electric Power Apparent power Baserotational peed	V=6.6 kV (+6%, -10%) P=6980 ekW, S=8725 kVA, Ω=720 rpm.
propellers	Rated power	P=4000 kW
thrusters	Rated power	P=1750 kW
Shifted Transformers	Transformed voltage	V=6.6 kV/715V
Non-linear loads	Rated power	P=700 kW
FC-TCR HF	Inductance capactitance	L=0.006 mH C=500 μF
PPFs	5^{th} harmonic filter 7^{th} harmonic filter	L5=0.002 H, C= 202.642 μF L5=0.002 H, C= 103.389 μF

$$G_{OL} = \frac{\dfrac{s \cdot L_{Fi}}{1 + s^2 \cdot L_{Fi} \cdot C_{Fi}}}{1 + \dfrac{s \cdot L_{Fi}}{1 + s^2 \cdot L_{Fi} \cdot C_{Fi}} \dfrac{1}{R_{lo} + s \cdot L_{lo}}} \cdot (k_p + \frac{k_i}{s}) \qquad \text{(IV-24)}$$

After some mathematical manipulation, the transfer function G_{OL} becomes [58]:

$$G_{OL} = (k_p + \frac{k_i}{s})$$

$$\frac{L_{Fi}(s^3 \cdot L_{Fi} \cdot C_{Fi} \cdot L_{lo} + s^2 \cdot L_{Fi} \cdot C_{Fi} \cdot R_{lo} + s \cdot L_{lo} + R_{lo})}{s^5 \cdot {L_{Fi}}^2 \cdot {C_{Fi}}^2 \cdot L_{lo} \cdot L_s + s^4 \cdot L_{Fi} \cdot C_{Fi} \cdot R_{lo} \cdot L_s + s^3 (L_{Fi} \cdot C_{Fi} \cdot L_s (2L_{lo} + L_{Fi})) + 2s^2 \cdot L_{Fi} \cdot C_{Fi} \cdot R_{lo} \cdot L_s + s \cdot L_s (2L_{lo} + L_{Fi}) + R_{lo} \cdot L_s}$$

(IV-25)

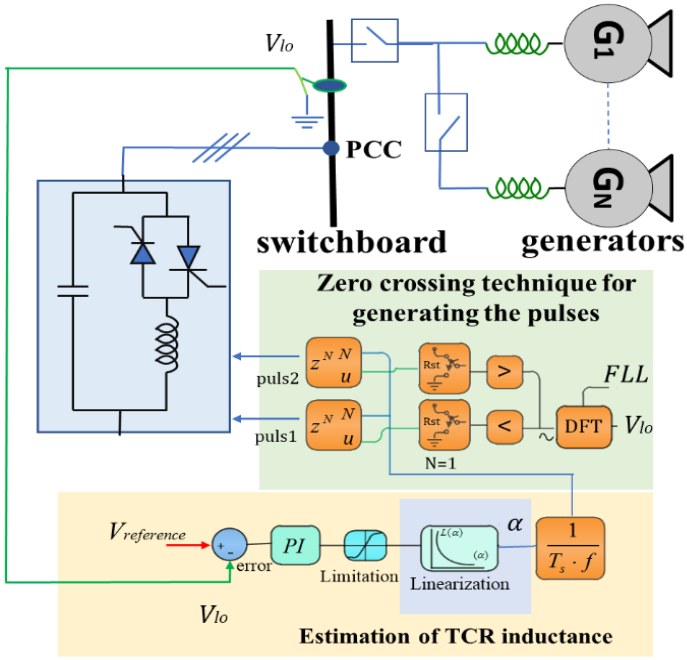

(a)

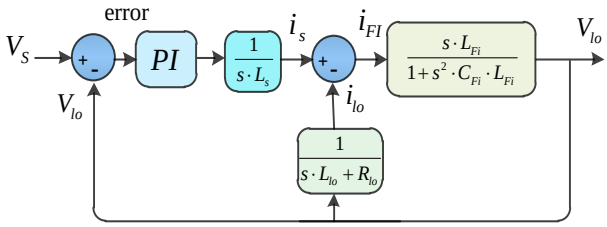

(b)

Fig. IV. 14 Control algorithm of the FC-TCR (a) Voltage based control of the FC-TCR. (b) Average model-based voltage control model of the FC-CTR [58].

Fig. IV. 15 displays the Bode plot of open-loop function and the step response of (IV-25) that are obtained using MATLAB software. As long as (IV-25) is a high order transfer function, finding the PI parameters is not straightforward. Therefore, applying some software like the toolbox of MATLAB can facilitate the procedure, then it will be easy to select the values that stabilize the system and offer an acceptable response.

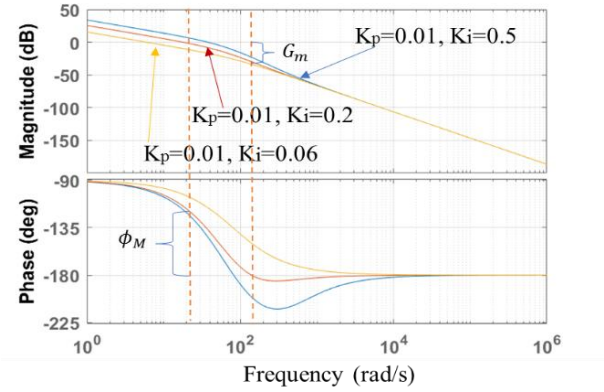

(a)

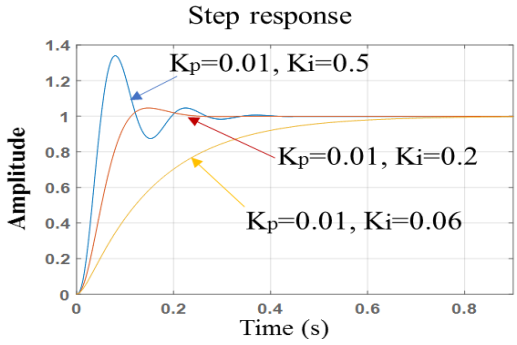

(b)

Fig. IV. 15 Bode diagram and step response of (IV-25) [58]

Fig. IV. 16 presents the behaviour of the FC-TCR compensator in suppressing the harmonics and compensating for the voltage drop under frequency variation. Before installing the compensator, it is obvious that both V_{lo} and I_s are harmonically contaminated with THDs of respectively 40% and 29% and the PF is higher than 0.9. The connection of the switched capacitor in the instant 0.06s improves the V_{lo} and I_s waveforms by decreasing their THDs to less than 5% and causes an overcompensating of the PF, which leads to an overvoltage. In the instant 0.14s, the FC-TCR is connected. It is evident that the FC-TCR compensates for the overvoltage to less than 1%, while the THDs of V_{lo} and I_s remain fixed. Furthermore, in the instant 0.25s a frequency drift of 4% occur. It is clear that the FC-TCR can work efficiently under frequency drifts due to adapting the DFT with the frequency locked-loop (FLL).

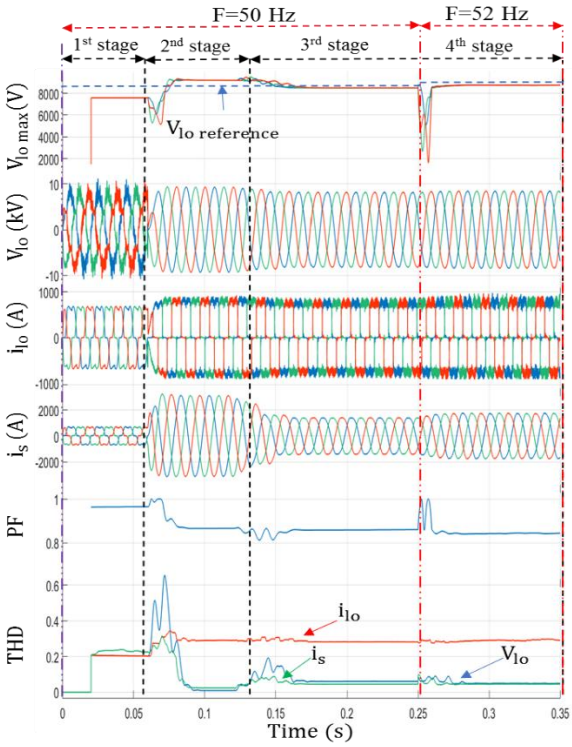

Fig. IV. 16 performance of the FC-TCR compensator under frequency variation [58].

Fig. IV. 17(a) presents the performance of the FC-TCR under load variation. It is clear that before connecting the FC-TCR, the voltage is dropped and distorted. After connecting the switched capacitor in the instant 0.06s, it acts as a low-pass filter leading to decrease the THDs of V_{lo} and I_s to less than 5%. However, the extra injected capacitive reactive power causes an overvoltage. After connecting the FC-TCR in the instant 0.13s, the overvoltage is decreased to follow the reference voltage, and the THDs of V_{lo} and I_s remain fixed. In the instant 0.25s, a load variation occurs. It is clear that the FC-TCR is flexible to flow the load variation by pushing the voltage to follow the reference. However, according to Fig. IV. 17(b), it is clear that the installation of the PPFs can only reduce the harmonics of both voltage and current by decreasing their THDs to values that do not respect the standards. Moreover, the PPFs are not flexible to enhance the voltage stability due to their fixed compensation characteristic.

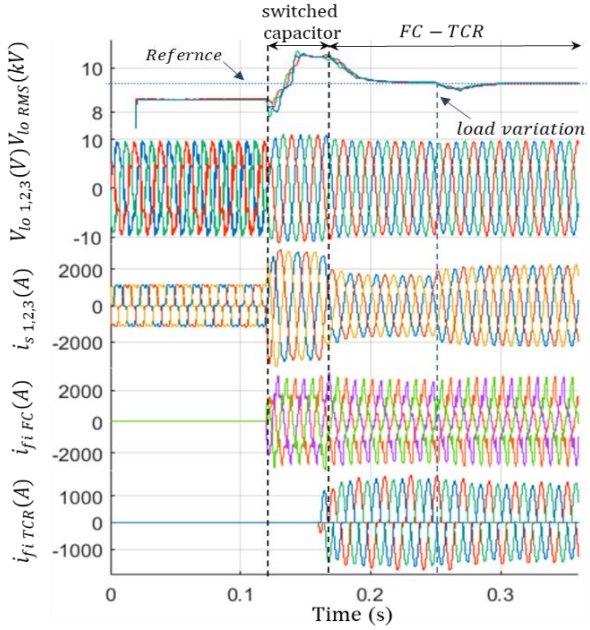

(b)

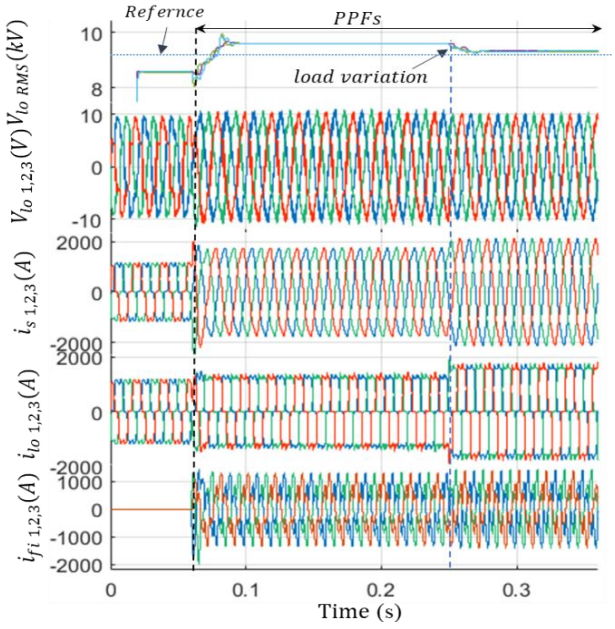

(a)

Fig. IV. 17 harmonic mitigation and voltage sags compensation under load variation. (a) Using the FC-TCR compensator. (b) Using the PPFs [57].

In case the main impedance value is not high enough to reduce the cut-off frequency of the FC-TCR to reject the low-order harmonics, the combined topology of the FC-TCRs with the APF can be an alternative. As it has been demonstrated in [56], the FC-TCRs can reject the high order harmonics and ensures the voltage stability, while the APF can suppress the low order harmonics. Fig. IV. 18 presents the single line diagram of the EPS of the SPS, which contains two synchronous generators, two propulsions, two variable speed drives, two FC-TCR compensators, and a hybrid APF.

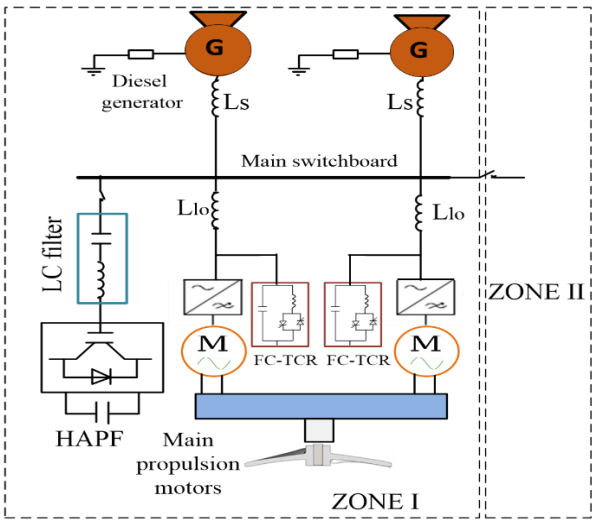

Fig. IV. 18 Single line diagram of a combined structure of the FC-TCRs with the APF [56].

Fig. IV. 19 (a) presents the performance of the combined filter in enhancing the THDs and the voltage stability of the SPS. Before the connection of the filter, it is clear that in this study case the voltage and current are harmonically contaminated. In the instant 0.05s, only the HAPF is connected. It is evident that the APF can filter the current by decreasing its THD to less than 5%. This is more clear in the second plot of Fig. IV. 19 (b). However, the Hybrid APF cannot filter the voltage. In the instant 0.12s, the FC-TCR is connected. It is obvious that the FC-TCR can act as a low pass filter and decrease the harmonics of the voltage to less than 5%. Moreover, as the FC-TCR is controlled to enhance the stability of the voltage it is clear in the first plot of Fig. IV. 19 (b) that the voltage drop is compensated from 9% to less than 1%.

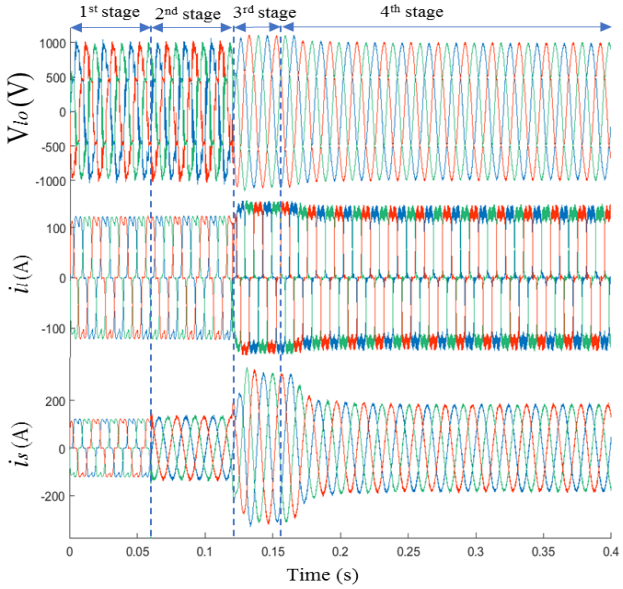

(a)

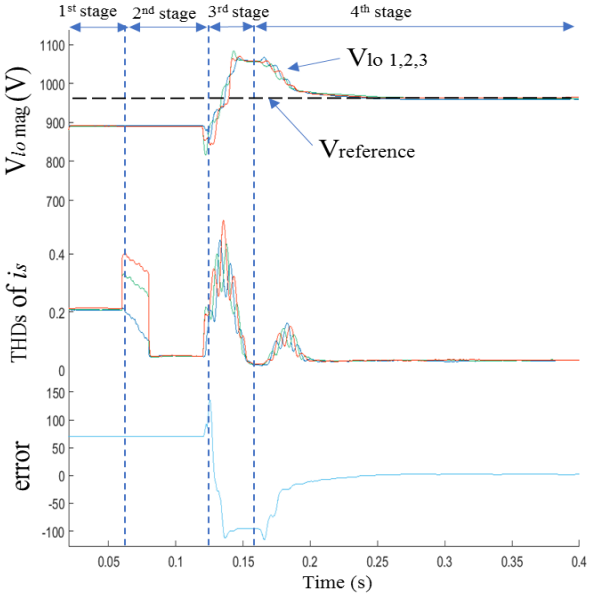

(b)

Fig. IV. 19 performance of the combined filter. (a) The waveform of the voltage and current before and after installing the combined filter. (b) evaluation of the voltage stability of and the THD of current after installing the combined filter [56].

IV. 5 Performance enhancement of fixed capacitor-thyristor controlled reactor based on numerical methods. A study case of a shipboard microgrid

In the last decades, the application of static var compensators (SVCs) such as the FC-TCR compensators has been increasing in different applications [76], [77]. In [27], the FC-TCR proved it is efficacy in reducing the harmonics and improving the PF of SPSs. Whereas in [58], [57] the FC-TCR compensator demonstrated its reliability in enhancing the voltage stability and suppressing the harmonics. The basic structure of the FC-TCR filter consists of a capacitor, which is shunted with an inductor. The capacitor generates a large amount of capacitive reactive power to drive the lagging PF into leading PF. Then, based on the anti-parallel thyristors of the TCR, the inductance is controlled either to tend the PF towards the unity or to force the load voltage to follow the reference voltage. Fig. IV. 20 presents the EPS of the selected hybrid ferry, which consists of two synchronous generators, two propulsion motors, energy storage system, hotel loads and the FC-TCR compensator.

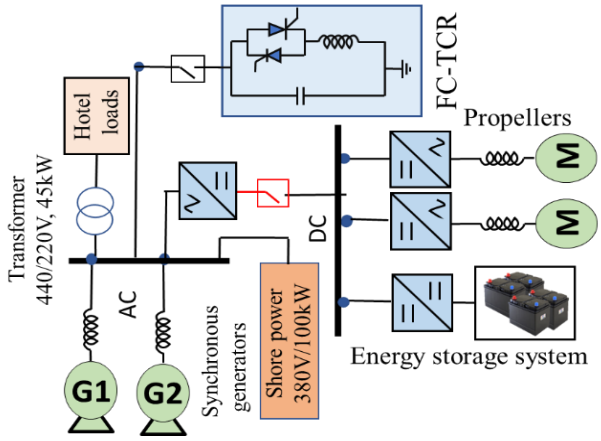

Fig. IV. 20 Single line diagram of the FC-TCR compensator connected to the EPS of the hybrid ferry [60].

The reactive power generated by the FC-TCR is defined by calculating the firing angle α as [60]:

$$-2\alpha + \sin(2\alpha) - 2\pi = \pi \frac{L_{FI}}{L_{FI}(\alpha)} \quad \text{(IV-26)}$$

where L_{Fi} indicate the total inductance of the TCR. $L_{Fi}(\alpha)$ is the estimated inductance that generates the desired amount of the reactive power. It is obvious that (IV-26) is a non-linear equation. Hence, extracting α is not straightforward. The traditional method to solve (IV-26) is to make an offline calculation and store it in the microprocessor of the signal processor cards. Then, based on the lookup table, α is approximated [25]. However, the performance of this method tends to worsen under-voltage and frequency variation. Therefore, in [60] the application of three simple and yet-effective numerical algorithms are suggested to estimate α of the FC-TCR compensator. These methods that are based on the Bisection (BS) method, Newton-Raphson (N-R) method and false position (FP) method can estimate α online with an effective approximation even under voltage and frequency variation.

IV. 5. 1 Newton-Raphson method

The N-R method is one of the dominant algorithms in numerical analysis, which can estimate the roots of real-valued functions [66]. Fig. IV. 21 presents the flowchart of the N-R algorithm. By defining an initial value α_0 and an error, the algorithm starts the linearization by using the derivative of (IV-26) as [60]:

$$x_i = \alpha - \frac{f(\alpha)}{df(\alpha)} \tag{IV-27}$$

For each iteration the condition S is evaluated as [60]:

$$S = \frac{x_i - \alpha_0}{\alpha} 100 \tag{IV-28}$$

Once the algorithm reaches a value of S that is less than the error, it means that the true root is satisfactory. Hence, it stops. The selected error should not be very small to reduce the number of iteration. It is worthy to highlight that the guess α_0 is always selected in the interval $\frac{\pi}{2} < \alpha(i) < \pi$, which is the maximum and minimum values of α for a star connected FC-TCR.

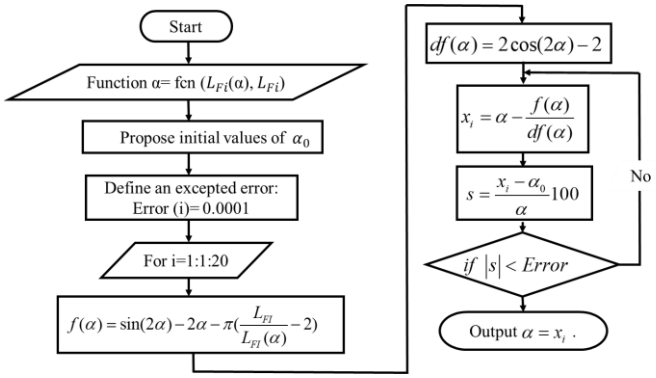

Fig. IV. 21 Flow chart of the Newton–Raphson method [60].

IV. 5. 2 Bisection method

The BS method is a simple algorithm, which is performed using Bolzano's theorem to find the roots of the non-linear function [66]. Fig. IV. 22 presents the flowchart of the BS algorithm. Contrary to the N-R method, which needs only one guess, this method starts by identifying the guesses α_1 and α_2. Since α varies in the interval $\frac{\pi}{2}<\alpha(i)<\pi$ for a star connected FC-TCR compensator, then selecting α_1 to $\alpha_1=\pi/2$ and α_2 to $\alpha_2=\pi$ improves the convergence. Then, an error should be defined to enable the algorithm to stop the iterations. There is always a compromise between good accuracy and a small computation burden. It will be demonstrated that setting the error to 0.0001 provides good results with a small number of iterations. After that the BS method starts the execution by decreasing the distance between α_1 and α_2 until it attains the best approximation as [60]:

$$\alpha=\frac{\alpha_1+\alpha_2}{2} \tag{IV-29}$$

Finally, the decision to stop the iteration is taking when $\alpha=\alpha_1+\alpha_2/2<error$, thus, outputs α.

IV. 5. 3 False position method

In numerical analysis, the FP method is an algorithm that can estimate the roots of non-linear functions. The difference between this method and the BS method is that the FP method is featured by the better adaptability to higher dimensions [16]. Fig. IV. 23 portrays the flowchart of the FP method. The execution of the FP method begins by defining an interval $[\alpha_1,\alpha_2]$, where the following conditions must be

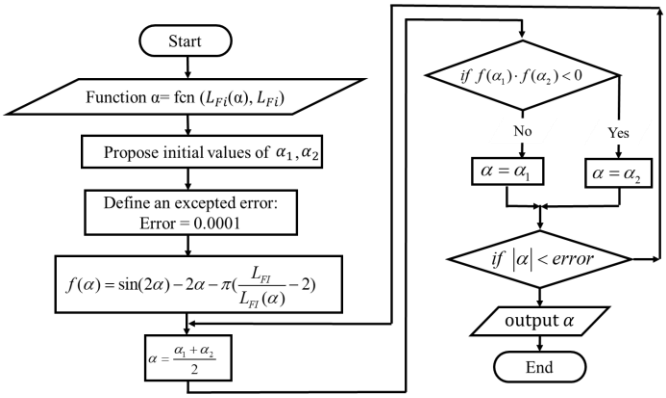

Fig. IV. 22 Flow chart of the Bisection method [60].

respected: $\alpha_1 < \alpha_2$, and $f(\alpha_1) \cdot f(\alpha_2) < 0$. Moreover, an error should be selected to enable the algorithm to stop the iteration once the answer's error is smaller than the selected error. Similar to the N-R method and the BS method, setting the error to 0.0001 provides a satisfactory compromise between the transient response and the accuracy. After that, the FP method performs the linearization of the non-linear equation using the following function [60]:

$$\alpha = \alpha_1 - f(\alpha_1) \frac{(\alpha_2 - \alpha_1)}{f(\alpha_2) - f(\alpha_1)} \tag{IV-30}$$

When the approximation's error crosses the selected error, α is extracted based on (IV-30) with the last approximated roots.

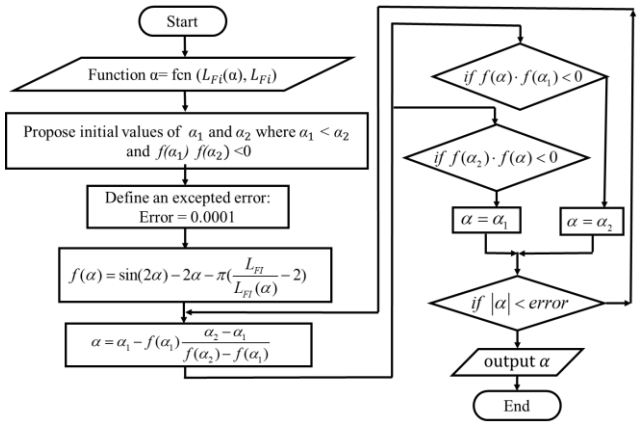

Fig. IV. 23 Flowchart of the false position method [60].

IV. 5. 4 Simulation results and discussions

The numerical results of a modelled ferry are carried out under the MATLAB/Simulink environment. The EPS parameters are summarized in Table. IV. 4. Fig. IV. 24 shows the performance of the FC-TCR compensator based on the proposed numerical methods. The plots of this figure present respectively the distorted load voltage with a THD of about 19%, distorted load current i_{lo} with a THD of 15%, the source current i_s, the PF, α, and the number of iteration operated by each method. The switched capacitor is connected in the instant 0.06s and the TCR is connected in the instant 0.12s. It is obvious that the three techniques provide the same accuracy. Hence, the THD of i_s is reduced from 15% to less than 5%, which respects the norms, and the PF is compensated from 0.89 to be close to unity. The last plot presents the iterations of each method to estimate the firing angle. It is clear that the N-R method provides a smaller number of iterations compared to the other methods. Furthermore, in contradiction with the BS method and the FP method that need two initial guesses α_1 and α_2, the N-R requires only one initial guess; thus, its implementation is featured by simplicity.

Fig. IV. 25 presents the behaviour of the N-R method and the lookup table method in estimating α of the FC-TCR compensator under frequency variation. It is clear that when connecting the capacitor in the instant 0.02s, it acts as a low-pass filter, which improves the THDs of the voltage and source current. Then in the instant 0.06s the TCR is connected. It is evident that both methods can provide a good estimation of α. However, when the frequency drifts in the instant 0.12s, the performance of the lookup table tends to worsen resulting in some fluctuations that appear on the PF, the

Table. IV. 4. Parameters of the EPS of the ferry [60].

Category	Parameters	Values
Synchronous generators	RMS voltage	V=450V
	Electric Power	P= 2x88 ekW
propellers	Rated power	2x112kW/1620rpm
Hotel loads	Nominal power	P=35 ekW
PPFs	5th harmonic filter	$L = 0.006 / 0.016H$
		$C = 67.54/25.3302\ \mu F$
	7th harmonic filter	$L = 0.006 / 0.016H$
		$C = 34.46/12.92\ \mu F$
	Supporter inductance	$L_{sup} = 0.06H\ \ R = 2\Omega$

RMS source current and α.

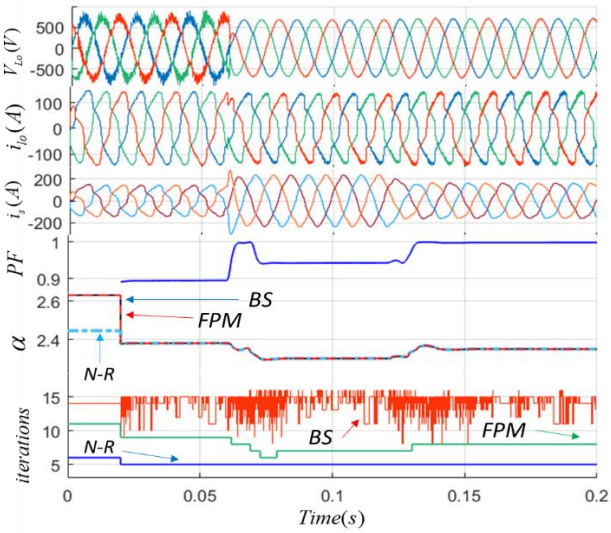

Fig. IV. 24 Behaviour of the FC-TCR compensator using the proposed numerical methods [60]

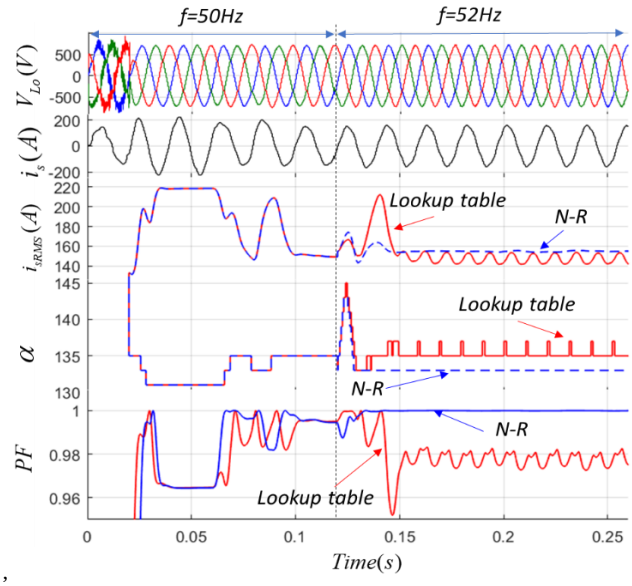

,

Fig. IV. 25 Comparison between the N-R method and the lookup table under frequency drift [60].

Chapter V. Conclusion and future work

Conclusion

In this Ph.D. thesis, a study and development of the power quality issues and voltage stability of terrestrial grids and shipboard power systems for low-voltage and medium-voltage level were investigated and summarized in each chapter as:

Chapter I presents a general introduction about some inherent power quality issues of terrestrial grids and shipboard power systems, then briefly describe some of the most used techniques to improve these power quality issue. And finally, present the objectives and contributions of this Ph.D. dissertation.

In Chapter II the roots of the most dominant power quality issues such as the harmonic contamination are presented. These harmonics have mainly resulted from the power electronic converters (PECs) that are growing vastly due to their non-linearity characteristic. Then it presents the advantages and disadvantages of the PPFs that are the traditional solution. These filters can reduce the dominant harmonics and compensate for a degree of PF. However, they struggle from several deficiencies such as susceptibilities to series and parallel resonance, sensitivity to frequency variation, fixed tuning, heavyweight and large size, etc. After that, the solution to overcome the weakness of the traditional solutions based on installing the APFs is presented. Besides the harmonics suppression, the APFs can compensate for the PF and unbalance. A crucial part of installing the APFs is the reference compensating current (RCC) algorithm. Hence, in this chapter, several reference compensating current algorithms and synchronization methods are presented. In [28], the dynamic performance of the APF under distorted and unbalanced grid voltage is enhanced by proposing a selective harmonic cancelation technique based on the multiple-complex coefficient-filter-based PLL (MCCF-PLL). The advantage of applying this type of PLL is to provide accurate information about each harmonic component of the voltage with its corresponding sequence during the estimation of the voltage phase/frequency. In [29], an optimized open-loop synchronization technique is proposed to enhances the dynamic performance of the APF. This technique, which is based on the non-linear least square approach can extract the fundamental voltage and estimates its phase within only a half cycle in the presence of odd harmonics and dc offset. And last but not least, in [30], a fast and yet effective open-loop synchronization (OLS) technique based on Cascaded Delayed Signal Cancellation (CDSC) to improve the performance of the APF is suggested.

Chapter III begins by introducing the harmonics contamination of the electrical power system of the shipboard power systems. These harmonics are caused mainly

due to the widespread of power electronic converters onboard shipboard power systems. Then it describes the importance of attaining precise information of harmonics, which is very crucial to assess the total distortion and verify if it respects the norms or poses a threat. After that, it explains proper methods to assess these harmonics based on the power quality standards. Next, it highlights the deficiency of the these standards requirements to assess the harmonics distortion mainly in the existence of the inetrharmonics and frequency drifts such as the application of the FFT with a window width of 10/12 times of the fundamental component that is not practical for the shipboard power systems. Finally, to overcome the weaknesses of the FFT, this chapter presents a signal periodicity-independent algorithms to assess the harmonics and interharmonics of distorted signals. This method, which is based on an enhanced MPM can estimate the harmonics and interharmonics with a short moving window width under large frequency drifts that makes its application to shipboard power systems more practical. The performance of this method is evaluated under MATLAB software, and then the experimental validation is attained by analyzing the current of a container ship.

Chapter IV starts by demonstrating that tuning the passive power filters (PPFs) at the aimed harmonic is not enough to improve their harmonics rejection capability. Hence, there are extra two most important factors that are the harmonic attenuation factor (HAF) and the filtering sensitivity factor (FSF) that can also influence on the filtering capability of PPFs. The smaller the HAF is the better filtering performance. However, seeking to decrease the HAF can affect the FSF if the filters are not properly designed. Therefore, in this chapter, a more in-depth harmonic analysis of the HAF and FSF of PPFs was investigated and improved. Moreover, a theoretical and analytical investigation on how to improve the trade-off between the HAF and FSF was addressed. Furthermore, a new topology of the PPFs is suggested for shipboar power systems to achieve a good compromise between the HAF and the FSF. Moreover, in this chapter, a combined topology of hybrid APF (hereafter called HAPF) and FC-TCR is proposed to enhance the power quality of shipboard power systems. The FC-TCR is connected to reduce the harmonic distortion and compensate for the voltage drop. Thus, enhances the voltage stability, whereas the HAPF rejects the dominant harmonic currents. Furthermore, it has been demonstrated in this chapter that if the FC-TCR compensator is well designed, it will function as a low-pass filter with a cut-off frequency that is lower than the frequencies of the low-order harmonics. Hence, it filters both the dominant and high-order harmonics of the shipboard power systems. In addition, to deal with the voltage stability issues of ships, it has been demonstrated that if the control algorithm of the FC-TCR compensator is a voltage control algorithm instead of a power factor control algorithm, then the FC-TCR compensator will compensate for the voltage sags and swells, and thus ensures the voltage stability of shipboard power systems. Besides, the estimation of the firing

angle to control the FC-TCR is not straightforward due to its non-linearity characteristics. Therefore, in this chapter, three simple and yet-effective numerical methods are suggested to estimate the firing angle of the FC-TCR compensator. These techniques that are based on the Bisection (BS) technique, Newton-Raphson (N-R) technique, and false position (FP) technique have demonstrated their capability in providing an accurate firing angle estimation of the FC-TCR compensator under load variation and frequency drifts.

Chapter V summarizes the contributions of this dissertation.

Future work

- The SPSs are distinguished by the redundancy of the synchronous generators (SGs). The number of these SGs differs depending on the type and the size of the ship. These SGs are connected and disconnected according to the load demand, which is managed by the power management system. During the connection/disconnection of these SGs, the total main impedance of the systems varies due to the sub-transient reactance variation. Hence, in future work, we consider designing a developed controller for the FC-TCR compensator to offer better stability of the FC-TCR under the main impedance variation.
- Prepare a more in-depth analysis of the optimal location of the FC-TCR compensators in case of connecting more than one compensator.
- Make a study on how to integrate other sophisticated filters of the second and third generation to improve the power quality issues of ships such as the electrical spring, the smart impedance, dynamic voltage restorer …etc.

LITERATURE LIST

[1] W. E. Reid, "Power quality issues-standards and guidelines," *IEEE Trans. Ind. Appl.*, vol. 32, no. 3, pp. 625–632, 1996.

[2] S. Jayasinghe, L. Meegahapola, N. Fernando, Z. Jin, and J. Guerrero, "Review of Ship Microgrids: System Architectures, Storage Technologies and Power Quality Aspects," *Inventions*, vol. 2, no. 1, p. 4, 2017.

[3] A. Micallef, M. Apap, C. Spiteri-Staines, and J. M. Guerrero, "Mitigation of Harmonics in Grid-Connected and Islanded Microgrids Via Virtual Admittances and Impedances," *IEEE Trans. Smart Grid*, pp. 1–11, 2015.

[4] G. Sulligoi, A. Tessarolo, V. Benucci, A. M. Trapani, M. Baret, and F. Luise, "Shipboard Power Generation: Design and Development of a Medium-Voltage dc Generation System," *IEEE Ind. Appl. Mag.*, vol. 19, no. 4, pp. 47–55, 2013.

[5] S. Sumsurooah, M. Odavic, S. Bozhko, and D. Boroyevic, "Toward Robust Stability of Aircraft Electrical Power Systems: Using a μ-Based Structural Singular Value to Analyze and Ensure Network Stability," *IEEE Electrif. Mag.*, vol. 5, no. 4, pp. 62–71, 2017,

[6] M. Shahbazi and A. Khorsandi, "Power Electronic Converters in Microgrid Applications," *Microgrid*, pp. 281–309, Jan. 201.

[7] A. Micallef, M. Apap, C. Spiteri-Staines, and J. M. Guerrero, "Mitigation of Harmonics in Grid-Connected and Islanded Microgrids Via Virtual Admittances and Impedances," *IEEE Trans. Smart Grid*, pp. 1–11, 2015.

[8] R. L. Smith and R. P. Stratford, "Power System Harmonics Effects from Adjustable-Speed Drives," *IEEE Trans. Ind. Appl.*, vol. IA-20, no. 4, pp. 973–977, Jul. 1984.

[9] T. H. Ortmeyer, K. R. Chakravarthi, and A. A. Mahmoud, "The Effects of Power System Harmonics on Power System Equipment and Loads," *IEEE Power Eng. Rev.*, vol. PER-5, no. 9, pp. 54–54, Sep. 1985.

[10] D. E. Rice, "Adjustable Speed Drive and Power Rectifier Harmonics-Their Effect on Power Systems Components," *IEEE Trans. Ind. Appl.*, vol. IA-22, no. 1, pp. 161–177, Jan. 1986.

[11] R. E. Hebner *et al.*, "Technical cross-fertilization between terrestrial microgrids and ship power systems," *J. Mod. Power Syst. Clean Energy*, vol. 4, no. 2, pp. 161–179, 2016.

[12] G. Sulligoi, A. Vicenzutti, V. Arcidiacono, and Y. Khersonsky, "Voltage Stability in Large Marine Integrated Electrical and Electronic Power Systems," *IEEE Trans. Ind. Appl.*, vol. 9994, no. c, pp. 1–1, 2016.

[13] R. Sachan and R. Srivastava, "Performance analysis of fixed shunt passive filters for harmonic mitigation," in *2016 International Conference on Emerging Trends in Electrical Electronics & Sustainable Energy Systems (ICETEESES)*, 2016, pp. 87–90.

[14] H. Akagi, *"Modern active filters and traditional passive filters."* Bulletin of the polish academy of sciences technical sciences 54, no. 3 (2006).

[15] A. Insleay, “A neural network controlled unity power factor three phase current source PWM front-end rectifier for adjustable speed drives,” in *Proceedings of 5th International Conference on Power Electronics and Variable-Speed Drives*, 1994, vol. 1994, pp. 251–255.

[16] R. R. Chavan and A. R. Thorat, “Modified PWM technique for bidirectional AC/DC converter to reduce switching loss with fuzzy logic control for grid tied microgrid system,” in *2016 International Conference on Computation of Power, Energy Information and Commuincation (ICCPEIC)*, 2016, pp. 392–397.

[17] Z. Jin, L. Meng, J. M. Guerrero, and R. Han, “Hierarchical Control Design for a Shipboard Power System With DC Distribution and Energy Storage Aboard Future More-Electric Ships,” *IEEE Trans. Ind. Informatics*, vol. 14, no. 2, pp. 703–714, Feb. 2018.

[18] J. Mindykowski, “Case Study—Based Overview of Some Contemporary Challenges to Power Quality in Ship Systems,” *Inventions*, vol. 1, no. 4, p. 12, 2016.

[19] and M. A. Akagi, Hirofumi, Edson Hirokazu Watanabe, “Instantaneous power theory and applications to power conditioning. Vol. 62. John Wiley & Sons, 2017.”

[20] S. Ouchen, J.-P. Gaubert, H. Steinhart, and A. Betka, “Energy quality improvement of three-phase shunt active power filter under different voltage conditions based on predictive direct power control with disturbance rejection principle,” *Math. Comput. Simul.*, Dec. 2018.

[21] P. Salmerón Revuelta, S. Pérez Litrán, J. Prieto Thomas, P. Salmerón Revuelta, S. Pérez Litrán, and J. Prieto Thomas, “Series Active Power Filters,” *Act. Power Line Cond.*, pp. 149–187, Jan. 2016.

[22] P. Salmerón Revuelta, S. Pérez Litrán, J. Prieto Thomas, P. Salmerón Revuelta, S. Pérez Litrán, and J. Prieto Thomas, “Combined Shunt and Series Active Power Filters,” *Act. Power Line Cond.*, pp. 231–284, Jan. 2016.

[23] I. Andrić *et al.*, “Improvement in Power Quality using Hybrid Power Filters based on RLS Algorithm,” *Energy Procedia*, vol. 138, pp. 723–728, 2017.

[24] J. E. R. Alves, L. A. S. Pilotto, and E. H. Watanabe, “Thyristor-Controlled Reactors Nonlinear and Linear Dynamic Analytical Models,” *IEEE Trans. Power Deliv.*, vol. 23, no. 1, pp. 338–346, Jan. 2008.

[25] R. M. Mathur and R. K. Varma, *Thyristor-based FACTS controllers for electrical transmission systems*. John Wiley & Sons, 2002.

[26] A. Hamadi, S. Rahmani, and K. Al-Haddad, “A hybrid passive filter configuration for VAR control and harmonic compensation,” *IEEE Trans. Ind. Electron.*, vol. 57, no. 7, pp. 2419–2434, 2010

[27] Y. Terriche *et al.*, “A Hybrid Compensator Configuration for VAR Control and Harmonic Suppression in All-Electric Shipboard Power Systems,” *IEEE Trans. Power Deliv.*, pp. 1–1, 2019.

[28] Y. Terriche, S. Golestan, J. M. Guerrero, and J. C. Vasquez, “Multiple-Complex Coefficient-Filter-Based PLL for Improving the Performance of Shunt Active Power Filter under Adverse Grid Conditions,” in *IEEE Power and Energy Society General Meeting*, 2018, vol. 2018-August.

[29] Y. Terriche, J. M. Guerrero, and J. C. Vasquez, “Performance improvement of shunt active power filter based on non-linear least-square approach,” *Electr. Power Syst. Res.*, vol. 160, 2018.

[30] Y. Terriche *et al.*, “Adaptive CDSC-Based Open-Loop Synchronization Technique for Dynamic Response Enhancement of Active Power Filters,” *IEEE Access*, vol. 7, pp. 96743–96752, 2019.

[31] Y. Terriche, D. Kerdoun, and H. Djeghloud, “A new passive compensation technique to economically improve the power quality of two identical single-phase feeders,” *2015 IEEE 15th Int. Conf. Environ. Electr. Eng. EEEIC 2015 - Conf. Proc.*, no. 2, pp. 54–59, 2015.

[32] B. Singh, K. Al-Haddad, and A. Chandra, “A review of active filters for power quality improvement,” *IEEE Trans. Ind. Electron.*, vol. 46, no. 5, pp. 960–971, 1999.

[33] Y. Terriche, S. Golestan, J. M. Guerrero, D. Kerdoune, and J. C. Vasquez, “Matrix pencil method-based reference current generation for shunt active power filters,” *IET Power Electron.*, vol. 11, no. 4, 2018.

[34] X. Guo, W. Wu, and Z. Chen, “Multiple-Complex Coefficient-Filter-Based Phase-Locked Loop and Synchronization Technique for Three-Phase Grid-Interfaced Converters in Distributed Utility Networks,” *IEEE Trans. Ind. Electron.*, vol. 58, no. 4, pp. 1194–1204, Apr. 2011.

[35] S. Golestan, M. Monfared, and F. D. Freijedo, “Design-oriented study of advanced synchronous reference frame phase-locked loops,” *IEEE Trans. Power Electron.*, vol. 28, no. 2, pp. 765–778, 2013.

[36] P. Xiao, K. A. Corzine, and G. K. Venayagamoorthy, “Multiple reference frame-based control of three-phase PWM boost rectifiers under unbalanced and distorted input conditions,” *IEEE Trans. Power Electron.*, vol. 23, no. 4, pp. 2006–2017, Jul. 2008.

[37] M. Qasim, P. Kanjiya, and V. Khadkikar, “Artificial-Neural-Network-Based Phase-Locking Scheme for Active Power Filters,” *IEEE Trans. Ind. Electron.*, vol. 61, no. 8, pp. 3857–3866, Aug. 2014.

[38] R. Chudamani, K. Vasudevan, and C. S. Ramalingam, “Real-Time Estimation of Power System Frequency Using Nonlinear Least Squares,” *IEEE Trans. Power Deliv.*, vol. 24, no. 3, pp. 1021–1028, Jul. 2009.

[39] R. Chudamani, C. S. Ramalingam, and K. Vasudevan, “Non-linear least-squares-based harmonic estimation algorithm for a shunt active power filter,” *IET Power Electron.*, vol. 2, no. 2, pp. 134–146, Mar. 2009.

[40] M. D. Kusljevic, J. J. Tomic, and L. D. Jovanovic, “Frequency Estimation of Three-Phase Power System Using Weighted-Least-Square Algorithm and Adaptive FIR Filtering,” *IEEE Trans. Instrum. Meas.*, vol. 59, no. 2, pp. 322–329, Feb. 2010.

[41] E. Robles, J. Pou, S. Ceballos, J. Zaragoza, J. L. Martin, and P. Ibañez, “Frequency-Adaptive Stationary-Reference-Frame Grid Voltage Sequence Detector for Distributed Generation Systems,” *IEEE Trans. Ind. Electron.*, vol. 58, no. 9, pp. 4275–4287, Sep. 2011.

[42] Y. F. Wang and Y. W. Li, “Grid Synchronization PLL Based on Cascaded Delayed Signal Cancellation,” *IEEE Trans. Power Electron.*, vol. 26, no. 7,

pp. 1987–1997, Jul. 2011.
[43] A. Bagheri, M. Mardaneh, A. Rajaei, and A. Rahideh, “Detection of Grid Voltage Fundamental and Harmonic Components Using Kalman Filter and Generalized Averaging Method,” *IEEE Trans. Power Electron.*, vol. 31, no. 2, pp. 1064–1073, Feb. 2016.
[44] C. A. Busada, H. G. Chiacchiarini, and J. C. Balda, “Synthesis of Sinusoidal Waveform References Synchronized With Periodic Signals,” *IEEE Trans. Power Electron.*, vol. 23, no. 2, pp. 581–590, Mar. 2008.
[45] S. Golestan, A. Vidal, A. G. Yepes, J. M. Guerrero, J. C. Vasquez, and J. Doval-Gandoy, “A True Open-Loop Synchronization Technique,” *IEEE Trans. Ind. Informatics*, vol. 12, no. 3, pp. 1093–1103, Jun. 2016.
[46] L. Asirninoaei, F. Blaabjerg, and S. Hansen, “Evaluation of harmonic detection methods for active power filter applications,” in *Twentieth Annual IEEE Applied Power Electronics Conference and Exposition, 2005. APEC 2005.*, vol. 1, pp. 635–641.
[47] G. Hostetter, “Recursive discrete Fourier transformation,” *IEEE Trans. Acoust.*, vol. 28, no. 2, pp. 184–190, Apr. 1980.
[48] Ö. C. Özerdem, S. K. Khadem, S. Biricik, M. Basu, and S. Redif, “Real-time control of shunt active power filter under distorted grid voltage and unbalanced load condition using self-tuning filter,” *IET Power Electron.*, vol. 7, no. 7, pp. 1895–1905, Jul. 2014.
[49] Terriche et al., "A Resolution-Enhanced Sliding Matrix Pencil Method for Evaluation of Harmonics Distortion in Shipboard Microgrids," IEEE Transactions on Transportation Electrification, 2020.
[50] M. Aiello, A. Cataliotti, S. Favuzza, and G. Graditi, “Theoretical and Experimental Comparison of Total Harmonic Distortion Factors for the Evaluation of Harmonic and Interharmonic Pollution of Grid-Connected Photovoltaic Systems,” *IEEE Trans. Power Deliv.*, vol. 21, no. 3, pp. 1390–1397, Jul. 2006.
[51] J. Borkowski, D. Kania, and J. Mroczka, “Interpolated-DFT-Based Fast and Accurate Frequency Estimation for the Control of Power,” *IEEE Trans. Ind. Electron.*, vol. 61, no. 12, pp. 7026–7034, Dec. 2014.
[52] S. M. Seo, “A Fast IE-FFT Algorithm to Analyze Electrically Large Planar Microstrip Antenna Arrays,” *IEEE Antennas Wirel. Propag. Lett.*, vol. 17, no. 6, pp. 983–987, Jun. 2018.
[53] S. Golestan, J. M. Guerrero, and A. M. Abusorrah, “MAF-PLL with phase-lead compensator,” *IEEE Trans. Ind. Electron.*, vol. 62, no. 6, pp. 3691–3695, 2015.
[54] Y. Hua and T. K. Sarkar, “On the total least squares linear prediction method for frequency estimation,” *IEEE Trans. Acoust.*, vol. 38, no. 12, pp. 2186–2189, Dec. 1990.
[55] Y. Terriche, S. Golestan, J. M. Guerrero, D. Kerdoune, and J. C. Vasquez, “Matrix pencil method-based reference current generation for shunt active power filters,” *IET Power Electron.*, vol. 11, no. 4, pp. 772–780, Apr. 2018, doi: 10.1049/iet-pel.2017.0351.
[56] Y. Terriche *et al.*, “Power quality and Voltage Stability improvement of

Shipboard Power Systems with Non-Linear Loads," in *2019 IEEE International Conference on Environment and Electrical Engineering and 2019 IEEE Industrial and Commercial Power Systems Europe (EEEIC / I&CPS Europe)*, 2019, pp. 1–6.

[57] Y. Terriche, M. U. Mutarraf, M. Mehrzadi, C. Su, J. M. Guerrero and J. C. Vasquez, "More in-depth analytical investigations of two Effective Harmonics Filters for More Electric Marine Vessel Applications," *2019 9th International Conference on Power and Energy Systems (ICPES)*, Perth, Australia, 2019, pp. 1-6

[58] Yacine Terriche, Abderezak Lashab 1, Muhammad. U. Mutarraf et al., "Voltage Stability and Harmonics Mitigation Analyses of Two Effective Compensators for More Electric Marine Vessel Applications,'' IEEE Transactions nn Industial Applications (under review).

[59] Y. Terriche, et al, "Harmonics Rejection Capability Enhancement of Passive Power Filters for All-Electric-Shipboard Micro-Grids." 2020 6th IEEE International Energy Conference (ENERGYCon 2020) (accepted).

[60] Y. Terriche, et al, "Harmonics Mitigation in Hybrid AC / DC Shipboard Microgrids Using Fixed Capacitor-Thyristor Controlled reactor." 2020 6th IEEE International Energy Conference (ENERGYCon 2020) (Accepted).

[61] Y. Terriche, D. Kerdoun, S. Golestan, A. Laib, H. Djehloud, and J. M. Guerrero, "Effective and low-cost passive compensator system to improve the power quality of two electric generators," *IET Power Electron.*, vol. 12, no. 7, pp. 1833–1840, Jun. 2019.

[62] C.-L. Su and C.-J. Hong, "Design of passive harmonic filters to enhance power quality and energy efficiency in ship power systems," in *49th IEEE/IAS Industrial & Commercial Power Systems Technical Conference*, 2013, pp. 1–8.

[63] Van Cutsem, Thierry, and Costas Vournas. Voltage stability of electric power systems. Springer Science & Business Media, 2007.

[64] P. Kundur, *Power System Stability and ontrol*. McGraw-Hill, 1994.

[65] Lamont, Lisa, and Ali Sayigh, eds. Application of Smart Grid Technologies: Case Studies in Saving Electricity in Different Parts of the World. Academic Press, 2018.

[66] MEZEI, Razvan A. An introduction to SAGE programming. John Wiley, and Sons, USA, 2016..

[67] Chih-Ju Chou, Chih-Wen Liu, June-Yown Lee, and Kune-Da Lee, "Optimal planning of large passive-harmonic-filters set at high voltage level," *IEEE Trans. Power Syst.*, vol. 15, no. 1, pp. 433–441, 2000.

[68] S. V. Giannoutsos and S. N. Manias, "A Systematic Power-Quality Assessment and Harmonic Filter Design Methodology for Variable-Frequency Drive Application in Marine Vessels," *IEEE Trans. Ind. Appl.*, vol. 51, no. 2, pp. 1909–1919, Mar. 2015.

[69] Y. Li *et al.*, "A controllably inductive filtering method with transformer-integrated linear reactor for power quality improvement of shipboard power system," *IEEE Trans. Power Deliv.*, vol. 32, no. 4, pp. 1817–1827, 2017.

[70] An Luo, Zhikang Shuai, Wenji Zhu, Ruixiang Fan, and Chunming Tu,

"Development of Hybrid Active Power Filter Based on the Adaptive Fuzzy Dividing Frequency-Control Method," *IEEE Trans. Power Deliv.*, vol. 24, no. 1, pp. 424–432, Jan. 2009.

[71] Control of Harmonics in Electrical Power Systems, American Bureau of Shipping Guidance, 2006.

[72] N. Conditions, C. Study, T. Tarasiuk, and M. Gorniak, "Load Sharing in Ship Microgrids Under," vol. 32, no. 2, pp. 810–819, 2017.

[73] IEEE recommended practice for electrical installations on shipboard, IEEE Standard 45–2002.

[74] IEC Standard 60 092-101-2002, Electrical installations in ships. Definitions and general requirement, 2002.

[75] Rules for Building and Classing Steel Vessels, American Bureau of Shipping, Houston, TX, USA, 2008.

[76] J. R. C. Orillaza and A. R. Wood, "Harmonic State-Space Model of a Controlled TCR," *IEEE Trans. Power Deliv.*, vol. 28, no. 1, pp. 197–205, Jan. 2013.

[77] S. Das, D. Chatterjee, and S. K. Goswami, "A GSA-Based Modified SVC Switching Scheme for Load Balancing and Source Power Factor Improvement," *IEEE Trans. Power Deliv.*, vol. 31, no. 5, pp. 2072–2082, Oct. 2016.

ISSN (online): 2446-1636
ISBN (online): 978-87-7210-805-6 AALBORG UNIVERSITY PRESS